ISSN 0252-1075
Contribution from IITM
Research Report No. RR-144
ESSO/IITM/SERP/SR/06(2018)/195

Spatial Patterns of Subseasonal Eddy Momentum and Heat Transport and its Probable Role in the Interannual Variability of Extratropical to Tropical Interaction during the Summer Monsoon Season

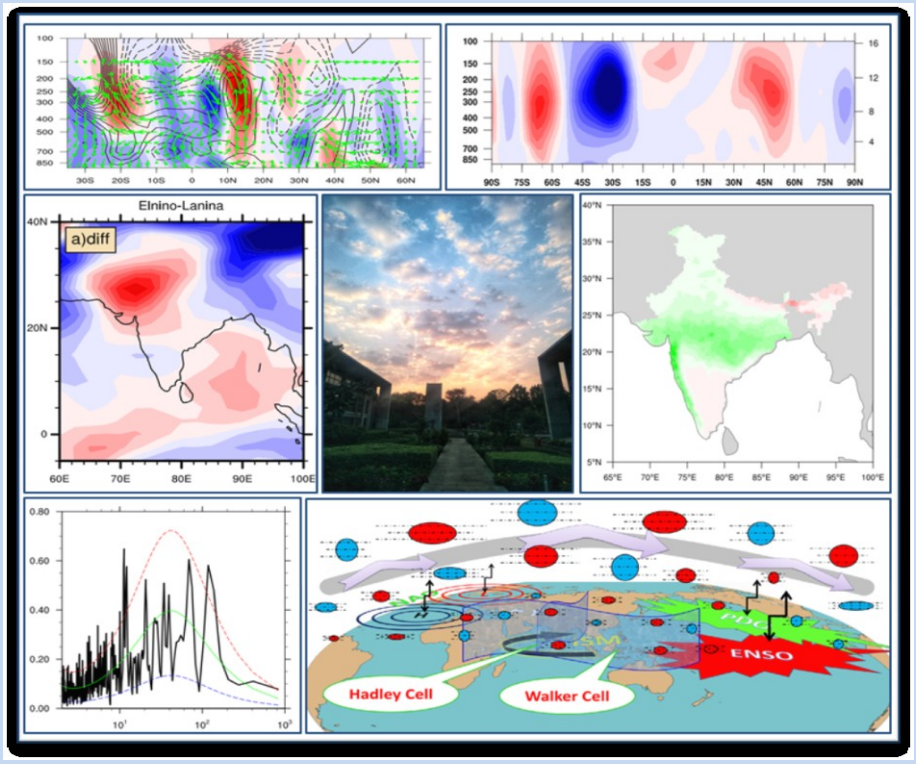

Mahesh Kalshetti, Rajib Chattopadhyay, Phani M. Krishna and A.K. Sahai

Indian Institute of Tropical Meteorology (IITM)
Earth System Science Organization (ESSO)
Ministry of Earth Sciences (MoES)
PUNE, INDIA
http://www.tropmet.res.in/

ISSN 0252-1075
Contribution from IITM
Research Report No. RR-144
ESSO/IITM/SERP/SR/06(2018)/195

Spatial Patterns of Subseasonal Eddy Momentum and Heat Transport and its Probable Role in the Interannual Variability of Extratropical to Tropical Interaction during the Summer Monsoon Season

Mahesh Kalshetti, Rajib Chattopadhyay, Phani M. Krishna and A.K. Sahai

***Corresponding Author Address:**

Rajib Chattopadhyay
Indian Institute of Tropical Meteorology,
Dr. Homi Bhabha Road, Pashan,
Pune – 411008, India.
E-mail: rajib@tropmet.res.in
Phone: +91-(0)20-25904523

Indian Institute of Tropical Meteorology (IITM)
Earth System Science Organization (ESSO)
Ministry of Earth Sciences (MoES)
PUNE, INDIA
http://www.tropmet.res.in/

DOCUMENT CONTROL SHEET

Earth System Science Organization (ESSO)
Ministry of Earth Sciences (MoES)
Indian Institute of Tropical Meteorology (IITM)

ESSO Document Number
ESSO/IITM/SERP/SR/06(2018)/195

Title of the Report
Spatial Patterns of Subseasonal Eddy Momentum and Heat Transport and its Probable Role in the Interannual Variability of Extratropical to Tropical Interaction during the Summer Monsoon Season

Authors
Mahesh Kalshetti, Rajib Chattopadhyay, Phani M. Krishna and A.K. Sahai

Type of Document
Scientific Report (Research Report)

Number of pages and figures
83, 33

Number of references
36

Keywords
Cospectra analysis, extratropical tropical interaction, Indian monsoon, eddy transport, teleconnections

Security classification
Open

Distribution
Unrestricted

Date of Publication
December 2018

Abstract
The current study uses a co-spectral analysis to study the horizontal and vertical structures of eddy heat and momentum transport during the monsoon season (June to September) over the Indian region. The co-spectral composite shows significant interannual variability of north-south eddy transport. Analysis suggesting vital role of global teleconnection patterns on eddy transports and its variability. Since the eddy transport is manifasted by the Rossby wave breaking through the subtropical Jetstream fluctuation. It is well known that such fluctuations can potentially impact the monsoonal low-frequency variability. Current study links such a modulation of eddy forcing by low-frequency extratropical teleconnections.

Summary

A co-spectral analysis is presented to study the northward and southward transport of eddy momentum and heat flux in the sub-seasonal range over the Indian region during the summer monsoon season. The horizontal and vertical structure of eddies shows strong interannual and spatial variability. The transport is studied for the El-Nino/La-Nina years, PDO years and NAO years to understand how the teleconnections impact the spatial structure of eddies. The study reveals the transport of eddies in a horizontal direction could act as an eddy forcing over the Indian region. Also, the results show that the global teleconnection patterns could modulate the transport of heat and momentum by the eddies.

Contents

1. Summary 1

2. Abstract 2

3. Introduction 4

4. Datasets 8

5. Methodology & definitions 8

5.1. Cospectra 8

5.2. Correlation coefficient analysis 9

5.3. Monsoon circulation index 10

5.4. Active and break composite 10

5.5. El Niño Southern Oscillation (ENSO) index and monsoon teleconnection 10

5.6. Pacific Decadal Oscillation (PDO) index and monsoon teleconnection 11

5.7. North Atlantic Oscillation (NAO) index and monsoon teleconnection 12

6. General circulation and eddy transport analysis 12

6.1. Climatic features of general circulation 12

6.2. Eddy transport analysis by the conventional method 15

6.3. Eddy transport analysis by the cospectra method 16

6.3.1. Eddy periodicity band selection 16

6.3.2. Comparison of eddy analysis method 17

6.3.3. Cospectra analysis in subseasonal scale 18

6.3.4. Interannual variation of cospectra analysis 19

6.4. Active and break spells 20

7. Eddy transport and teleconnection 21

7.1. Correlation analysis 21

7.2. A climatic feature of eddies in ENSO phases 22

7.3. EMF transport and ENSO teleconnection 23

7.4. EHF transport and ENSO teleconnection 26

7.5. A climatic feature of eddies in PDO and NAO phases 28

7.6. EMF transport and PDO teleconnection 29

7.7. EMF transport and NAO teleconnection 31

7.8. EHF transport and PDO teleconnection 33

7.9. EHF transport and NAO teleconnection 36

8. Conclusion 39

9. List of abbreviations 41

10. List of figures 42

11. List of Tables 46

12. References 47

13. Tables 50

14. Figures 53

Spatial Patterns of Subseasonal Eddy Momentum and Heat Transport and its Probable Role in the Interannual Variability of Extratropical to Tropical Interaction during the Summer Monsoon Season

Mahesh Kalshetti, Rajib Chattopadhyay, Phani M. Krishna, and A.K. Sahai
Indian Institute of Tropical Meteorology, Pune, India

1. Summary

A co-spectral analysis is presented to study the northward and southward transport of eddy momentum and heat flux in the sub-seasonal range over the Indian region during the summer monsoon season. The horizontal and vertical structure of eddies shows strong interannual and spatial variability. The transport is studied for the El-Nino/La-Nina years, PDO years and NAO years to understand how the teleconnections impact the spatial structure of eddies. The study reveals the transport of eddies in a horizontal direction could act as an eddy forcing over the Indian region. Also, the results show that the global teleconnection patterns could modulate the transport of heat and momentum by the eddies.

2. Abstract

The current study uses a co-spectral analysis to study the horizontal and vertical structures of eddy heat and momentum transport during the monsoon season (June to September) over the Indian region. The co-spectral composites during different years show significant north to south or south to north transport during the monsoon season with distinct spatial features. There is a strong interannual variability in the co-spectral transport over Indian region, and it shows distinct vertical structures, In some year structures shows barotropic (uniform sign of the spectral variance) and in some year it shows baroclinic variation (spectral signature changes sign) with height. It implies distinct year to year variability of poleward and equatorward transport during different monsoon seasons.

To understand eddy transports and its variability associated with distinct teleconnection pattern, a correlation analysis is made with global teleconnection indices, e.g., NAO, PDO, monsoon Hadley, and ENSO indices. The study shows a significant correlation between 20-40, 40-60 day cospectral band and phases of PDO and NAO and in some cases (i.e., in some frequency band) with ENSO. Since the eddy transport is also associated with fluctuations of the subtropical westerly Jetstreams, fluctuations in co-spectral eddy transport and its significant teleconnection potentially indicate a distinct control mechanism of the fluctuations of the subseasonal variability of the Jetstream.

Since the eddy transport is associated with the Rossby wave breaking, it is related to the fluctuations of the subtropical Jetstream. It is well known that such fluctuations can potentially impact the monsoonal low-frequency variability. Hence the analysis potentially shows a mechanism by which extratropical eddy transport fluctuation mediated by large-scale low-frequency teleconnection could potentially regulate intraseasonal monsoon variability. This mechanism is important as earlier studies shows the internal monsoon dynamics strongly

controls the monsoon interannual variability and hence, also, predictable component of low-frequency variability could improve monsoon predictability. The seasonal and spatial variation in eddy forcing could indicate an externally forced teleconnection mechanism in which the monsoon low-frequency variability is influenced by intraseasonal eddy forcing modulated by low-frequency extratropical teleconnections.

3. Introduction

The Atmospheric general circulation plays a significant role in the modulation of climate and weather patterns across the globe; unequal heating drives it over the tropics and high latitudes. To balance such differential heating, the components of general circulation get interacted by exchanging heat, mass, and momentum (Willett, 1948, Namias, 1950, Lorenz, 1969). This interaction may occur through the direct and indirect way. The direct interaction manifested by Hadley cell, Walker cell, and polar cell, for example, the interaction of Walker and Hadley cells with Indian summer monsoon (ISM) rainfall (ISMR). The indirect interaction is manifested by propagations of waves and eddies, for example, midlatitude weather system.

Over the midlatitude region due to the north and south stronger temperature gradient, small perturbation gives rise to strong baroclinic instabilities and generation of eddies (Saltzman & Tang, 1975, Peixto & Oort, 1984). Eddies are a vital component of Ferrel Cell, and it maintains the general circulation at higher latitudes. Eddies are inhomogeneity in space (persistent zonal asymmetric) and time (departure from time mean) by atmospheric variables, and it is a significant contributor to the zone of mixing region (mid-latitude). Eddy mediates induced-circulation over extratropical regions.

Eddies can term as an "additional forcing" in the zonal momentum or temperature equation. Thus they influence the heat and momentum transfer. The study reveals the transport of eddies in the horizontal direction could act as an eddy forcing. Formally eddies are defined as departures from products of two average fields. Suppose $\boldsymbol{A}$ and $\boldsymbol{B}$ are any scalar atmospheric variables, the time-space decomposition of $\boldsymbol{A}$ and $\boldsymbol{B}$ variables mathematically is expressed as:

$$[\overline{\mathbf{AB}}] = [\overline{\mathbf{A}}][\overline{\mathbf{B}}] + [\overline{\mathbf{A}}^{*}\,\overline{\mathbf{B}}^{*}] + \left[\overline{\boldsymbol{A'B'}}\right]$$

First-term in above expression represents the zonal mean of time mean of product ***AB***. It is clear that the total flux term decomposed into three-term viz. mean circulation, stationary eddies, and transient eddies respectively (Peixto & Oort, 1984). The extratropical region gives rise to baroclinic eddies. The extratropical eddies manifested as anomalous weather patterns and waves propagation and are interacting with the global circulation as well as regional circulation. Hence the interaction is responsible for local as well as a teleconnected response in climate.

On a global scale, for example, the correlation between the 500mb height from mid-latitude and outgoing longwave radiation from the tropical region suggests that energy propagates from upper troposphere of mid-latitudes (in the Northern hemisphere) into tropics and triggers the convections over the tropics (Liebmann & Hartmann, 1984). The diagnostic analysis shows that the remote influence of North Atlantic Oscillation (NAO), Pacific Decadal Oscillation (PDO) during interannual to decadal scale is modifying Extratropical to Tropical (E2T) interactions (Walker & Bliss, 1932, Wallace & Gutzler, 1981, Krishnan & Sugi 2003, Krishnamurthy & Krishnamurthy, 2017).

Over the Indian region, the impact of anomalous extratropical circulation on monsoon break has been shown decades back by Ramaswamy, 1962; Chart analysis indicates that extratropical originated westerly wave trough intrusion occurs over north-west Indian mid-troposphere. Atmospheric General Circulation Model (AGCM) simulation has demonstrated the extended monsoon breaks linked with mid-latitude anomalous circulation, the intrusion of extratropical cold and dry winds into northwest Indian region weakens the monsoon flow (Krishnan et al., 2009). A recent study by Chattopadhyay et al., 2015 have shown a pathway for extratropical interaction over Indian region that enabled through Sea Surface Temperature (SST) anomalies pattern over North Pacific and North Atlantic basin whose association with seasonal variability give rise to potential monsoon predictability in dynamical models. The

role of extratropical circulation on extreme rainfall over Himalayan region is highlighted by Joseph et al., 2015, Vellore et al., 2016 and Joseph et al., 2016. Another diagnostic analysis by Fadnavis & Chattopadhyay, 2017 for prolonged rainfall break spells of ISM suggests its linkage with the extratropical stratospheric intrusion. This intrusion occurs over the North Indian region through eddy dissipation and Rossby wave breaking. Rossby wave breaking near vicinity of the subtropical westerly jet is manifested by eddy dissipation; cold and dry air mass characterizes this eddy. Such a stratospheric intrusion is one of the factors for subdued rainfall over the Indian region. Above studies suggest direct pathways for E2T interaction over Indian region through eddy transport and modulation of mean monsoon flow.

On what factors do these eddy generation and transport depend? Local variability influences eddies. Beside local factor, eddy transport also influenced by teleconnection. Teleconnection enables indirect interaction between general circulation components through eddies and wave transport. Teleconnection can be defined as significant simultaneous correlations between temporal fluctuations in meteorological parameters at widely separated points on Earth (Wallace and Gutzler, 1981). It excites the atmosphere to behave like a ‘‘bridge’’ linking between different parts of the oceanic region, and it excites the ocean to behave like a ‘‘tunnel’’ linking between different atmospheric regions (Liu & Alexander, 2007). Linkages of numerous atmospheric and oceanic global patterns (steady state like El Niño Southern Oscillation (ENSO) as well as a dynamic state like Madden Julian Oscillation (MJO)) are associated with energy transport and wave propagation in subseasonal to decadal scale which creates weather patterns that can be viewed as an eddy mediated weather pattern. Global teleconnections patterns observed with the help of the monthly data sets shows two distinct modes, one is for ISM which linked with entire globe and another for western North Pacific summer monsoon, which linked with southern hemispheric wave trains (Lin, 2009). Such teleconnections are essential for local eddy response (Leung & Zhou, 2018).

Although monsoon climate shows the strong influence of eddies, the general spatiotemporal evolution of eddy heat and momentum transfer during monsoon season over Indian region are not well studied. The general climatological features of eddy transport could shed more light on the monsoon interannual to intraseasonal variability.

In this study, we focus on spatial distribution of eddy momentum and heat transport based on co-spectra analysis of Indian region during the monsoon season. The model and observational studies suggest E2T interaction mediated by eddy transport. The extratropical eddies are influencing the ISMR by modifying the circulation. However, the properties such as vertical and horizontal patterns of eddies, timescale existence of such eddies are still unclear. In this research report, we have examined,

A. The properties of eddies with the help of spectral information of meteorological variables which yields idiosyncratic bands of eddies; Present findings indicate that existence of idiosyncratic eddy bands from the frequency domain analysis is similar to conventional time domain analysis. A significant distinction between the present and previous work is that here we emphasize the essential properties of eddies derived from spectral covariance method.

B. The interannual variations of the subseasonal eddies and its linkage with global teleconnection patterns. The interannual variability of subseasonal eddies could provide a significant understanding of the teleconnections of global patterns.

The detailed outline is as follows; **section 4** describes the datasets specifications of the study, **section 5** explains the data, methodology, and definitions of some terms which have targeted in this study. **Section 6** deals with climatic features of general circulation, cospectra analysis, and level-latitudinal eddy transport variations. **Section 7** deals with the teleconnection affecting the eddy transport.

4. Datasets

In this study the analysis for wind circulation, power spectra of wind components, eddy transport (by heat and momentum flux) and Hadley cell discussed, for this analysis we used daily average data sets from the National Centers for Environmental Prediction/National Centers for Environmental Information **(**NCEP/NCAR) reanalysis (Kalnay & The, 1996). The data sets based on 2.5° x 2.5° with 17 Pressure levels (mb). Wind components (***u, v, w***) and temperature have been used for the period 1950 to 2016 (June, July, August and September (JJAS) and November, December, and January, (NDJ)). High resolution gridded (0.25° x 0.25°) daily rainfall data set from the year 1950-2016 (JJAS) have used (India Meteorological Department (IMD), Pai et al., 2015). Active and Break period composites analysis are done based on techniques discussed in Rajeevan et al., 2010.

5. Methodology & definitions

Standardized indices (NAO, PDO) were obtained from National Centers for Environmental Information and Climate Prediction Center (https://www.ncdc.noaa.gov, (ftp://ftp.cpc.ncep.noaa.gov/wd52dg/data/indices/tele_index.nh.), Nino 3.4 SST from ERSST v4 (https://www.esrl.noaa.gov/psd/data/correlation/nina34.data) for JJAS months from the year 1950-2016. In the following subsection we discuss cospectra analysis which is new method imposed for eddy analysis compare to conventional time-space decomposition methods; additionally, the sources of different indices such as monsoon circulation, ENSO, PDO, and NAO index and their role in ISM will be discussed.

5.1. Cospectra

It is a real part of cross-spectrum analysis; it determines the relationship between two time series as a function of frequency. In given covariance of the two time series, a cospectrum calculates in-phase oscillation in the frequency domain, i.e., it explains the

particular frequency from one-time series is equals in amplitude to other time series at the same frequency. The mathematical expression of cross spectra can be written as:

$$\Gamma_{xy}(f) = \mathcal{F}\{\gamma_{xy}\}(f) = \sum_{\tau=-\infty}^{\infty} \gamma_{xy}(\tau)\, e^{-2\pi i \tau f}$$

$$\Gamma_{xy}(f) = C_{xy}(f) + i\Psi_{xy}(f)$$

Where $\gamma_{xy}(\tau)$ represents Cross Covariance of two time series x and y, $\Gamma_{xy}(f)$ is cross-spectrum, $\mathcal{F}$ represents Fourier transform, $C_{xy}(f)$ is a real part of $\Gamma_{xy}(f)$ and it is known as cospectra and $\Psi_{xy}(f)$ is imaginary part of $\Gamma_{xy}(f)$ and it is known as a quadrature spectrum. Any physical parameter A (in this study u, and T) and meridional wind component v and its positive (negative) cospectra $C_f(A,v)$ gives a measure of the poleward (equatorward) transport of the quantity A due to particular eddy frequency by f (Nitta, 1970). In this study $C_f(u,v)$ and $C_f(T,v)$ cospectra (eddy momentum and heat transport) are discussed. The level-latitudinal distribution of the zonal mean of time-space decomposition of A and B component ($\overline{[A'B']}$ i.e., Transient Eddy) and $C_f(A,v)$ cospectra analysis are shown in **Figure 4** and **Figure 9** respectively, this analysis is discussed in the section 6.3.2.

5.2. Correlation coefficient analysis

The correlation coefficient is a measure of the statistical relationship between two sets of samples. The correlation coefficient values lie between +1 to -1 range, near to +1 and -1 values represents robust agreements and disagreement between two sets of given samples respectively. If the correlation coefficient is near to 0 values, it states that there is no significant relation between given sets of samples. If the sample sets of x and y are distributed from $i = 1$ to n, the Pearson' a correlation coefficient of x and y samples can be written as follows.

$$r = \frac{\sum_{i=1}^{n}(x_i - \bar{x})(y_i - \bar{y})}{\sqrt{\sum_{i=1}^{n}(x_i - \bar{x})^2}\sqrt{\sum_{i=1}^{n}(y_i - \bar{y})^2}}$$

From the above formula, ***r*** represents the Pearson' correlation coefficient. In this analysis the Pearson' a correlation coefficient technique is used to calculate the correlation of $C_f(u,v)$, $C_f(T,v)$ cospectra with ENSO, PDO, NAO, and MH index. These correlation coefficients are shown in **Table** *1* and **Table** *2* respectively.

Monsoon circulation index (Monsoon Hadley index, i.e., MH index, Goswami et al., 1999) defined as meridional wind shear anomalies (850hPa and 200hPa) averaged over extended monsoon rainfall region (70°E-110°E, and 10°N-30°N). This MH index used as to measure anomalous Hadley circulation strength, MH index captures the dominant quasi-biennial variability of ISM. MH index is teleconnected to south equatorial Indian Ocean (EIO). In this study the Cospectra correlation with the MH index is used, this correlation shown in **Table** *1* and **Table** *2* (JJAS, 1950-2016).

5.3. Active and break composite

It is an intraseasonal phenomenon of monsoon season in which series of days are classified with and without rain events. During peak monsoon months, standardized rainfall anomaly of the monsoon core zone, when it exceeds 1.0 (less than −1.0) for more than consecutive three days are classified as Active (Break) day (Rajeevan et al., 2010). The composite patterns of rainfall distribution over the Indian region for active and break spells (1950-2016) shown in **Figure 17**.

5.4. El Niño Southern Oscillation (ENSO) index and monsoon teleconnection

ENSO is the crucial coupled ocean-atmosphere phenomenon over interannual timescales. On the interannual scale, ENSO influences indirectly on ISM. The study is suggesting that epochal behaviors of ISMR are slightly modified by ENSO frequency, such

ENSO frequency is linked with Pacific decadal time-scale variations (Kripalani & Kulkarni, 1997). Warm phases of ENSO shifts Walker cell East of its climatic mean, due to this shift EIO experiences enhancement in convection, that creates anomalous subsidence over Indian landmass through Hadley cell (Goswami, 1998). Interdecadal scale variation of Pacific SST possesses several strong and weak interannual variations of ENSO phases. During warm (cold) Pacific phase, El Niño (La Niña) condition reinforces (weakens) prevailing regional anomalous interdecadal Hadley cell and thus, ISM is more prone to drought (excess rainfall) conditions when El Niño (La Niña) appears during the warm (cold) Pacific phase (Krishnamurthi & Goswami, 2000). The phases of ENSO, i.e., La Niña and El Niño are classified based on SST anomalies averaged over the Nino 3.4 regions (5°N-5°S, 170°W - 120°W). Warmer (cold) phases of SST anomalies above a threshold over Nino 3.4 region is known as El Niño (La Niña).

5.5. Pacific Decadal Oscillation (PDO) index and monsoon teleconnection

PDO (Yuan Zhang et al., 1997) is one of the dominant SST patterns; it extends from mid-latitudes to the tropical region of the Pacific basin. During the positive phase of PDO (+PDO), i.e., warm phase, equatorial eastern Pacific becomes warmer than northwestern Pacific and during the negative phase of PDO (-PDO), i.e., in the cool phase, it gets reversed. Over Indian region, the diagnostic analysis shows the coherent remote influence of PDO on the monsoon; it exhibits strong signal over the tropics and southern Indian ocean on a decadal scale (Krishnan & Sugi, 2003). ISM is more vulnerable to the combined impact of the PDO and ENSO phases. When ENSO and PDO are in (out) phase, it enhances (suppresses) monsoon-ENSO relation (Krishnamurthy & Krishnamurthy, 2017). In this study, the PDO index based on NOAA's (National Oceanic and Atmospheric Administration) extended reconstruction of SST (ERSST Version 4). It is constructed by regressing the ERSST anomalies against the Mantua PDO index for their overlap period, to compute a PDO

regression map for the North Pacific ERSST anomalies. The ERSST anomalies then projected onto the PDO regression map for computing the National Centers for Environmental Information (NCEI) index. The NCEI PDO index closely follows the Mantua PDO index (Mantua et al., 1997).

5.6. North Atlantic Oscillation (NAO) index and monsoon teleconnection

The NAO (Barnston & Livezey, 1987) based on the surface sea-level pressure difference between the subtropical (Azores) high and the subpolar (Iceland) low. The positive phase of the NAO (+NAO) reflects above normal geopotential heights and atmospheric pressure over the central North Atlantic, the eastern United States, and western Europe and below-normal heights and pressure across the high latitudes of the North Atlantic. The negative phase (-NAO) reflects an opposite pattern of height and pressure anomalies over these regions. Over Indian region positive (negative) phase of NAO increases (decreases) meridional tropospheric temperature gradient, it enhances (suppresses) ISM (Goswami et al., 2006). The NAO index is obtained by projecting the NAO loading pattern to the daily anomaly 500mb height field over 0-90°N. The NAO loading pattern has been chosen as the first mode of a Rotated Empirical Orthogonal Function (EOF) analysis using monthly mean 500mb height anomaly data from 1950 to 2000 over 0-90°N latitude.

6. General circulation and eddy transport analysis

6.1. Climatic features of general circulation

The mean meridional circulation over both the hemisphere is essential to balance excess warming over tropics and excess cooling over high latitudes. The zonal mean of the latitudinal distribution of meridional circulation characterized by wind cells; those are Hadley cells, Ferrel Cells, and Polar Cells. These closed circulations get modulated with season change regarding structure as well as the intensification of rising and subsiding motions. **Figure 1** represents a long-term climatic feature (averaged from the year 1950-2016 and

65°E-100°E) of mean meridional circulation. During summer time (JJAS) intense (**Figure 1a**) rising branch of the Hadley cell located over 10°N to 20°N latitude and subsidizing over 15°S to 25°S latitude. Midlatitude westerly jet stream reached to its maximum north position (near 40°N) and its associated isotachs widely separated with weak core, but in winter season (NDJ, **Figure 1b**), Hadley cell gets completely reversed over the same region also intensified jetstream is now at minimum north position (near 30°N), and its associated isotachs firmly separated with strong core. Thus seasonal reversing of the Hadley cell and 10° latitude migration of midlatitude jet stream feature is noticed. The cross-equatorial flow, i.e., low level easterly over 20°S to 5°S and low level westerly (0° to 20°N) is present during the summer season, in winter season this feature is absent. Tropical Easterly Jet (TEJ) is present during the summer season over the mid-troposphere, and it centered over 15°N.

A similar analysis of mean meridional circulation carried out for ENSO, and PDO phases (**Figure *2***). Difference between El Niño & La Niña phase (**Figure *2*c**) shows increase in anomalous subsiding of air mass over 20°S to 35°N latitude (it gets reduced from 5°S to 5°N & 10°N to 20°N) along with anomalous ascending motion over 35°N to 45°N latitude during El Niño phase as compare to La Niña phase. The anomalous easterlies over 40°N suggest a drastic weakening of mid-latitude westerly jet stream during the El Niño phase. Difference +PDO & -PDO (**Figure *2*f**) phase shows anomalous alternative bands of subsiding and rising air mass. Over Indian region, four alternative bands of upward and downward motions we can see clearly. Vicinity of 20°N latitude during -PDO phase is showing relatively strong convection. Above analysis shows La Niña and –PDO favors for enhanced convections during ISM. Mid-latitude jet streams weaken in El Niño (from **Figure *2*a,** and **Figure *2*c**) case as compared to other cases.

Figure *3* represents a similar analysis as compare to above except daily mean climatology removed. In the summer season, the region over 10°N to 20°N experiences

anomalous convection and region over 10°S to 10°N experiences anomalous subsidence of air mass (**Figure *3*a**). Anomalous low-level westerlies and easterlies are present over the region 10°N to 20°N and 15°S to 5°S; this is part of the cross-equatorial flow in JJAS. During summer time subtropical westerly jet stream weakens in the northern hemisphere and it is robust in the southern hemisphere (**Figure *3*d**). In winter season large-scale anomalous subsidence zone present over 15°S to 10°N region, cross-equatorial flow is also absent. The southward shift of north hemispheric subtropical jet stream manifested by anomalous strong westerlies over 20°N to 30°N.

The circulation during El Niño period (**Figure *3*b**) behaves like winter time anomalous circulation, except narrow rising branch of air mas confined between 10°N to 15°N and an extended region of mid to upper tropospheric anomalous westerlies. The circulation during La Niña period (**Figure *3*e**) behaves like mean anomalous summertime circulation, except a broad rising branch of air mass present over the entire Indian landmass. The -PDO (**Figure *3*f**) phase is similar to mean anomalous summertime circulation. During +PDO phase anomalous circulation matches with summertime circulation (**Figure *3*c**), but fascinating feature apart from mean summer season is that strong mid to upper tropospheric westerlies are present as discussed in El Niño period. Tropical easterly jet becomes anomalous westerly in the El Niño and +PDO phase (**Figure *3*b,** and **Figure *3*c**).

ENSO and PDO phases likely to modulate zonal and meridional circulation patterns and affecting ISMR. However, the model analysis suggested that from the total ISMR variability out of 50% is contributed by internal dynamics (Goswami, 1998), and the rest of variability may arise from the teleconnections mediated by the large-scale global oscillating patterns through waves and eddy interactions. In the following section, we will discuss observed features of large-scale eddy mechanism over the globe in the subseasonal scale and its year to year variability. We try to answer the following questions such as; whether this

large-scale eddy transport affects the weather and/or climate of the Indian region by modifying ISM large-scale circulation? If so, what is the role behind large-scale global oscillating patterns (such as ENSO, PDO, and NAO) on eddy generation or modification? Is there any teleconnection present between such patterns and eddy over the Indian region? On what spatial and temporal extent of these teleconnection exists? We have tried to address some fundamental aspects of transient eddy transport and its interaction over broader Indian region.

6.2. Eddy transport analysis by the conventional method

The midlatitude is the source of eddy generation, which drives the indirect general circulation cell, i.e., Ferrell cell embedded with eddy is a carrier of mass and energy for balancing meridional thermal contrast. The flux term $[\overline{A'B'}]$ from space-time decomposition $[\overline{AB}]$ of A and B variables is known as a transient eddy. In this analysis eddy momentum flux (EMF) term i.e. $[\overline{u'v'}]$ (**Figure 4a)** and eddy heat flux (EHF) term i.e. $[\overline{T'v'}]$ are analyzed for level-latitude distribution (**Figure 4b**). EMF and EHF analysis carried out from the year 1950 to 2016 of JJAS season averaged over 65°E to 100°E. These eddy fluxes are dominated in midlatitude; transient eddies are relatively stronger in the southern hemisphere than the northern hemisphere.

Overall interaction among E2T region attracts to the investigation, especially in ISM season. The similar eddy analysis from Oort, Abraham H.Peixóto, 1983 is extended from the year 1950 to 2016, and it resembles the original result (Oort, Abraham H.Peixóto, 1983, Peixto & Oort, 1984). The EHF transport distribution is broader than EMF transport. Poleward EMF transport shows peaks at 250hPa (**Figure 4a**, near 30°S and 50°N) and for equatorward transport it shows peaks at 350hPa (near 65°S and 85°N), but poleward EHF transport shows multiple peaks, one is at 250hPa (**Figure 4b**, near 30°S and 50°N and other is

broader in nature (35°S to 65°S and 65°N to 75°N) present over entire lower troposphere. Over tropical region in the long-term mean picture of meridional eddy transport is not stronger than higher latitude but the presence of such eddy cannot be ruled out.

The small magnitude of EMF and EHF transport (**Figure 5a**, and **Figure 5b** respectively) over the tropical region can be seen clearly. The similar EMF and EHF transport analysis further classified into ENSO and PDO phases (**Figure 6a1-f1** for EMF, and **Figure 6a2-f2** for EHF). During the ENSO phase difference of meridional EMF transport (**Figure 6c1**) shows robust poleward flux transport over midlatitude during El Niño than La Niña phase. Similarly, for the difference between PDO phases (**Figure 6f1**) shows stronger eddy transport in +PDO than –PDO. For EHF transport suggests, El Niño and +PDO phases strengthening the eddy activity than La Niña and –PDO phases (**Figure 6c2,** and **Figure 6f1**). Eddy transport activities during JJAS season during ENSO and PDO phases are partially different.

6.3. Eddy transport analysis by the cospectra method

6.3.1. Eddy periodicity band selection

Before we do eddy analysis with the help of frequency domain analysis, the space-time variability associated with the mid-latitude westerly jet stream is important to study first. Over extratropical region, systematic space-time evolution of wave train anomalies is enabling coupling mechanism over tropics, and it shows quasi-period of 40-50 days (Lau & Phillips, 1986). Over Indian region, with the help of spectral analysis of precipitation datasets shows 40-50 days significant spectral peaks corresponding to MJO and 5-7 day peaks corresponding to monsoon lows are found (Hartmann & Michelsen, 1989). This analysis is suggesting that ISMR variability can fall in subseasonal to seasonal scale. By use of power spectrum analysis of wind components vicinity of jet stream shows two distinct significant

peaks near 60 days and 15 days (**Figure 7a-b**, averaged over 400hPa to 100hPa level, 65°E to 100°E, and 30°N to 50°N). These peaks are showing stronger variance at 200hPa between 35°N to 45°N latitudes (**Figure 7c-d**, averaged over 65°E to 100°E). Thus, mean variability feature associated with midlatitude jet stream over Indian region is present from sub-seasonal to seasonal scale. In the cospectra $C_f(A,v)$ analysis to see such variability, eddy transport by f frequencies has grouped into four bands (5-10 days, 10-20 days, 20-40 days and 40-60 days). In this periodic band, variability associated with jet stream (by 60 and 15 days) is involved.

The seasonal (JJAS) averaged eddies from cospectra analysis shows interannual to interdecadal variability (**Figure** *8*). Here, the interval between two orange lines shows significant PDO signal from monthly (**Figure** *8***a**) and seasonal mean (**Figure** *8***b**) power spectra get captured in $C_f(uv)$ (**Figure** *8***c**) and $C_f(Tv)$ (**Figure** *8***d**) power spectra.

6.3.2. Comparison of eddy analysis method

Figure 4 and **Figure 9** resemble each other; it is a striking feature of eddy analysis by conventional space-time decomposition method and frequency domain analysis. **Figure 4** represents the mean meridional transient eddy transport (averaged over 65°E-100°E, and 1950-2016 year, JJAS months) by EMF $[\overline{u'v'}]$ and EHF $[\overline{T'v'}]$, which are extended result of Oort, Abraham H.Peixóto, 1983, whereas the **Figure 9** represents EMF ($C_f(uv)$) and EHF ($C_f(Tv)$) transport based on mean cospectra analysis (averaged over 2 to 60 day period , 65°E-100°E , and 1950-2016 year for JJAS months). Both the analysis are matching in terms of the direction of eddy transport and magnitude. **Figure 4** analysis is done with help of u, v, and T anomalies of JJAS season, **Figure 9** analysis associated with 2 to 60 day period uv and Tv cospectra, hence slightly higher magnitude present in cospectra analysis, we can conclude that transient eddy response by particular period eddy can be achieved with help of cospectra analysis. Here onward we will call local cellular structure present in zonal mean, meridional

distribution in **Figure 4** and **Figure 9** belonging to particular latitude as a primary cell transport.

6.3.3. Cospectra analysis in subseasonal scale

Over Pacific region, with the help of observed datasets over 13 Pacific stations (April to July 1962) suggests that EMF and EHF eddies with 4 day period over equatorial region, 6 and more than 10 days period over the subtropical region plays a significant role (**Figure 10,** Nitta, 1970**,** 2 to 20 days filtered). Poleward EMF transport $C_f(uv)$ is dominating at 200hPa level over subtropical stations (**Figure 10a**). At equatorial stations (**Figure 10b)** 6 day period disturbance shows equatorward transport of EMF. Analysis of $C_f(Tv)$ cospectra over subtropical stations (**Figure 10c**) shows a strong correlation between ***T*** and ***v*** over lower and upper troposphere with more than 10 days period, a negative correlation centered near 200hPa level for 6 day period eddies (**Figure 10c**). The eddy period less than 10 days are transporting equatorward in the lower troposphere over the equator (**Figure 10d**). Middle troposphere shows strong equatorward transport contributed by eddy period greater than 10 days in the equator region (**Figure 10d**).

Similar analysis over Indian region conducted (April to July 1962, **Figure 11**), we have found some exciting features, over subtropical region (**Figure 11a**) equatorward EMF transport at upper tropospheric level (around 100hPa) associated with greater than 15 day period and another peak of nearly 8 day period (around 200hPa) entering towards tropics. Over equatorial region (**Figure 11b**), entire troposphere witnesses poleward transport by 10 to 15 day period EMF and up to mid-level witnesses poleward transport by 15 to 20 day period. Over the subtropical region (**Figure 11c**) EHF transport by 12 day period is equatorward at 200hPa, while over the equatorial region (**Figure 11d**) shows equatorward transport of EHF, it is peaked around 850hPa and 200hPa by 20 to 8 day period. It confirmed

that EMF and EHF are actively contributing in subseasonal scale over equatorial and subtropical Indian region. Such high-frequency eddies could not be traced in time domain analysis discussed in the conventional method of eddy transport.

6.3.4. Interannual variation of cospectra analysis

In this section interannual variation (From 1950 to 2016) of EMF and EHF transport over Pacific and Indian regions will be discussed (**Figure 12** to **Figure 155**), Over equatorial Pacific stations, the EMF transport (***$C_f(uv)$*, Figure 12a-d**) exhibits alternative directional bands in all the period. Most of the time such a band is confined between 400hPa to 100hPa, and it centered at 200hPa. Smaller magnitude eddy transport present in low level with the smaller periodic band. Over subtropical Pacific stations, the robust EMF transport (**Figure 12e-h**) is poleward contributed by the all period bands in most of the year, maximum peak centered near 200hPa level. Some year notices a decrease in amplitude and very few years showing a reverse in direction, i.e., equatorward EMF transport. Over equatorial region (**Figure 13a-d**); poleward EHF transport by 5-10 day period eddy over upper troposphere. EHF transport (***$C_f(Tv)$***) over equatorial Pacific stations associated with non-uniform level wise distribution, but over subtropical Pacific region (**Figure 13e-h**) it is associated with uniform distribution along discontinuity boundary between 300hPa to 200hPa, such a fascinating feature is present in all the bands. Over Subtropical Pacific region (**Figure 13e-h**) EHF transport above 200hPa level contributes to poleward transport with an interannual change in intensity while below the 300hPa level contributes to equatorward transport with an interannual change in intensity, Baroclinic nature of EHF can be seen. Equatorial and subtropical Pacific stations show interannual variations (direction and magnitude) of EMF and EHF transport (***$C_f(uv)$*** and ***$C_f(Tv)$***) by all the bands.

Over the Indian region, a similar analysis is carried out (averaged over 25°N to 35°N and 65°E to 100°E, **Figure 14**, and **Figure 15**). Most of the year the EMF transported (**Figure 14a-d**) by all the bands is poleward, and it confined to 400hPa to 100hPa level. Few cases (around 7 years) associated with equatorward transport contributed by 20 days and above period bands while most of the cases (around 20 years) upper troposphere (above 200hPa) of this region is transporting equatorward by below 20 day bands. Interannual variability of EHF transport can be seen in all the bands (**Figure 15a-d**). The major feature of eddy transport over upper and middle troposphere shows most of the year equatorward and poleward respectively (except for 5-10 day period band, it gets reversed). As compared to sub-tropical Pacific region the EHF transport is a nonuniform level-latitudinal distribution. In Indian region analysis of both eddy transport activity by all the bands are associated with larger in magnitude as compared to the Pacific region.

6.4. Active and break spells

During dominant mode of intra-seasonal Oscillation, i.e., active and break spells, the latitudinal distribution of (averaged from the year 1950 to 2016) circulation shown in **Figure 16.** During active spell (**Figure 16a**) the strong rising branch of Hadley cell present over 20°N to 30°N and descending branch splits into two, one descends over 35°N to 40°N and other over 7°N to 20°N up to mid-troposphere. Low-level westerly jet confined between the equator to 20°N, and upper level easterly (10°S to 20°N) can be seen in **Figure 16a**. Midlatitude jet stream core gets enhanced and shifts little north. Over the southern hemisphere, another complete weak Hadley cell (35°S to 5°N) can be seen clearly.

During break spell (**Figure 16a**) Hadley cell gets reversed in the northern hemisphere while for southern hemisphere it weakens further, westerly jet stream moves relatively southward in break spells. Spatial rainfall pattern composites during active and break spells

has shown in **Figure 17**. Active spells are excess spells of rainfall (positive rainfall anomalies) over a wide region of India (Western Ghats, Central India) and Break spells with negative anomalies over the same region.

The active and break cycles of ISMR is related to 10-20 days and 30-60 days oscillations. Northward propagating 30-60 days mode originates over Indian ocean and westward propagating 10-20 days mode originates in the Pacific (Kulkarni et al., 2011). The shift in jet core region implies the meridional temperature distribution, and eddies may develop closer to the Indian region due to Rossby wave breaking. Hence the study of this eddy interaction to such a dominate ISMR mode is needed.

7. Eddy transport and teleconnection

7.1. Correlation analysis

In this section, with the help of cospectra analysis, the behavior of eddies during global teleconnection patterns will be discussed. Correlation analysis between cospectra (***$C_f(uv)$*** and ***$C_f(Tv)$***, averaged over 25°N-35°N, 65°E- 100°E, and 1950-2016 year of JJAS) and different indices (PDO, NAO, ENSO, and MH) tabulated in **Table** *1* and **Table** *2*. EMF of 40-60 and 20-40 days period (**Table** *1*, averaged over 300hPa to 150hPa level) shows strong positive correlation with the PDO index, while 20-40 and 10-20 days period shows moderately positive correlation with NAO index. For EHF of 5-10, 10-20, and 20-40 days eddies show moderately positive correlation and 40-60 days shows weak positive correlation with PDO index, while 20-40 days period shows a strong correlation and 40-60 days period shows moderate positive correlation with NAO index. Nino 3.4 index showing poor correlation with all the bands of ***$C_f(uv)$*** and ***$C_f(Tv)$*** except moderate positively correlated with EMF of 40-60 days period. MH index, (Goswami et al., 1999) is moderate negatively correlated with EHF for 20-40 days as well as 40-60 days period.

Table *2* represents similar to the above mention analysis except for level averaged between 850hPa to 400hPa. MH index is moderate positively correlated with EMF of 10-20 and 40-60 days period of eddies and with EHF of 10-20, 20-40 and 40-60 days period eddies. Over the same level, PDO shows a positive correlation with 5-10 days EHF and NAO shows a negative correlation with 10-20 days period EHF. Rest of the cases in **Table** *2* correlation is weak. Over 25°N to 35°N latitude $C_f(uv)$ shows a stronger relationship with PDO then followed by NAO, and $C_f(Tv)$ shows a stronger relationship with NAO then followed by PDO patterns in the vicinity of 200hPa. Correlation analysis manifests that PDO and NAO phases are significantly modulating meridional transient eddy transport near vicinity of the mid-latitude westerly jet than ENSO and MH index.

7.2. A climatic feature of eddies in ENSO phases

In this section, we can see the level-latitudinal distribution of zonally averaged cospectra ($C_f(uv)$, $C_f(Tv)$, i.e., EMF and EHF respectively) for the eddy period from 2 to 60 days during ENSO phases (**Figure 18**). Along with ENSO composite cospectra distribution, the composites of zonal and meridional wind superimposed. The zonal and meridional anomalous wind pattern discussed in **Figure 3**.

A fascinating feature of this analysis is that cospectra analysis contributed by all the period is comparable with **Figure 4** and **Figure 6** of transient eddy analysis. Strong EMF near 50°N (**Figure 18a**) transported towards the pole, it centered near 300hPa in ENSO phase, but such a feature is absent in climatology (**Figure 18f**). Strong EHF near 55°N (**Figure 18d**) is being transported to poleward and centered near 200hPa in ENSO phases. EMF is entering in the equatorial lower tropospheric region from the upper troposphere over 15°N to 30°N latitude (**Figure 18b-c**). In La Niña case, such upper tropospheric intrusion shifted equatorward. Mid-troposphere witnesses poleward EHF transport over 10°N to 20°N (**Figure**

18e-f), This eddy transport is narrower in La Niña than El Niño event, EHF is entering in the equatorial lower tropospheric region from upper troposphere of 30°N to 40°N latitude. During La Niña phase such continuous feature is remarkable than a broken segment in El Niño case.

Horizontal distribution of eddy transport analysis over Indian region is divided into two major group based on averaged level (850hPa to 400hPa, and 300hPa to 150hPa) by all the bands. For level-latitudinal distribution of eddy transport analysis are divided into two major groups of averaged longitudinal regions (65°E to 80°E, and 80°E to 100°E) by all bands. All the analysis EMF and EHF analysis carried out for climatic mean, ENSO, PDO, and NAO phases during the year 1950 to2016. Based on a different combination of averaging regions we have found that above mention level and longitude regions show idiosyncratic eddy bands related to EMF and EHF transport, discussed in details in following subsections.

7.3. EMF transport and ENSO teleconnection

In this section, we can see a spatial (**Figure 19**, averaged over 850-400hPa and 300-150hPa level) and level-latitudinal (**Figure 20**, averaged over the 60°E-80°E and 80°E-100°E) analysis of ***uv*** cospectra by all the periodic bands during ENSO phases.

a) Spatial analysis of EMF transport (avg. 850-400hPa)

i. Climatology (avg. 850-400hPa)

In the climatology plots, the mean of ***uv*** cospectra analysis is shown in **Figure 19a1-d1** by all four bands. It shows equatorward transport of EMF over the Gangetic plain (GP) by 5-10 and 10-20 days band (**Figure 19a1-b**), this EMF equatorward transport gets extended from north-central India and western Bay of Bengal (BoB) in the 20-40 and the 40-60 days bands. Entire Arabian Sea (AS) shows poleward EMF transport by 20-40 and 40-60 days bands (**Figure 19c1-d1**). Poleward EMF transport is restricted up to north-central and central

AS region by 20-40 and 40-60 days eddy bands (**Figure 19a1-b1**). A diagonal strip of poleward EMF transport by 5-10 and 10-20 days band is present over the north-central AS, west-central India up to the west-central BoB. The Tibetan Plateau (TP) region shows poleward transport of EMF by all the bands.

ii. ENSO phases (avg. 850-400hPa)

Composites of El Niño, La Niña phase, and their difference are shown in **Figure 19a2-d2**, **Figure 19a3-d3,** and **Figure 19a4-d4** respectively. By analyzing all the panels, the following distinct features are noted. During La Niña phase cospectra analysis shows robust equatorward transport of EMF over the GP, east coast and up to the western BoB as compare to El Niño phase followed by climatology by 20-40 and 40-60 days band (**Figure 19c-d**).

Similarly over the central AS and northwestern of Indian region (Indus plain) shows strong poleward transport of EMF by 40-60 days period during El Niño phase as compared to climatology followed La Niña phase (**Figure 19d**). Similar transport properties are present during the La Niña phase by 20-40 days band (**Figure 19c3**). Over the Tibetan Plateau, the poleward EMF transport by all the eddy bands is maximum during the La Niña phase followed by El Niño and climatic mean (**Figure 19a3-d3**). During La Niña phase the EMF poleward transport is maximum in the southeastern side of Tibetan Plateau (**Figure 19a3-d3**), during the El Niño phase this region shifts to the northwestern side (**Figure 19a2-d2**).

b) Spatial analysis of EMF transport (avg. 300-150hPa)

i. Climatology (avg. 300-150hPa)

In this level averaged case, the climatological mean of ***uv*** cospectra analysis is shown in **Figure 19e1-h1** by all four bands. Over north-central India and its adjoining region (Indo-Pak-Afghan region, 25°N to 40°N) a strong poleward transport of EMF present in all the eddy bands. Entire AS show moderate and strong positive EMF transport by all the bands. In

the north-eastern side, the negative EMF transport is tilted in the southwest-northeast direction for all the eddy bands (over southern India, entire BoB, Myanmar, and Thailand region). This negative transport is almost zonal in the 5-10 and 10-20 days band extending between the equator to 30°N (**Figure 19e1-f1**).

ii. ENSO phases (avg. 300-150hPa)

For this case, in comparison to climatological mean, the ***uv*** cospectra during El Niño phase show that it is positive and narrower band over North of Indian region in 20-40 and 40-60 days band (**Figure 19g2-h2**). In the south of this band, there is a diagonal strip which shows stronger equatorward transport south of positive EMF region. This transport is larger in magnitude during El Niño followed by climatic mean, and La Niña phase.

c) Vertical structure of EMF transport (avg. 60°E to 80°E)

i. Climatology (avg. 60°E to 80°E)

The vertical distribution of EMF cospectra analysis in the vicinity of the midlatitude jet stream region during the ENSO phases is shown in **Figure 20**. In the climatology mean the EMF transport shows southward extension of the EMF cell (**Figure 20c1-d1**, over 25°N to 40°N, centered over 150hPa, south of jet core). The southward extension is not in the 5-10 and 10-20 days band. There is no significant equatorward transport in any of the cases.

ii. ENSO phases (avg. 60°E to 80°E)

The southward extension of a primary cell is more prominent in the El Niño phase (**Figure 20c2-d2**) than the climatology (**Figure 20c1-d1**) and the La Niña phase (**Figure 20c3-d3**). The jet core region during the La Niña phase (**Figure 20b3-d3**) witnesses robust poleward EMF transport than El Niño phase. It means a significant northward and southward movement of the primary cell during the El Niño phase and La Niña phase respectively.

d) Vertical structure of EMF transport (avg. 80°E to 100°E)

i. Climatology (avg. 80°E to 100°E)

As discussed in the previous section an extension of EMF transport is missing in the 80°E to 100°E zonal averaged analysis (**Figure 20e1-h1**). Positive EMF transport it is confined to the jet region by all the bands. The important feature of this vertical structure is a negative EMF transport present over 20°N to 30°N and centered near 150hPa level.

ii. ENSO phases (avg. 80°E to 100°E)

Vertical profile analysis shows an increase in the EMF transport during El Niño (**Figure 20e2-h2**) as compare to climatological and La Niña (except by 20-40 days band during La Niña). Equatorward EMF transport in the upper troposphere is seen above 20°N up to 35°N latitude by all the bands (**Figure 20**). It is stronger in the El Niño phase followed by the La Niña phase and the climatology.

7.4. EHF transport and ENSO teleconnection

a) Spatial analysis of EHF transport (avg. 850-400hPa)

i. Climatology (avg. 850-400hPa)

In the climatology plots of the EHF transport, the north-east region of TP associated with poleward transport while Pak-Afghan region associated with equatorward transport by all the bands. Northcentral AS also shows equatorward EHF transport by the 20-40 and the 40-60 days bands (**Figure 21c1-d1**). Southcentral AS shows poleward EHF transport by the 20-40 and the 40-60 days bands (**Figure 21c1-d1**). In 5-10 and 10-20 days, bands (**Figure 21a1-b1**) the poleward EHF transport is present over the Indian peninsula and the BoB.

ii. ENSO phases (avg. 850-400hPa)

Horizontal analysis of EHF transports shows an enhancement in the equatorward transport during the El Niño phases over northwestern, western Pak-Afghan region and northeastern AS for all the eddy bands (**Figure 21a2-d2**). During the La Niña 20-40 and 40-

60 days band of the EHF transport shows a poleward transport over the south-central AS (**Figure 21c3-d3**). This feature is absent in the El Niño phase (**Figure 21c2-d2**). Over the northeast region of the TP enhanced EHF transport is present during the La Niña phase contributed by the 20-40 and 10-20 days period eddies (**Figure 21a3-c3**). The enhancement reduced in the climatology (**Figure 21a1-c1**) and the El Niño phase (**Figure 21a2-c2**). However, for the El Niño phase, the poleward EHF transport get stronger in the 40-60 days eddies over this region (**Figure 21d2**).

b) Spatial analysis of EHF transport (avg. 300-150hPa)

i. Climatology (avg. 300-150hPa)

The spatial climatology pattern of the EHF transport is comparable to the pattern for the 850hPa to 400hPa as discussed in the previous section except, over the Pak-Afghan region where it is associated with equatorward transport that is extended northward. In the 40-60 days band over west-central India, AS, and western region of maritime continent shows equatorward EHF transport (**Figure 21h1**).

ii. ENSO phases (avg. 300-150hPa)

During the El Niño phase, the poleward EHF transport gets stronger by 40-60 days period eddies over the northeast region of TP (**Figure 21h2**) whereas it is stronger in La Niña phase by the 10-20 and the 20-40 days band (**Figure 21f3-g3**). In the region over Pak-Afghan, the equatorward transport of the EHF is stronger in the El Niño phase by the 40-60 bands (**Figure 21h2**). The EHF transport becomes stronger during the La Niña phase by the 10-20 and the 20-40 days band (**Figure 21f3-g3**).

c) Vertical structure of EHF transport (avg. 60°E to 80°E)

i. Climatology (avg. 60°E to 80°E)

As compared to the level-latitudinal EMF analysis (section 7.3.c.ii), the southward extension of the primary cells (**Figure 20**) is absent in the case of EHF analysis. A dipole

transport structure of the eddy transport is present (**Figure 22**). In the climatological mean EFH analysis, a northward tilted dipole structure is present. It shows equatorward EHF transport up to middle troposphere (over 30°N to 40°N, and is centered over 300hPa) and a poleward EHF transport over upper troposphere (over 50°N to 60°N, and is centered over 200hPa) (**Figure 22a1-d1**).

ii. ENSO phases (avg. 60°E to 80°E)

The dipole structure is enhanced during the El Niño phase by the 40-60 days band of eddy as compared to the other cases; the middle level shows strong equatorward and the upper troposphere shows strong poleward EHF transport (**Figure 22d2**). However, such transport by the dipole structure gets enhanced during the La Niña phase for the other cospectra eddy bands (**Figure 22a3-d3**).

d) Vertical structure of EHF transport (avg. 80°E to 100°E)

i. Climatology (avg. 80°E to 100°E)

As compared to the previous section, the longitude averaged dipole transport structure of the eddy transport is now reversed and vertically oriented (**Figure 22e-h**). In the climatic mean EFH analysis, equatorward EHF transport up to upper troposphere (over 35°N to 45°N, and is centered over 100hPa) and poleward EHF transport over lower troposphere (over 35°N to 45°N, and is centered over 300hPa) (**Figure 22e1-h1**) except in the 5-10 days band.

ii. ENSO phases (avg. 80°E to 100°E)

The vertically oriented dipole structure of the EHF transport gets enhanced in the El Niño phase (**Figure 22f2-h2**) which is reduced in the La Niña phase (**Figure 22f3-h3**) and the climatological mean (**Figure 22f1-h1**) except in the 5-10 days band.

7.5. A climatic feature of eddies in PDO and NAO phases

In this section, we will discuss the latitudinal distribution of zonally averaged cospectra for the eddy band 2-60 days during the PDO and the NAO phases (**Figure *23***, and

Figure *24*). The composites of the zonal and the meridional winds are the superimposed over cospectra. The zonal and meridional anomalous wind patterns discussed in **Figure 3**. Low-level cross-equatorial flow gets reversed in the +PDO phase than –PDO and NAO phases. Tropical easterly jet becomes anomalous westerly in the +PDO phase, and it is easterly in other cases (**Figure *23*3b-e**). Subtropical westerly jet becomes anomalous easterly in +PDO and –NAO phase. During –PDO and +NAO phase the analysis shows strong anomalous convection over the 5°N to 15°N and anomalous strong subsidence present vicinity of 30°S as compared to the +PDO and the –NAO phase.

A fascinating feature of this analysis is that cospectra analysis contributed by all the period is comparable with **Figure 4** and **Figure 6** of transient eddy analysis. Strong EMF (**Figure *23*a**, near 50°N) transported towards the pole, and it is centered near 300hPa in the PDO and the NAO phases than the climatic mean. Composites of EMF (**Figure *23***) and EHF (**Figure *24***) transport are similar in all the PDO and NAO phases. The poleward EMF transport centered over the midlatitude region, and the poleward EHF transport centered near the subpolar region in both the hemispheres. As discussed in **Figure 18** tropical flux activity by the EMF and the EHF during the ENSO phase, a similar transport is present during the PDO and NAO phases.

7.6. EMF transport and PDO teleconnection

In this section, the spatial (**Figure *25***, averaged over 850-400hPa and 300-150hPa level) and level-latitudinal (**Figure 26**, averaged over the 60°E-80°E and 80°E-100°E) analysis of EMF transport by all the periodic bands during PDO phases will be discussed.

a) Spatial analysis of EMF transport (avg. 850-400hPa)

i. Climatology (avg. 850-400hPa)

We have already discussed climatological mean ***uv*** cospectra in **Figure 19a1-d1** this is repeated in **Figure *25*a1-d1** for the sake of comparison. For discussion please refer the section 7.3.a.i.

ii. PDO phases (avg. 850-400hPa)

Northwest-southeast tilted band of EMF transport by 5-10 days is present over Indian region in +PDO phase (**Figure 25a2**). Over the central AS, Gujarat and Rajasthan region EMF transport shows strong poleward flux in the 20-40 days band in the –PDO phase than climatological and +PDO phase (**Figure 25c3**). Such transport by the 20-40 days period present in La Niña phase also (refer **Figure *19*c3**). There is no significant difference in EMF transport over the TP during the +PDO and –PDO phases in all the bands. Over Odisha to west-central BoB stronger EMF transport during +PDO is seen except for the 5-10 days band (**Figure 25b2-d2**).

b) Spatial analysis of EMF transport (avg. 300-150hPa)

i. Climatology (avg. 300-150hPa)

We have already discussed climatological EMF transport in **Figure 19e1-f1** and repeated in **Figure *25*e1-h1** for sake of comparison, please refer the section 7.3.b.i.

ii. PDO phases (avg. 300-150hPa)

Figure 25e-h represents EMF transport averaged over 300hPa to 150hPa level. It is seen that over the north of Indian region (Pak-Afghan and north-western Indian region) there is a strong poleward transport of EMF by the 40-60 days period during the +PDO phase as compared to the -PDO phase (**Figure 25h1-h4**). The EMF transport by the 10-20 days period is equatorward over the central and over eastern India during the +PDO phase (**Figure 25f2**). The transport is not strong in another band over this region as evident in difference plot.

c) Vertical structure of EMF transport (avg. 60°E to 80°E)

i. Climatology (avg. 60°E to 80°E)

We have already discussed climatological mean ***uv*** cospectra in **Figure 20a1-d1** this is repeated in **Figure 26a1-d1** for the sake of comparison, please refer the **section 7.3.c.i**.

ii. PDO phases (avg. 60°E to 80°E)

Figure *26* shows the vertical distribution of EMF cospectra during PDO phases. The extension of the poleward EMF transport (25°N to 40°N, south of jet core) is seen in the 20-40 and 40-60 days band (**Figure *26*c-d**). It is centered near the 200hPa level and is stronger in the +PDO phase for the 40-60 days band. Climatological jet core region shows stronger poleward EMF transport during the +PDO phase by the 40-60 days band (**Figure *26*d2**) and during the –PDO phase it is by the 20-40 days band (**Figure *26*c3**).

d) Vertical structure of EMF transport (avg. 80°E to 100°E)

i. Climatology (avg. 80°E to 100°E)

We have already discussed climatological mean ***uv*** cospectra in **Figure 20e1-h1** this is repeated in **Figure 26e1-h1** for the sake of comparison, please refer the **section 7.3.d.i**.

ii. PDO phases (avg. 80°E to 100°E)

The extension transport of EMF is missing in the plot. In **Figure *26*e-h** (80°E to 100°E zonal averaged) the EMF transport is confined to the jet region. It is stronger in the magnitude during the +PDO phase as compared to the climatology and the -PDO phase for all the band. The Equatorward EMF transport over upper the troposphere above 20°N to 35°N latitude (**Figure *26***), it is stronger in the +PDO phase for all the bands than other cases (i.e., in the -PDO and the climatology).

7.7. EMF transport and NAO teleconnection

a) Spatial analysis of EMF transport (avg. 850-400hPa)

i. Climatology (avg. 850-400hPa)

We have already discussed climatological mean ***uv*** cospectra in **Figure 19a1-d1** this is repeated in **Figure 27a1-d1** for the sake of comparison. For discussion please refer the section 7.3.a.i.

ii. NAO phases (avg. 850-400hPa)

The plot shows similarity in the characteristics with the features as discussed in **Figure 19** and **Figure *25***. Southcentral AS during the +NAO phase shows strong poleward EMF transport than the –NAO and the climatic mean for the 40-60 days eddy (**Figure 27d**).

b) Spatial analysis of EMF transport (avg. 300-150hPa)

i. Climatology (avg. 300-150hPa)

We have already discussed climatological mean ***uv*** cospectra in **Figure 19e1-h1** this is repeated in **Figure 27e1-h1** for sake of comparison. For discussion please refer the section 7.3.b.i.

ii. NAO phases (avg. 300-150hPa)

There is no significant change in poleward EMF transport over the TP during the NAO phases. Westward shift of EMF core region over north of Indian region is present during the –NAO phase (**Figure *27*e3-h3**) as compared to the +NAO phase (**Figure *27*e2-h2**).

c) Vertical analysis of EMF transport (avg. 60°E to 80°E)

i. Climatology (avg. 60°E to 80°E)

We have already discussed climatological mean ***uv*** cospectra in **Figure 20a1-d1** this is repeated in **Figure 288a1-d1** for the sake of comparison. For discussion please refer the section 7.3.c.i.

ii. NAO phases (avg. 60°E to 80°E)

In the –NAO phase all the eddy bands are (**Figure 28a3-d3**) associated with stronger poleward EMF transport followed by the climatological transport (**Figure 28a1-d1**) and the

+NAO phase (**Figure 28a2-d2**) respectively. There is a strong poleward transport is seen in the 60°E to 80°E region (**Figure 28a-d**, over 25°N to 40°N, south of jet core) during the NAO phase in the 40-60 days band.

d) Vertical analysis of EMF transport (avg. 80°E to 100°E)

i. Climatology (avg. 80°E to 100°E)

We have already discussed climatological mean ***uv*** cospectra in **Figure 20e1-h1** this is repeated in **Figure 28e1-h1**for sake of comparison. For discussion please refer the **section 7.3.d.i**.

ii. **NAO phases (avg. 80°E to 100°E)**

The climatological jet core region during -NAO phase (**Figure *28*a-d**) and +NAO phase (**Figure *28*e-h**) witnesses strong poleward EMF transport. Equatorward EMF transport over upper troposphere is present in the 20°N-35°N latitude for the all the bands (**Figure *28*h**). The transport is stronger in the –NAO phase followed by the +NAO phase and the climatology.

7.8. EHF transport and PDO teleconnection

a) Spatial analysis of EHF transport (avg. 850-400hPa)

i. Climatology (avg. 850-400hPa)

We have already discussed climatological mean ***Tv*** cospectra in **Figure 21a1-d1** this is repeated in **Figure 29a1-d1** for the sake of comparison. For discussion please refer the **section 7.4.a.i**.

ii. PDO phases (avg. 850-400hPa)

Equatorward strong EHF transport by the all period bands is present over the North AS during the +PDO phase (**Figure 29a2-d2**) as compared to the other cases. Over central India, the EHF transport is equatorward in the 40-60 band during the +PDO phase and such a

transport absent in all the other cases (**Figure 29d2)**. The fascinating feature of the cospectra analysis averaged over the 850-400hPa level is that TP shows strong poleward EHF transport in the +PDO phase (**Figure 29a2-d2**) as compared to the climatology (**Figure 29a1-d1**) and the –PDO phase (**Figure 29a3-d3**). This is similar during the La Niña phase (**Figure 21d3-c3**) for the 20-40 and 10-20 days band.

b) Spatial analysis of EHF transport (avg. 300-150hPa)

i. Climatology (avg. 300-150hPa)

We have already discussed climatological mean ***Tv*** cospectra in **Figure 21e1-h1** this is repeated in **Figure 29e1-h1** for sake of comparison. For discussion please refer the **section 7.4.b.i**.

ii. PDO phases (avg. 300-150hPa)

The Equatorward EHF transport is extended from the east-central AS to west-central India. It is stronger in the –PDO phase (**Figure 29h3**) than the +PDO phase (**Figure 29h2**) in the 40-60 days period eddy. There is strong poleward EHF transport present over a north-western region of the TP during the +PDO phase in all the bands (**Figure 29e2-h2**), and it gets reduced in the climatic mean (**Figure 29e1-h1**) followed by the –PDO phase (**Figure 29e3-h3**).

c) Vertical analysis of EHF transport (avg. 60°E to 80°E)

i. Climatology (avg. 60°E to 80°E)

We have already discussed climatological mean ***Tv*** cospectra in **Figure 22a1-d1**this is repeated in **Figure 30a1-d1** for the sake of comparison. For discussion please refer the **section 7.4.c.i.**

ii. PDO phases (avg. 60°E to 80°E)

The level-latitudinal analysis of the EHF transport during the PDO phases is shown in **Figure 30**. In the longitude averaged region from 60°E to 80°E, a northward tilted dipole structure is present. It shows equatorward EHF transport up to the middle troposphere (centered over 40°N) and poleward EHF transport over the upper troposphere (centered over 55°N). EHF transport by the 40-60 days period during the +PDO phase (**Figure 30d2**) shows equatorward transport over the 35°N to 45°N and up to 200hPa. This is stronger as compared to the other case. In the 20-40 day band strong transport is centered over the 55°N is associated with the poleward EHF transport and it is stronger in the –PDO (**Figure 30c3**) as compare to the climatology mean (**Figure 30c1**) and the +PDO phase (**Figure 30c3**).

d) Vertical analysis of EHF transport (avg. 80°E to 100°E)

i. Climatology (avg. 80°E to 100°E)

We have already discussed climatological mean ***Tv*** cospectra in **Figure 22e1-h1**this is repeated in **Figure 30e1-h1** for the sake of comparison. For discussion, please refer the **section 7.4.d.i.**

ii. PDO phases (avg. 80°E to 100°E)

A vertically oriented dipole structure (middle troposphere associated positive transport and upper troposphere associated negative transport) is present between 30°N to 50°N (**Figure 30f-h**). The middle tropospheric positive band of the EHF is centered over 300hPa. The transport is stronger in +PDO (**Figure 30e2-h2**) year followed by climatology (**Figure 30e1-h1**) and the –PDO year (**Figure 30e3-h3**) respectively. Another poleward EHF transport we can see from 50°N up to 60°N over upper troposphere (centered near 100hPa). It is stronger in the 40-60 day band for the +PDO (**Figure 30h2**). For the rest of the bands, the transport is stronger in the –PDO phase (**Figure 30e3-g3**). This dipole structure is much weaker in the high-frequency eddy bands.

7.9. EHF transport and NAO teleconnection

a) Spatial analysis of EHF transport (avg. 850-400hPa)

i. Climatology (avg. 850-400hPa)

We have already discussed climatological mean ***Tv*** cospectra in **Figure 21a1-d1** this is repeated in **Figure 31a1-d1** for the sake of comparison. For discussion, please refer the section 7.4.a.i.

ii. NAO phases (avg. 850-400hPa)

The entire EHF bands show strong equatorward transport over the north of Pak-Afghan region and Indus plain region during the +NAO phase (**Figure 31a2-d2**), This transport is weaker in the climatological mean (**Figure 31a1-d1**), and it is further weakened in the –NAO phase (**Figure 31a3-d3**). TP region shows enhanced poleward EHF transport in the +NAO by the 20-40 and 40-60 days bands (**Figure 31c2-d2**). South of Iran, Pakistan, and North AS region associated with the equatorward EHF transport except for the 5-10 period bands. This equatorward EHF transport is stronger during the –NAO phase (**Figure 31b3-d3**) than other cases. In the 40-60 and 20-40 days band, the poleward EFH transport vicinity of the north of BoB region during the –NAO phase (**Figure 31c3-d3**) is stronger than the +NAO phase (**Figure 31c3-d3**).

b) Spatial analysis of EHF transport (avg. 300-150hPa)

i. Climatology (avg. 300-150hPa)

We have already discussed climatological mean ***Tv*** cospectra in **Figure 21e1-h1** this is repeated in **Figure 31e1-h1** for the sake of comparison. For discussion, please refer the section 7.4.b.i.

ii. NAO phases (avg. 300-150hPa)

Over the upper troposphere, the north of the Indian region shows strong poleward EHF transport during –NAO phase (**Figure 31h2**) by 40-60 day eddy while such transport is seen during the +NAO phase in the 20-40 (**Figure 31g3**) day band.

c) Vertical analysis of EHF transport (avg. 60°E to 80°E)

i. Climatology (avg. 60°E to 80°E)

We have already discussed climatological mean ***Tv*** cospectra in **Figure 22a1-d1** this is repeated in **Figure 32a1-d1** for the sake of comparison. For discussion, please refer the section 7.4.c.i.

ii. NAO phases (avg. 60°E to 80°E)

Vertical distribution of EHF cospectra analysis in the vicinity of the midlatitude jet stream region during the NAO phases is shown in **Figure 32**. In the longitude averaged region from 60°E to 80°E case, the northward tilted dipole structure is present, similarly as discussed in the ENSO and the PDO phases. The equatorward EHF transport gets weaker in all the bands of the –NAO phase (**Figure 32a3-d3**) as compared to the +NAO phase.

d) Vertical analysis of EHF transport (avg. 80°E to 100°E)

i. Climatology (avg. 80°E to 100°E)

We have already discussed climatological mean ***Tv*** cospectra in **Figure 22e1-h1** this is repeated in **Figure 32e1-h1** for the sake of comparison. For discussion, please refer the section 7.4.d.i.

ii. NAO phase (avg. 80°E to 100°E)

A vertically oriented the dipole structure is present similar to the ENSO and the PDO phases. However, the exciting feature is that middle tropospheric EHF poleward transport is stronger in –NAO phase followed by the climatological transport and the +NAO phase, it is

visible in the 20-40 and the 40-60 days band. This dipole EHF transport is more prominent in the –NAO (**Figure 32f3-h3**) phase as compared to the +NAO phase.

The EMF and the EHF transport (averaged over 300-150hPa) over the Indian region during the ENSO, the PDO, and the NAO phases are summaries in **Table** *3* and **Table** *4* respectively. In these tables, we have partially distinguished the Indian subcontinent region into 7 sectors. Symbolized representation of respective eddy transport for 5-10, 10-20, 20-40, and 40-60 bands can be seen clearly. The EMF and EHF transport are dominated during all the ENSO, PDO, and NAO phases in the all the bands over the Afghan-Pak, Northern of Indian region, and Tibetan Plateau. Most of the cases the EMF transport is poleward over the Afghan-Pak, Northern of Indian region, whereas it is equatorward over the Tibetan Plateau. In contrast, most of the cases the EHF transport is poleward over the Tibetan Plateau, whereas it is equatorward over the Afghan-Pak except Northern of Indian region exhibits transition zone between poleward (west of it) and equatorward (east of it) EMF transport.

The poleward EMF transport in the all the bands is stronger over the Afghan-Pak during the La Niña and -NAO phases. It is stronger over Northern of the Indian region during the El Niño, +PDO, -NAO phases. The equatorward EMF transport in the all the band is weaker over TP during +PDO, and +NAO phases. In the stronger. An interesting feature is that over central India relatively weak poleward EMF is present in the all the bands during NAO phases. The over the Afghan-Pak region equatorward EHF transport is relatively weaker during the El Niño, -PDO, -NAO phases, the transition zone (i.e., dipole structure) is the dominant feature present over the north of Indian region is weaker during ENSO phases. The poleward EHF transport over the TP is relatively stronger during the +PDO phase.

8. Conclusion

Eddy forcing in the form of momentum flux and heat flux can lead to significant variation in regional weather and climate and is documented by several studies. Over Indian region, the role of eddy flux is also documented in the intraseasonal scale. However, a comprehensive study depicting the spatial structure of eddy momentum and heat flux is not available for the monsoon period. The current study aims to document the spatiotemporal structure of eddy based on the co-spectra analysis. Also, the seasonality and interannual variability of the eddy fields are also discussed in detail. Based on the observed analysis, several important perspectives on the role of eddies emerge over the Indian region. The following important points are highlighted:

- Mean meridional and zonal circulation get modified during different phases of ENSO, PDO, and NAO.
- During El Niño year there is a decrease in the strength of mid-latitude westerly jet.
- A significant variation is noticed in northward or southward flux transport during different phases of ENSO, PDO, and NAO.
- Spectral analysis jet core vicinity suggested a significant variability in the 15-60 days range is present.
- Over subseasonal scale, bidirectional (northward and southward) transport of eddies is present in the subtropical and equatorial region of the Indian region.

To summarise all this aspect, a representative schematic is shown in **Figure 33**. The black double arrow connectors symbolize the presence of air-sea interaction underneath large-scale global patterns (such as ENSO, PDO, and NAO). The semi-transparent bluish wave-like structure is representing Hadley and Walker cell. The curved black arrow at the surface manifests the mean ISM flow. The east-west oriented gray line along with pinkish

arrow represents subtropical westerly jet. The different size and shape of eddy are represented by red (for poleward transport) and blue (for equatorward transport) circle with dash lines on it. The extratropical baroclinic atmosphere is a significant source of eddy production. The variation of magnitude and direction of eddies is occurred during seasonal change as well as in the presence of large-scale global patterns. Eddies are interacting over Indian region through modification of mean summertime monsoonal flow.

Acknowledgment

Indian Institute of Tropical Meteorology (IITM, Pune) is an autonomous institute under the Ministry of Earth Sciences, Government of India; and is fully supported by Government of India. We are thankful to Prof. Ravi Shankar Nanjundiah, Director, IITM for the support. We are also thankful to IMD and NCEP/NCAR for providing required daily gridded data sets.

9. List of abbreviations

AGCM	: -	Atmospheric General Circulation model
AS	: -	Arabian Sea
BoB	: -	Bay of Bengal
E2T	: -	Extratropical to Tropical
EHF	: -	Eddy Heat Transport
EIO	: -	Equatorial Indian Ocean
EMT	: -	Eddy Momentum Transport
ENSO	: -	El Niño Southern Oscillation
EOF	: -	Empirical Orthogonal Function
ERSST V4	:-	Extended Reconstructed Sea Surface Temperature Version 4
GFDL	: -	Geophysical Fluid Dynamics Laboratory
GP	: -	Gangetic plain
IMD	: -	India Meteorological Department
ITCZ	: -	Intertropical Convergence Zone
JJAS	: -	June, July, August and September
MH	: -	Monsoon Hadley
MJO	: -	Madden Julian Oscillation
NAO	: -	North Atlantic Oscillation
NCAR	: -	National Center for Atmospheric Research
NCEI	: -	National Centers for Environmental Information
NCEP	: -	National Centers for Environmental Prediction
NDJ	: -	November, December and January
NOAA	: -	National Oceanic and Atmospheric Administration
PDO	: -	Pacific Decadal Oscillation
SST	: -	Sea Surface Temperature
TP	: -	Tibetan plateau

10. List of figures

Figure 1: Mean (65°E-100°E, 1950-2016 year) meridional circulation (green arrow), zonal mean wind (line contour, continuous lines (westerlies), and dotted lines (easterlies)) and vertical mean wind component (shaded contour, red (upward), blue (downward), scaled by 100) during a) summer season (JJAS) and b) winter season (NDJ). 53

Figure 2: Mean (65°E-100°E, 1950-2016 year, JJAS months) meridional circulation (green arrow), zonal mean wind (line contour, continuous lines (westerlies), and dotted lines (easterlies) and mean vertical wind component (shaded contour, red (upward), blue (downward), scaled by 100) during a) El Niño, b) La Niña, c) difference between El Niño & La Niña year, d) +PDO, e) -PDO and f) difference between +PDO & -PDO year. 53

Figure 3: Anomalous mean (65°E-100°E, 1950-2016 year, JJAS months) meridional circulation (green vector), mean zonal wind (line contour, continuous lines (westerlies), and dotted lines (easterlies) and mean vertical wind component (shaded contour, red (upward), blue (downward), scaled by 100) during a) Summer (JJAS), b) El Niño, c) +PDO, d) Winter (NDJ), e) La Niña, and f)– PDO year. 54

Figure 4: Mean (65°E-100°E, 1950-2016 year, JJAS months) meridional transient eddy transport (shaded contour, red (northward), blue (southward)) for a) EMF, and b) EHF (the extended result of Oort, Abraham H.Peixóto, 1983). 55

Figure 5: Mean (65°E-100°E, 1950-2016 year, JJAS months) meridional transient eddy transport (shaded contour, red (northward), blue (southward)) zoomed region for a) EMF, and b) EHF (the extended result of Oort, Abraham H.Peixóto, 1983). 55

Figure 6: Mean (65°E-100°E, 1950-2016 year, JJAS months) meridional transient eddy transport (shaded contour, red (northward), blue (southward)) during ENSO and PDO phases (a1 to f1 represents EMF transport, and a2 to f2 represents for EHF transport). 56

Figure 7: Mean (65°E-100°E, 2000-2016 year, JJAS months) power spectra of **u** and **v** wind component, a) **u** wind, and b) **v** wind (averaged over 400hPa-100hPa and 30°N-50°N). c) **u** wind, and d) **v** wind (averaged over 200hPa and 35°N-45°N). 56

Figure 8 : Power spectra of PDO index (a. all months, b. JJAS months), uv cospectra (C_f(uv), c. JJAS months), and Tv cospectra (C_f(uv), d. JJAS months) from the year 1950 to 2016 (60°E-100°E, 25°N-60°N, and 300hPa-150hPa level).The area between two orange lines represents the PDO signal in all figures. 57

Figure 9: Mean cospectra analysis (2 to 60 day period, 65°E-100°E, 1950-2016 year, JJAS months, **uv** cospectra (**C_f(uv)**) and b is **Tv** cospectra (**C_f(Tv)**), Both figures show zonal mean of meridional distribution of respective cospectra (shaded contour, red (positive) northward, blue (negative) equatorward transport), This analysis resembles **Figure 4,** i.e., Mean meridional transient

eddy transport for momentum and heat (65°E-100°E / 1950-2016 year / JJAS), Oort, Abraham H.Peixóto, 1983. 57

Figure 10: Cospectra of 2-20 days (continuous line represents positive cospectra and northward transport, dashed line represents negative cospectra and equatorward transport) periodicity over the Pacific region from April to July 1962. Classified as a) **uv** cospectra ($\mathbf{C_f(uv)}$) subtropical region, b) **uv** cospectra equatorial region, c) **Tv** cospectra ($\mathbf{C_f(Tv)}$) subtropical region, and d) **Tv** cospectra equatorial region reproduced from Nitta, 1970. 58

Figure 11: Cospectra of 2-20 days (continuous line represents positive cospectra and northward transport, dashed line represents negative cospectra and equatorward transport) periodicity over Indian region from April to July 1962. Classified as a) **uv** cospectra ($\mathbf{C_f(uv)}$) subtropical region, b) **uv** cospectra equatorial region, c) **Tv** cospectra ($\mathbf{C_f(Tv)}$) subtropical region, and d) **Tv** cospectra equatorial region reproduced from Nitta, 1970. 58

Figure 12: Seasonal-mean (Pacific region, 1950-2016 year, JJAS months) interannual **uv** cospectra ($\mathbf{C_f(uv)}$, shaded contour, red (positive) northward, blue (negative) equatorward), Over equatorial Pacific from (a) to (b) and over subtropical Pacific from (e) to (h) represents eddy bands of 5-10 days, 10-20 days, 20-40 days and 40-60 days respectively. (For station details Nitta, 1970). 59

Figure 13: Seasonal-mean (Pacific region, 1950-2016 year, JJAS months) interannual **Tv** cospectra ($\mathbf{C_f(Tv)}$, shaded contour, red(positive) northward, blue(negative) equatorward),Over equatorial Pacific from (a) to (b) and over subtropical Pacific from (e) to (h) represents eddy bands of 5-10 days, 10-20 days, 20-40 days and 40-60 days respectively. (For station details Nitta, 1970). 60

Figure 14: Seasonal-mean (25°N-35°N, 65°E-100°E, 1950-2016 year, JJAS months) interannual **uv** cospectra ($\mathbf{C_f(uv)}$, shaded contour, red(positive) northward, blue(negative) equatorward),eddy bands from a) 5-10 days, b) 10-20 days, c) 20-40 days and d) 40-60 days respectively. 61

Figure 15: Seasonal-mean (25°N-35°N, 65°E-100°E, 1950-2016 year, JJAS months) interannual **Tv** cospectra ($\mathbf{C_f(Tv)}$, shaded contour, red(positive) northward, blue(negative) equatorward), eddy bands from a)5-10 days, b)10-20 days, c)20-40 days and d)40-60 days respectively. 61

Figure 16: Mean (65°E-100°E, 1950-2016 year, JJAS months) monsoonal Hadley cell during the dominant mode of intraseasonal oscillation (ISO), i.e., a) Active and b) Break spells, Days are classified according to Rajeevan et al., 2010. Zonal mean wind (line contour, continuous lines (westerlies), and dotted lines (easterlies)), mean meridional circulation (green arrow), and vertical mean wind component (shaded contour, red (upward), blue (downward), scaled by 100). 62

Figure 17: Mean (1950-2016 year / JJAS months) spatial pattern of rainfall anomalies (mm/day) during dominant mode intraseasonal oscillation (ISO), i.e., a) Active and b) Break spells, Days are classified according to Rajeevan et al., 2010. 62

Figure 18: Seasonal-mean(65°E-95°E, 1950-2016 year, JJAS months) meridional distribution of cospectra (shaded contour, red(positive) northward, blue(negative) equatorward) by averaged 2 to 60 days period with zonal mean wind anomalies (black line) and meridional wind vector (green arrow) for **C_f(uv)** during a) El Niño, b) La Niña and c) mean (1950 to 2016). For **C_f(Tv)** during d) El Niño, e) La Niña and f) mean (1950 to 2016) cases. 63

Figure 19: Spatial distribution of **uv** cospectra (**C_f(uv**), red(+ve) and blue(-ve) shading) with zonal wind (green line) over Indian region (5°S-40°N/60°E-100°E / JJAS) during ENSO cases. The columnar plot is 1.Climatology, 2.El Niño,3. La Niña, and 4.Difference between El Niño & La Niña. Averaged over 850hPa to 400hPa level for (a) 5-10 days, (b) 10-20 days, (c) 20-40 days and (d) 40-60 days bands. Averaged over 300hPa to 150hPa level for (e) 5-10 days, (f) 10-20 days, (g) 20-40 days and (h) 40-60 days bands. Green solid (dash) line represents positive (negative) **u** wind component (m/s, -50 to 50 by 5)..... 64

Figure 20: Vertical distribution of **uv** cospectra (**C_f(uv**), red(+ve) and blue(-ve) shading) with the zonal mean wind (black line) over 20°N -60°N and 500hPa-70hPa during ENSO cases. The columnar plot is 1.Climatology, 2.El Niño, 3.La Niña, and 4.Difference between El Niño & La Niña. Averaged over 60°E to 80°E longitude for (a) 5-10 days, (b) 10-20 days, (c) 20-40 days and (d) 40-60 days bands and averaged over 80°E to 100°E longitude for (e) 5-10 days, (f) 10-20 days, (g) 20-40 days and (h) 40-60 days bands. Black solid (dash) line represents positive (negative) **u** wind component (m/s, -50 to 50 by 5). 65

Figure 21: Spatial distribution of **Tv** cospectra (**C_f(Tv)**, red(+ve) and blue(-ve) shading) with zonal wind (green line) over Indian region (5°S-40°N/60°E-100°E) during ENSO cases. The columnar plot is 1.Climatology, 2.El Niño, 3.La Niña, and 4.Difference between El Niño & La Niña. Averaged over 850hPa to 400hPa level for (a)5-10 days, (b)10-20 days, (c)20-40 days and (d)40-60 days bands and averaged over 300hPa to 150hPa level for(e)5-10 days, (f)10-20 days, (g)20-40 days and (h)40-60 days bands. Green solid (dash) line represents positive (negative) **u** wind component (m/s, -50 to 50 by 5)..... 66

Figure 22: Vertical distribution of **Tv** cospectra (**C_f(Tv**), red (+ve) and blue (-ve) shading) with the zonal mean wind (black line) over 20°N -60°N and 500hPa-70hPa during ENSO cases. The columnar plot is 1.Climatology, 2.El Niño, 3.La Niña, and 4.Difference between El Niño & La Niña. Averaged over 60°E to 80°E longitude for (a) 5-10 days, (b) 10-20 days, (c) 20-40 days and (d) 40-60 days bands and averaged over 80°E to 100°E longitude for (e) 5-10 days, (f) 10-20 days, (g) 20-40 days and (h) 40-60 days bands. Black solid (dash) line represents positive (negative) **u** wind component (m/s, -50 to 50 by 5). 67

Figure 23: Seasonal-mean (65°E-95°E / 1950-2016 year / JJAS months) meridional distribution of **uv** cospectra (**C_f(uv),** shaded contour, red(positive) northward, blue(negative) equatorward) by averaged 2 to 60 days period with zonal mean wind anomalies (black line) and meridional wind vector (green arrow) during a)+PDO, b)-PDO, c)+NAO, d)-NAO and c) mean (1950 to 2016) Cases..... 68

Figure 24: Seasonal-mean (65°E-95°E / 1950-2016 year / JJAS months) meridional distribution of **Tv** cospectra (**C_f(Tv)**, shaded contour, red(positive) northward, blue(negative)

equatorward) by averaged 2 to 60 days period with zonal mean wind anomalies (black line) and meridional wind vector (green arrow) during a)+PDO, b)-PDO, c)+NAO, d)-NAO and c) mean (1950 to 2016) Cases. 69

Figure 25: Spatial distribution of **uv** cospectra (**C_f(uv)**, red(+ve) and blue(-ve) shading) with zonal wind (green line) over Indian region (5°S-40°N/60°E-100°E) during PDO cases. Columnar plot are 1.Climatology, 2. +PDO, 3.-PDO and 4.Difference between +PDO & -PDO. Averaged over 850hPa to 400hPa level by (a)5-10 days, (b)10-20 days, (c)20-40 days and (d)40-60 days bands and averaged over 300hPa to 150hPa level for (e)5-10 days, (f)10-20 days, (g)20-40 days and (h)40-60 days bands. Green solid (dash) line represents positive (negative) **u** wind component (m/s, -50 to 50 by 5). 70

Figure 26: Vertical distribution of **uv** cospectra (**C_f(uv)**, red (+ve) and blue (-ve) shading) with the zonal mean wind (black line) over 20°N -60°N and 500hPa-70hPa during PDO cases. Columnar plot are 1.Climatology, 2. +PDO 3.-PDO and 4.Difference between +PDO & -PDO. Averaged over 60°E to 80°E longitude for (a) 5-10 days, (b) 10-20 days, (c) 20-40 days and (d) 40-60 days bands and averaged over 80°E to 100°E longitude for (e) 5-10 days, (f) 10-20 days, (g) 20-40 days and (h) 40-60 days bands. Black solid (dash) line represents positive (negative) **u** wind component (m/s, -50 to 50 by 5). 71

Figure 27: Spatial distribution of **uv** cospectra (**C_f(uv)**, red(+ve) and blue(-ve) shading) with zonal wind (green line) over Indian region (5°S-40°N/60°E-100°E) during NAO cases. The columnar plot is 1.Climatology, 2. +NAO, 3.-NAO and 4.Difference between +NAO&-NAO. Averaged over 850hPa to 400hPa level for (a)5-10 days, (b)10-20 days, (c)20-40 days and (d)40-60 days bands and over 300hPa to 150hPa level for (e)5-10 days, (f)10-20 days, (g)20-40 days and (h)40-60 days bands. Green solid (dash) line represents positive (negative) **u** wind component (m/s, -50 to 50 by 5). 72

Figure 28: Vertical distribution of **uv** cospectra (**C_f(uv)**, red (+ve) and blue (-ve) shading) with the zonal mean wind (black line) over 20°N -60°N and 500hPa-70hPa during NAO cases. The columnar plot is 1.Climatology, 2. +NAO 3.-NAO and 4.Difference between +NAO & -NAO. Averaged over 60°E to 80°E longitude for (a) 5-10 days, (b) 10-20 days, (c) 20-40 days and (d) 40-60 days bands and averaged over 80°E to 100°E longitude for (e) 5-10 days, (f) 10-20 days, (g) 20-40 days and (h) 40-60 days bands. Black solid (dash) line represents positive (negative) **u** wind component (m/s, -50 to 50 by 5). 73

Figure 29: Spatial distribution of **Tv** cospectra (**C_f(Tv)**, red(+ve) and blue(-ve) shading) with zonal wind (green line) over Indian region (5°S-40°N/60°E-100°E) during PDO cases. Columnar plot are 1.Climatology, 2. +PDO, 3.-PDO and 4.Difference between +PDO & -PDO. Averaged over 850hPa to 400hPa level for (a)5-10 days, (b)10-20 days, (c)20-40 days and (d)40-60 days bands and averaged over 300hPa to 150hPa level for (e)5-10 days, (f)10-20 days, (g)20-40 days and (h)40-60 days bands. Green solid (dash) line represents positive (negative) **u** wind component (m/s, -50 to 50 by 5). 74

Figure 30: Vertical distribution of **Tv** cospectra (**C_f(Tv)**, red (+ve) and blue (-ve) shading) with the zonal mean wind (black line) over 20°N -60°N and 500hPa-70hPa during PDO cases. Columnar plot are 1.Climatology, 2. +PDO 3.-PDO and 4.Difference between +PDO & -PDO.

Averaged over 60°E to 80°E longitude for (a) 5-10 days, (b) 10-20 days, (c) 20-40 days and (d) 40-60 days bands and averaged over 80°E to 100°E longitude for (e) 5-10 days, (f) 10-20 days, (g) 20-40 days and (h 40-60 days bands. Black solid (dash) line represents positive (negative) **u** wind component (m/s, -50 to 50 by 5). 75

Figure 31: Spatial distribution of **Tv** cospectra ($\mathbf{C_f(Tv)}$, red(+ve) and blue(-ve) shading) with zonal wind (green line) over Indian region (5°S-40°N/60°E-100°E) during NAO cases. The columnar plot is 1.Climatology, 2. +NAO, 3.-NAO and 4.Difference between +NAO&-NAO. Averaged over 850hPa to 400hPa level for (a)5-10 days, (b)10-20 days, (c)20-40 days and (d)40-60 days bands and averaged over 300hPa to 150hPa level for (e)5-10 days, (f)10-20 days, (g)20-40 days and (h)40-60 days bands. Green solid (dash) line represents positive (negative) **u** wind component (m/s, -50 to 50 by 5). 76

Figure 32: Vertical distribution of **Tv** cospectra ($\mathbf{C_f(Tv)}$, red (+ve) and blue (-ve) shading) with the zonal mean wind (black line) over 20°N -60°N and 500hPa-70hPa during NAO cases. The columnar plot is 1.Climatology, 2. +NAO 3. -NAO and 4.Difference between +NAO & -NAO. Averaged over 60°E to 80°E longitude for (a) 5-10 days, (b) 10-20 days, (c) 20-40 days and (d) 40-60 days bands and averaged over 80°E to 100°E longitude for (e) 5-10 days, (f) 10-20 days, (g) 20-40 days and (h) 40-60 days bands. Black solid (dash) line represents positive (negative) **u** wind component (m/s, -50 to 50 by 5). 77

Figure 33: Schematic representation of air-sea interaction and teleconnection which may indirectly modulate Indian summer monsoon through eddy transport. On a different scale, such eddy fluctuation may associate with known global patterns such as ENSO, PDO, and NAO. 78

11. List of Tables

Table 1: *Correlation between the JJAS averaged co-spectra ($C_f(uv)$ and $C_f(Tv)$) and the large scale indices (PDO, NAO, Nino 3.4 index (SSTA) and MH index (Goswami et al., 1999), (300-150hPa)) for the years 1950-2016 (67 years). Green background color represents statistical significant at 5%, level and the orange background color represents statistical significant at 10% level.* 50

Table 2*: Same as Table-1 but co-spectral values calculated for the vertical level averaged between 850-400hPa.* 50

Table 3*: EMF transport averaged over 300-150 hPa for composites of ENSO, PDO, and NAO phases in all the bands.* 51

Table 4*: EHF transport averaged over 300-150 hPa for composites of ENSO, PDO, and NAO phases in all the bands.* 52

12. References

Barnston, A. G., & Livezey, R. E. (1987). Classification, Seasonality and Persistence of Low-Frequency Atmospheric Circulation Patterns. *Monthly Weather Review*. https://doi.org/10.1175/1520-0493(1987)115<1083:CSAPOL>2.0.CO;2

Chattopadhyay, R., Phani, R., Sabeerali, C. T., Dhakate, A. R., Salunke, K. D., Mahapatra, S., et al. (2015). Influence of extratropical sea-surface temperature on the Indian summer monsoon: An unexplored source of seasonal predictability. *Quarterly Journal of the Royal Meteorological Society*, *141*(692), 2760–2775. https://doi.org/10.1002/qj.2562

Fadnavis, S., & Chattopadhyay, R. (2017). Linkages of subtropical stratospheric intraseasonal intrusions with Indian summer monsoon deficit rainfall. *Journal of Climate*, *30*(13), 5083–5095. https://doi.org/10.1175/JCLI-D-16-0463.1

Goswami, B. N. (1998). Interannual variations of Indian summer monsoon in a GCM: external conditions versus internal feedbacks. *Journal of Climate*, *11*(4), 501–522. https://doi.org/10.1175/1520-0442(1998)011<0501:IVOISM>2.0.CO;2

Goswami, B. N., Krishnamurthy, V., & Annmalai, H. (1999). A broad-scale circulation index for the interannual variability of the Indian summer monsoon. *Quarterly Journal of the Royal Meteorological Society*, *125*(554), 611–633. https://doi.org/10.1002/qj.49712555412

Goswami, B. N., Madhusoodanan, M. S., Neema, C. P., & Sengupta, D. (2006). A physical mechanism for North Atlantic SST influence on the Indian summer monsoon. *Geophysical Research Letters*, *33*(2), 1–4. https://doi.org/10.1029/2005GL024803

Hartmann, D. L., & Michelsen, M. L. (1989). Haartmann and Michelin.pdf. *Journal of Atmospheric Sciences*. https://doi.org/10.1175/1520-0469(1989)046<2838:IPIIR>2.0.CO;2

Joseph, S., Sahai, A. K., Sharmila, S., Abhilash, S., Borah, N., Chattopadhyay, R., et al. (2015). North Indian heavy rainfall event during June 2013: diagnostics and extended range prediction. *Climate Dynamics*, *44*(7–8), 2049–2065. https://doi.org/10.1007/s00382-014-2291-5

Joseph, S., Sahai, A. K., Chattopadhyay, R., Sharmila, S., Abhilash, S., Rajeevan, M., et al. (2016). Extremes in June rainfall during the Indian summer monsoons of 2013 and 2014: Observational analysis and extended-range prediction. *Quarterly Journal of the Royal Meteorological Society*, *142*(696), 1276–1289. https://doi.org/10.1002/qj.2730

Kalnay, E., & The, N. (1996). NCAR 40-year reanalysis project. *Bull Amer Meteor Soc*, *77 SRC*-, 437–470.

Kripalani, R. H., & Kulkarni, A. (1997). Climatic impact of El Niño/La Niña on the Indian monsoon: A new perspective. *Weather*, *52*(2), 39–46. https://doi.org/10.1002/j.1477-8696.1997.tb06267.x

Krishnamurthi, V., & Goswami, B. N. (2000). Indian Monsoon ENSO relationship on interdecadal timescale. *American Meteorological Society*, *13*, 579–595. https://doi.org/10.1175/1520-0442(2000)013<0579:IMEROI>2.0.CO;2

Krishnamurthy, L., & Krishnamurthy, V. (2017). Indian monsoon's relation with the decadal part of PDO in observations and NCAR CCSM4. *International Journal of Climatology*, *37*(4), 1824–1833. https://doi.org/10.1002/joc.4815

Krishnan, R., & Sugi, M. (2003). Pacific decadal oscillation and variability of the Indian summer monsoon rainfall. *Climate Dynamics*, *21*(3–4), 233–242. https://doi.org/10.1007/s00382-003-0330-8

Krishnan, R., Kumar, V., Sugi, M., & Yoshimura, J. (2009). Internal Feedbacks from Monsoon–Midlatitude Interactions during Droughts in the Indian Summer Monsoon. *Journal of the Atmospheric Sciences*, *66*(3), 553–578. https://doi.org/10.1175/2008JAS2723.1

Kulkarni, A., Kripalani, R., Sabade, S., & Rajeevan, M. (2011). Role of intra-seasonal oscillations in modulating Indian summer monsoon rainfall. *Climate Dynamics*, *36*(5–6), 1005–1021. https://doi.org/10.1007/s00382-010-0973-1

Lau, K.-M., & Phillips, T. J. (1986). Coherent Fluctuations of Fxtratropical Geopotential Height and Tropical Convection in Intraseasonal Time Scales. *Journal of the Atmospheric Sciences*. https://doi.org/10.1175/1520-0469(1986)043<1164:CFOFGH>2.0.CO;2

Leung, M. Y. T., & Zhou, W. (2018). Circumglobal teleconnection and eddy control of variation in summer precipitation over Northwest China. *Climate Dynamics*, *51*(4), 1351–1362. https://doi.org/10.1007/s00382-017-3958-5

Liebmann, B., & Hartmann, D. L. (1984). An Observational Study of Tropical–Midlatitude Interaction on Intraseasonal Time Scales during Winter. *Journal of the Atmospheric Sciences*. https://doi.org/10.1175/1520-0469(1984)041<3333:AOSOTI>2.0.CO;2

Lin, H. (2009). Global Extratropical Response to Diabatic Heating Variability of the Asian Summer Monsoon. *Journal of the Atmospheric Sciences*, *66*(9), 2697–2713. https://doi.org/10.1175/2009JAS3008.1

Liu, Z., & Alexander, M. (2007). ATMOSPHERIC BRIDGE , OCEANIC TUNNEL , AND GLOBAL CLIMATIC TELECONNECTIONS, (2005), 1–34. https://doi.org/10.1029/2005RG000172.1.INTRODUCTION

Lorenz, E. N. (1969). The nature of the global circulation of the atmosphere: a present view. *The Global Circulation of the Atmosphere*.

Mantua, N. J., Hare, S. R., Zhang, Y., Wallace, J. M., & Francis, R. C. (1997). Pacific interdecadal climate oscillation with impacts on salmon production. *Am. Meteorol. Soc*, *78*(6), 1069–1079. https://doi.org/10.1175/1520-0477(1997)078<1069:apicow>2.0.co;2

Namias, J. (1950). the Index Cycle and Its Role in the General Circulation. *Journal of Meteorology*. https://doi.org/10.1175/1520-0469(1950)007<0130:TICAIR>2.0.CO;2

Nitta, T. (1970). On the Role of Transient Eddies in the Tropical Troposphere. *Journal of the Meteorological Society of Japan*, *48*(4), 348–359.

Oort, Abraham H.Peixóto, J. P. (1983). Global Angular Momentum and Energy Balance Requirements from Observations. *Advances in Geophysics*, *25*, 355. https://doi.org/10.1016/S0065-2687(08)60177-6

Pai, D. S., Sridhar, L., Badwaik, M. R., & Rajeevan, M. (2015). Analysis of the daily rainfall events over India using a new long period (1901–2010) high resolution (0.25° × 0.25°) gridded rainfall data set. *Climate Dynamics*, *45*(3–4), 755–776. https://doi.org/10.1007/s00382-014-2307-1

Peixto, J. P., & Oort, A. H. (1984). Physics of climate. *Reviews of Modern Physics*. https://doi.org/10.1103/RevModPhys.56.365

Rajeevan, M., Gadgil, S., & Bhate, J. (2010). Active and break spells of the indian summer monsoon. *Journal of Earth System Science*, *119*(3), 229–247. https://doi.org/10.1007/s12040-010-0019-4

RAMASWAMY, C. (1962). Breaks in the Indian summer monsoon as a phenomenon of interaction between the easterly and the sub-tropical westerly jet streams. *Tellus*, *14*(3), 337–349. https://doi.org/10.1111/j.2153-3490.1962.tb01346.x

Saltzman, B., & Tang, C.-M. (1975). Formation of meanders, fronts, and cutoff thermal pools in a baroclinic ocean current. *Journal of Physical Oceanography*. https://doi.org/10.1175/1520-0485(1975)005<0086:FOMFAC>2.0.CO;2

Vellore, R. K., Kaplan, M. L., Krishnan, R., Lewis, J. M., Sabade, S., Deshpande, N., et al. (2016). Monsoon-extratropical circulation interactions in Himalayan extreme rainfall. *Climate Dynamics*, *46*(11–12), 3517–3546. https://doi.org/10.1007/s00382-015-2784-x

Walker, G. T., & Bliss, E. W. (1932). World Weather V - NAO. *Memoirs of the Royal Meteorological Society*. https://doi.org/10.1002/qj.49705422601

Wallace, J. M., & Gutzler, D. S. (1981). Teleconnections in the Geopotential Height Field during the Northern Hemisphere Winter. *Monthly Weather Review*. https://doi.org/10.1175/1520-0493(1981)109<0784:TITGHF>2.0.CO;2

Willett, H. C. (1948). Patterns of world weather changes. *Eos, Transactions American Geophysical Union*, *29*(6), 803–809. https://doi.org/10.1029/TR029i006p00803

Yuan Zhang, Wallace, J. M., & Battisti, D. S. (1997). ENSO-like interdecadal variability: 1900-93. *Journal of Climate*, *10*(5), 1004–1020. https://doi.org/10.1175/1520-0442(1997)010<1004:ELIV>2.0.CO;2

13. Tables

Table 1: *Correlation between the JJAS averaged co-spectra (**C_f(uv)** and **C_f(Tv))** and the large scale indices (PDO, NAO, Nino 3.4 index (SSTA) and MH index (Goswami et al., 1999), (300-150hPa)) for the years 1950-2016 (67 years). Green background color represents statistical significant at 5%, level and the orange background color represents statistical significant at 10% level.*

Avg. over 300-150hPa, 25°-35°N, 65°-100°E, and running 3 years								
Period (1/f)	Cf(uv)				Cf(Tv)			
	PDO	NAO	SSTA	MH	PDO	NAO	SSTA	MH
5-10	0.1	0.12	0.09	-0.14	0.27	0.05	-0.06	-0.09
10-20	0.06	0.18	0.03	-0.15	0.23	0.11	-0.08	-0.02
20-40	0.42	0.24	0.06	0.05	0.27	0.4	-0.09	-0.27
40-60	0.55	0.05	0.18	0.12	0.11	0.21	0	-0.25

Table 2: *Same as Table-1 but co-spectral values calculated for the vertical level averaged between 850-400hPa.*

Avg. over 850-400hPa, 25°-35°N, 65°-100°E, and running 3 years								
Period (1/f)	Cf(uv)				Cf(Tv)			
	PDO	NAO	SSTA	MH	PDO	NAO	SSTA	MH
5-10	0.04	-0.03	0.02	-0.1	0.32	0.09	0.1	-0.2
10-20	0	0.19	0.07	0.26	0.03	-0.26	0.14	0.11
20-40	0.07	0.12	0.08	0.09	-0.15	-0.02	-0.2	0.17
40-60	0.07	-0.1	-0.06	0.27	-0.05	-0.02	-0.25	0.22

Table 3: *EMF transport averaged over 300-150 hPa for composites of ENSO, PDO, and NAO phases in all the bands.*

Eddy Transport		
Northward		Equatorward
	Weaker	
	Moderate	
	Stronger	
NS = Not Significant		
	= Dipole	

$C_f(uv)$, averaged over 300-150hPa, and from the year 1950 to 2016																		
Pattern	**ENSO**						**PDO**						**NAO**					
Period (1/*f*)	*El Niño*	*La Niña*	*El Niño*	*La Niña*	*El Niño*	*La Niña*	*+PDO*	*-PDO*	*+PDO*	*-PDO*	*+PDO*	*-PDO*	*+NAO*	*-NAO*	*+NAO*	*-NAO*	*+NAO*	*-NAO*
	Afghan-Pak		**Northern India**		**Tibetan Plateau**		**Afghan-Pak**		**Northern India**		**Tibetan Plateau**		**Afghan-Pak**		**Northern India**		**Tibetan Plateau**	
5-10					NS	NS					NS	NS					NS	NS
10-20																	NS	
20-40																		
40-60																		
	Arabian Sea		**Central India**		**Bay of Bengal**		**Arabian Sea**		**Central India**		**Bay of Bengal**		**Arabian Sea**		**Central India**		**Bay of Bengal**	
5-10	NS	NS	NS	NS	NS	NS	NS	NS	NS	NS	NS	NS	NS	NS			NS	NS
10-20	NS	NS	NS	NS	NS	NS	NS	NS		NS	NS	NS	NS	NS			NS	NS
20-40	NS	NS			NS	NS	NS	NS	NS	NS	NS	NS	NS	NS			NS	NS
40-60	NS	NS	NS	NS	NS	NS	NS	NS		NS	NS	NS	NS	NS			NS	NS
			Peninsular						**Peninsular**						**Peninsular**			
5-10			NS	NS					NS	NS					NS	NS		
10-20			NS	NS					NS	NS					NS	NS		
20-40			NS						NS	NS					NS	NS		
40-60			NS	NS					NS	NS					NS	NS		

Table 4: *EHF transport averaged over 300-150 hPa for composites of ENSO, PDO, and NAO phases in all the bands.*

Eddy Transport		
Northward		Equatorward
	Weaker	
	Moderate	
	Stronger	
NS = Not Significant		
= Dipole		

$C_f(Tv)$, averaged over 300-150hPa, and from the year 1950 to 2016																		
Pattern	**ENSO**						**PDO**						**NAO**					
Period (1/*f*)	*El Niño*	*La Niña*	*El Niño*	*La Niña*	*El Niño*	*La Niña*	*+PDO*	*-PDO*	*+PDO*	*-PDO*	*+PDO*	*-PDO*	*+NAO*	*-NAO*	*+NAO*	*-NAO*	*+NAO*	*-NAO*
	Afghan-Pak		Northern India		Tibetan Plateau		Afghan-Pak		Northern India		Tibetan Plateau		Afghan-Pak		Northern India		Tibetan Plateau	
5-10		NS	NS	NS	NS	NS	NS	NS	NS	NS		NS	NS	NS	NS	NS	NS	NS
10-20	NS		NS	NS														
20-40	NS							NS						NS				
40-60														NS				
	Arabian Sea		Central India		Bay of Bengal		Arabian Sea		Central India		Bay of Bengal		Arabian Sea		Central India		Bay of Bengal	
5-10	NS	NS	NS	NS	NS	NS	NS	NS	NS	NS	NS	NS	NS	NS	NS	NS	NS	NS
10-20	NS	NS	NS	NS	NS	NS	NS	NS	NS	NS	NS	NS	NS	NS	NS	NS	NS	NS
20-40	NS	NS	NS	NS	NS	NS	NS	NS	NS	NS	NS	NS	NS	NS	NS	NS	NS	NS
40-60		NS	NS	NS	NS	NS	NS	NS	NS	NS	NS	NS	NS	NS	NS	NS	NS	NS
			Peninsular						Peninsular						Peninsular			
5-10			NS	NS					NS	NS					NS	NS		
10-20			NS	NS					NS	NS					NS	NS		
20-40			NS	NS					NS	NS					NS	NS		
40-60			NS	NS					NS	NS					NS	NS		

14. Figures

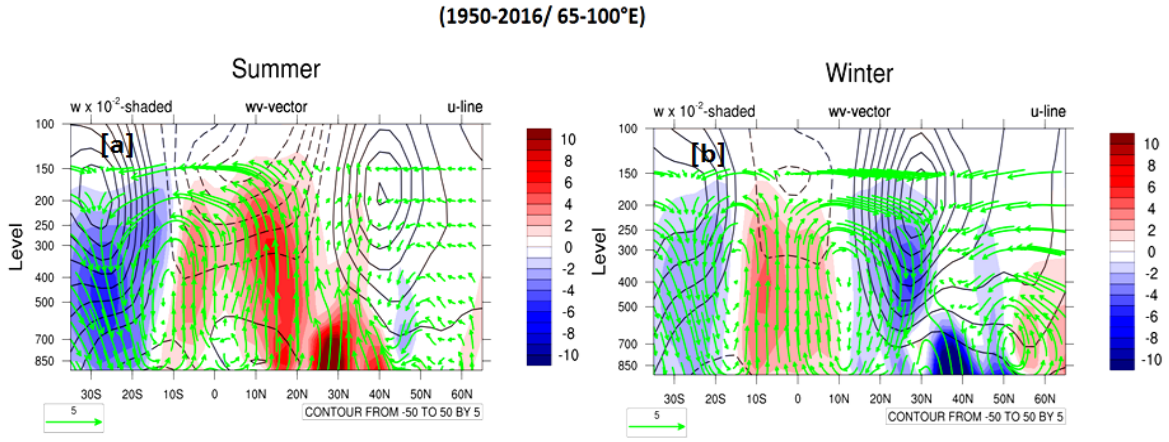

Figure 1: *Mean (65°E-100°E, 1950-2016 year) meridional circulation (green arrow), zonal mean wind (line contour, continuous lines (westerlies), and dotted lines (easterlies)) and vertical mean wind component (shaded contour, red (upward), blue (downward), scaled by 100) during a) summer season (JJAS) and b) winter season (NDJ).*

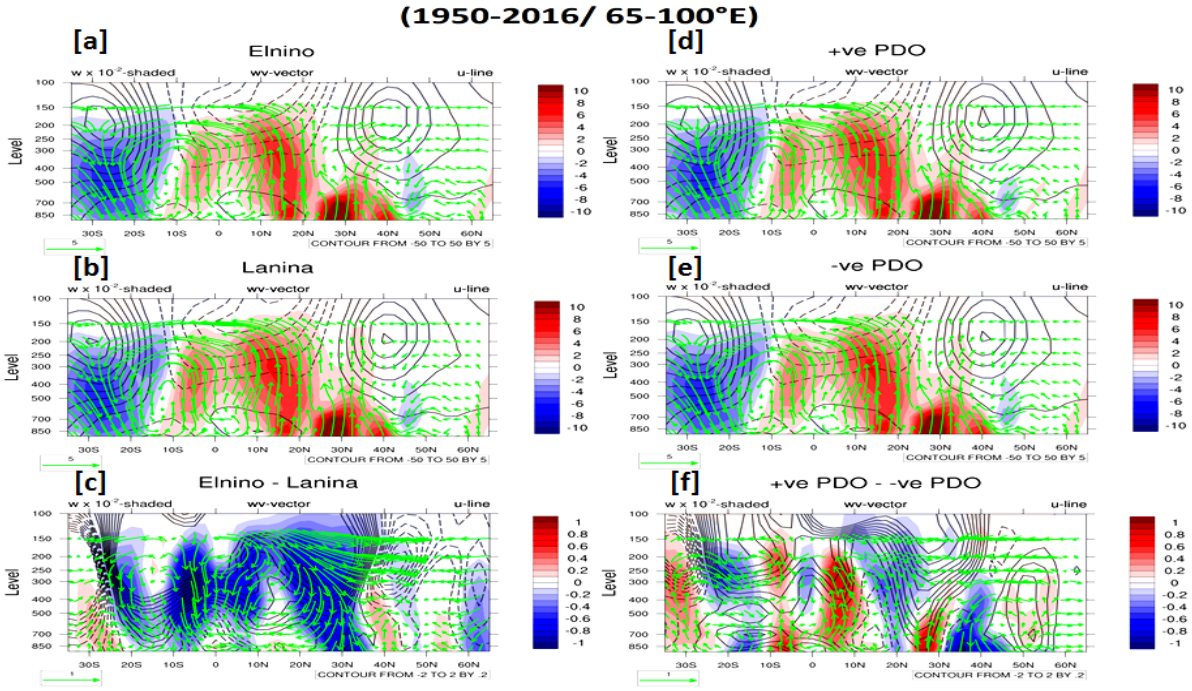

Figure 2: *Mean (65°E-100°E, 1950-2016 year, JJAS months) meridional circulation (green arrow), zonal mean wind (line contour, continuous lines (westerlies), and dotted lines (easterlies) and mean vertical wind component (shaded contour, red (upward), blue (downward), scaled by 100) during a) El Niño, b) La Niña, c) difference between El Niño & La Niña year, d) +PDO, e) -PDO and f) difference between +PDO & -PDO year.*

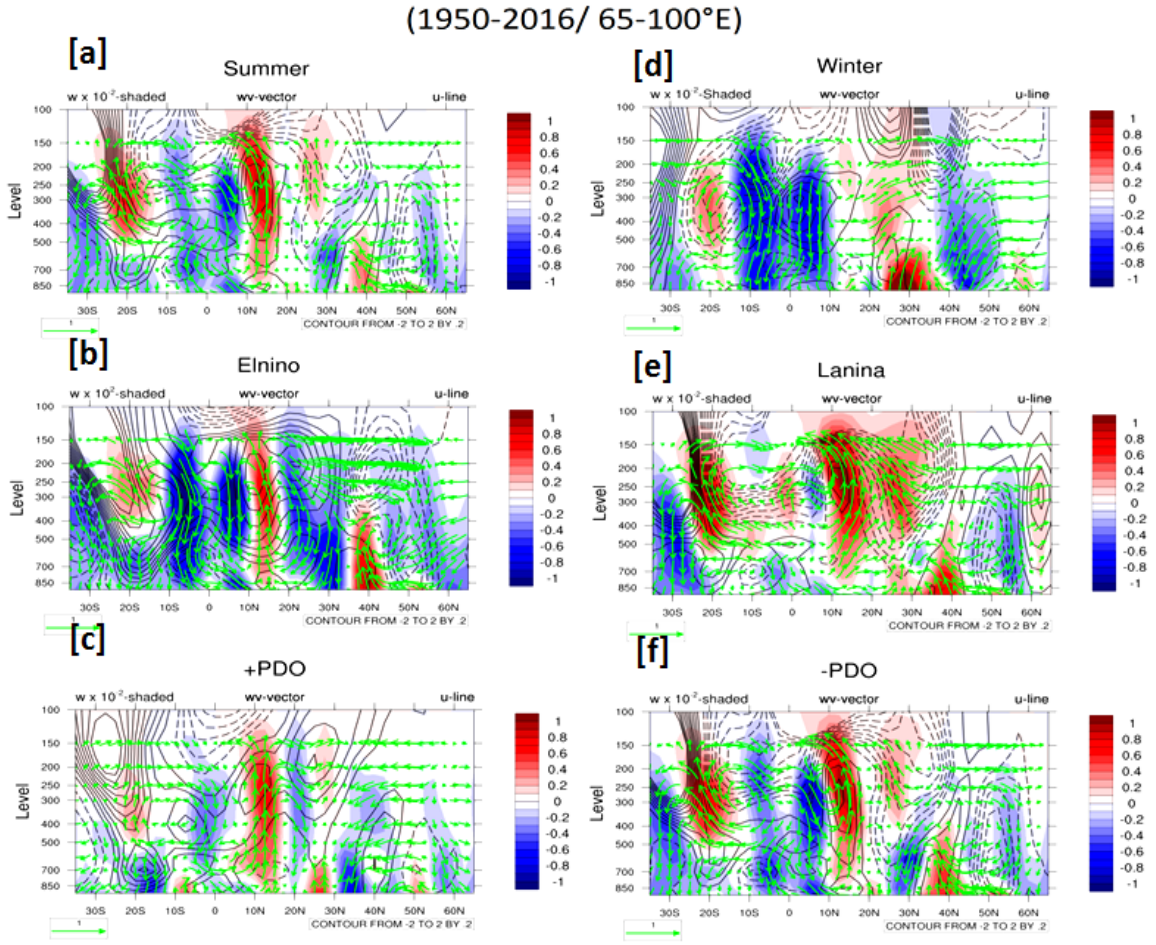

Figure 3: *Anomalous mean (65°E-100°E, 1950-2016 year, JJAS months) meridional circulation (green vector), mean zonal wind (line contour, continuous lines (westerlies), and dotted lines (easterlies) and mean vertical wind component (shaded contour, red (upward), blue (downward), scaled by 100) during a) Summer (JJAS), b) El Niño, c) +PDO, d) Winter (NDJ), e) La Niña, and f)–PDO year.*

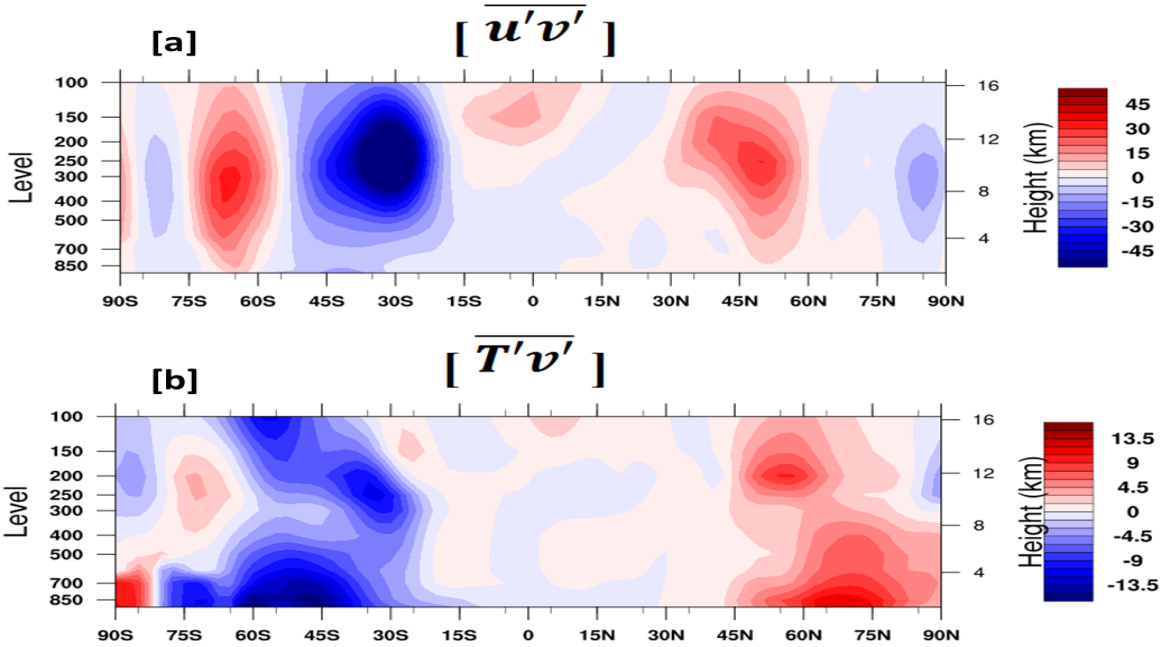

Figure 4: *Mean (65°E-100°E, 1950-2016 year, JJAS months) meridional transient eddy transport (shaded contour, red (northward), blue (southward)) for a) EMF, and b) EHF (the extended result of Oort, Abraham H.Peixóto, 1983).*

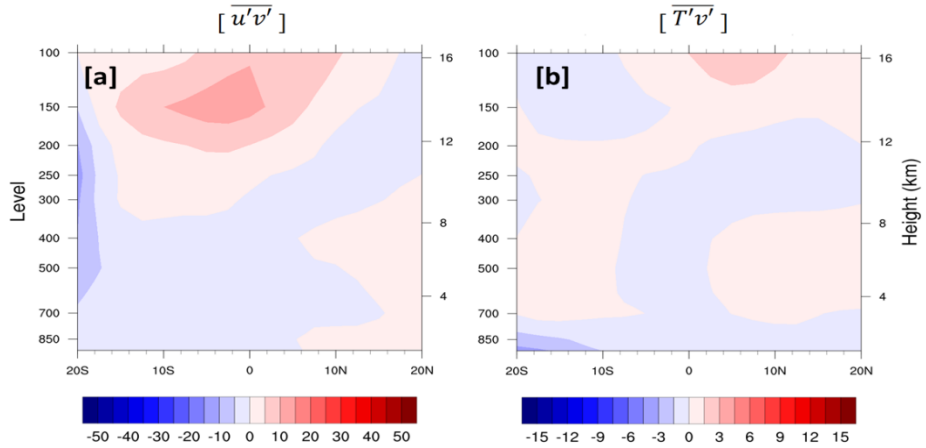

Figure 5: *Mean (65°E-100°E, 1950-2016 year, JJAS months) meridional transient eddy transport (shaded contour, red (northward), blue (southward)) zoomed region for a) EMF, and b) EHF (the extended result of Oort, Abraham H.Peixóto, 1983).*

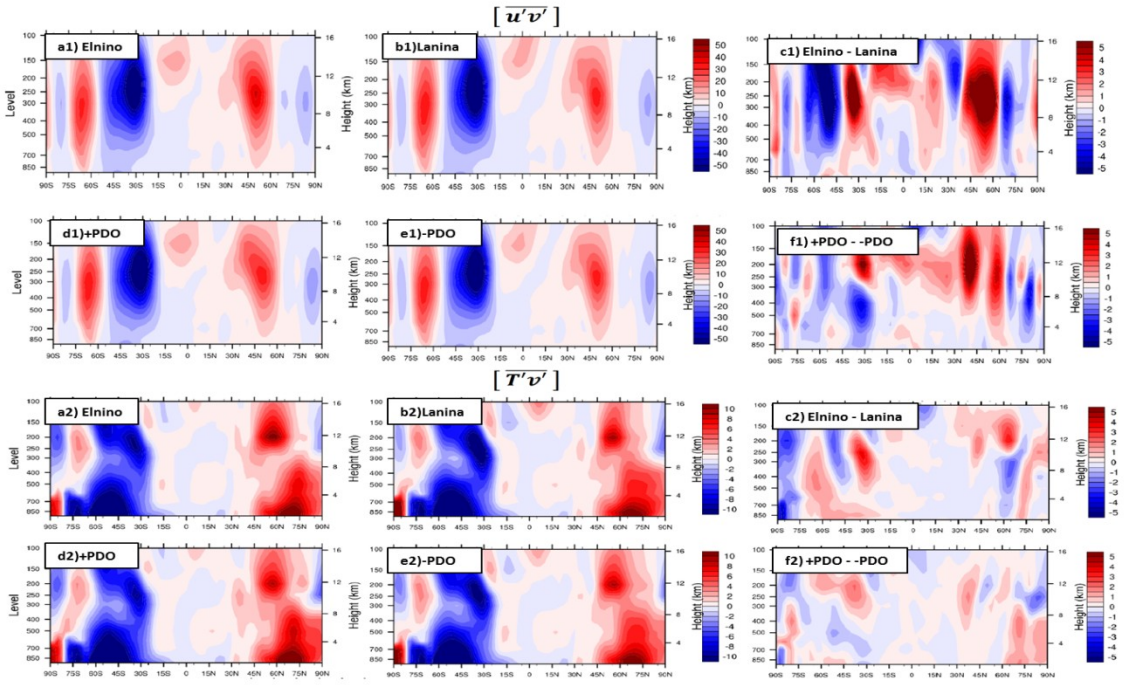

Figure 6: *Mean (65°E-100°E, 1950-2016 year, JJAS months) meridional transient eddy transport (shaded contour, red (northward), blue (southward)) during ENSO and PDO phases (a1 to f1 represents EMF transport, and a2 to f2 represents for EHF transport).*

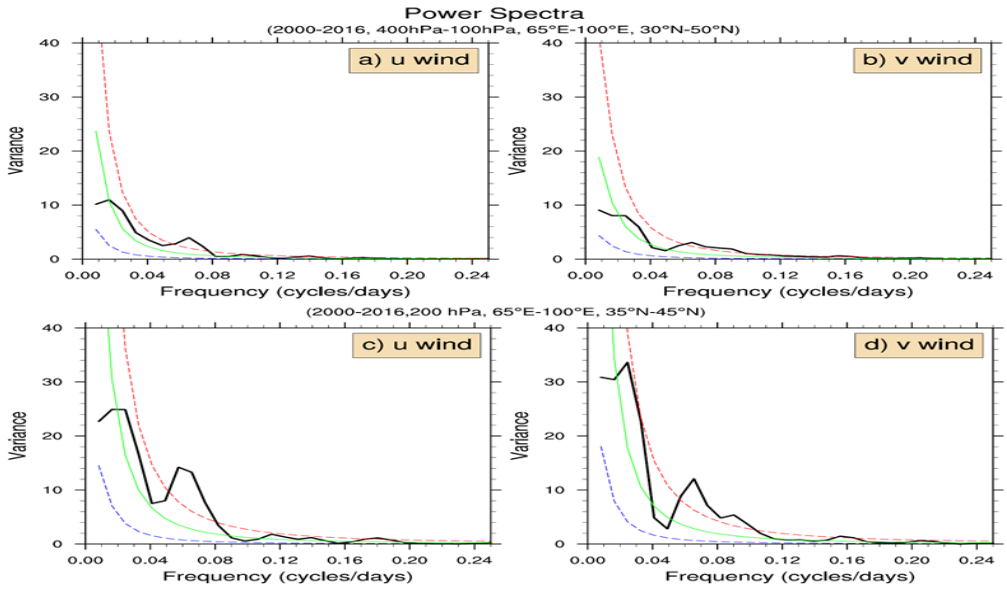

Figure 7: *Mean (65°E-100°E, 2000-2016 year, JJAS months) power spectra of* ***u*** *and* ***v*** *wind component, a)* ***u*** *wind, and b)* ***v*** *wind (averaged over 400hPa-100hPa and 30°N-50°N). c)* ***u*** *wind, and d)* ***v*** *wind (averaged over 200hPa and 35°N-45°N).*

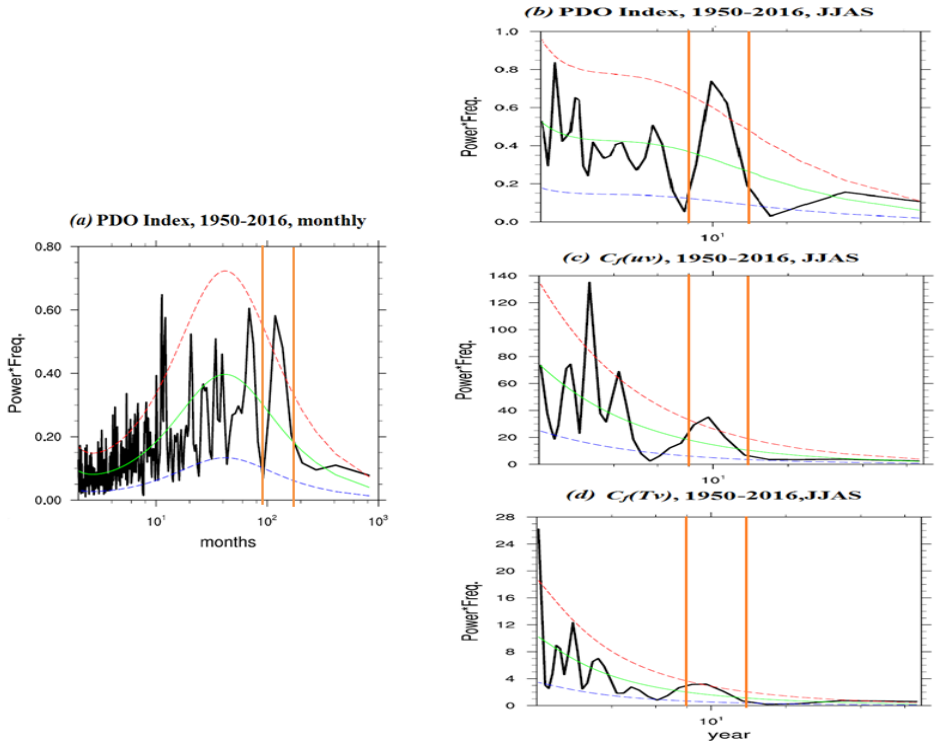

Figure 8 : *Power spectra of PDO index (a. all months, b. JJAS months),* ***uv*** *cospectra (**C_f(uv)**, c. JJAS months), and* ***Tv*** *cospectra (**C_f(uv)**, d. JJAS months) from the year 1950 to 2016 (60°E-100°E, 25°N-60°N, and 300hPa-150hPa level).The area between two orange lines represents the PDO signal in all figures.*

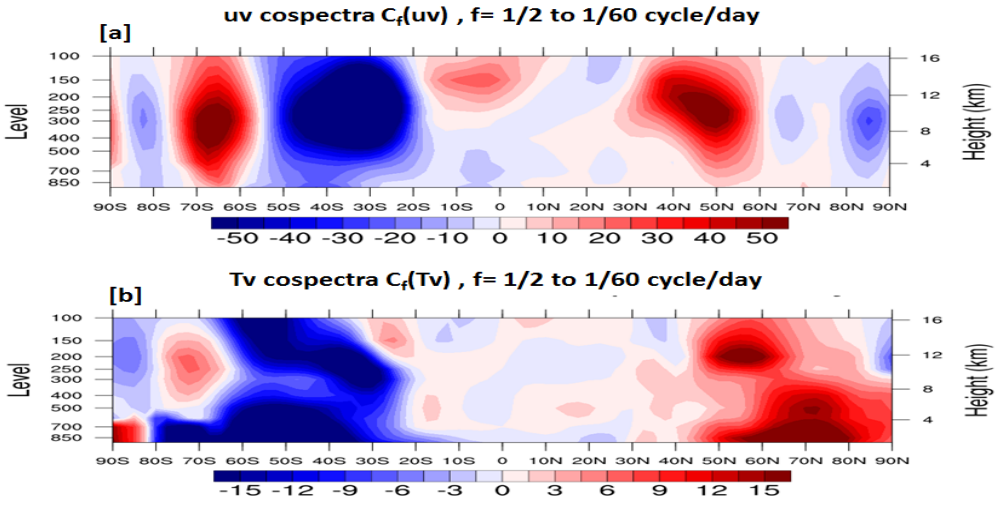

Figure 9: *Mean cospectra analysis (2 to 60 day period, 65°E-100°E, 1950-2016 year, JJAS months,* ***uv*** *cospectra (**C_f(uv)**) and b is* ***Tv*** *cospectra (**C_f(Tv)**), Both figures show zonal mean of meridional distribution of respective cospectra (shaded contour, red (positive) northward, blue (negative) equatorward transport), This analysis resembles* ***Figure 4,*** *i.e., Mean meridional transient eddy transport for momentum and heat (65°E-100°E / 1950-2016 year / JJAS), Oort, Abraham H.Peixóto, 1983.*

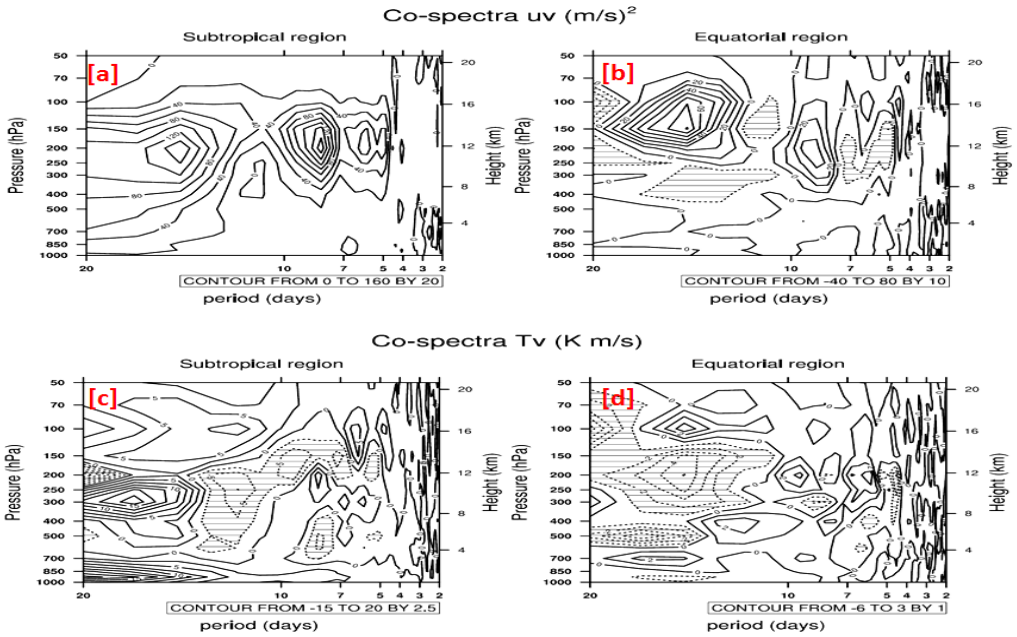

***Figure 10**: Cospectra of 2-20 days (continuous line represents positive cospectra and northward transport, dashed line represents negative cospectra and equatorward transport) periodicity over the Pacific region from April to July 1962. Classified as a) **uv** cospectra (**C_f(uv)**) subtropical region, b) **uv** cospectra equatorial region, c) **Tv** cospectra (**C_f(Tv)**) subtropical region, and d) **Tv** cospectra equatorial region reproduced from Nitta, 1970.*

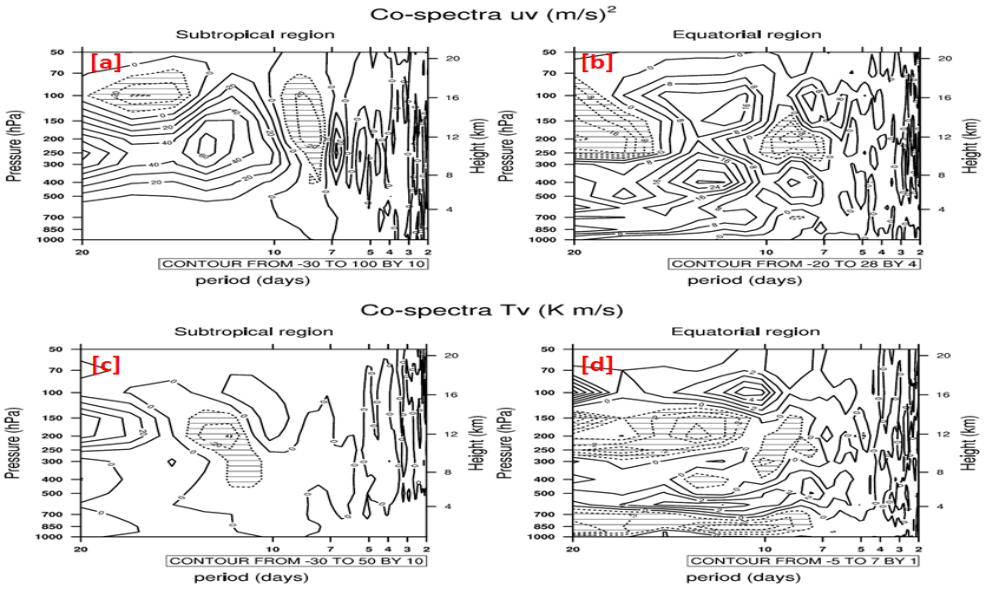

***Figure 11:** Cospectra of 2-20 days (continuous line represents positive cospectra and northward transport, dashed line represents negative cospectra and equatorward transport) periodicity over Indian region from April to July 1962. Classified as a) **uv** cospectra (**C_f(uv)**) subtropical region, b) **uv** cospectra equatorial region, c) **Tv** cospectra (**C_f(Tv)**) subtropical region, and d) **Tv** cospectra equatorial region reproduced from Nitta, 1970.*

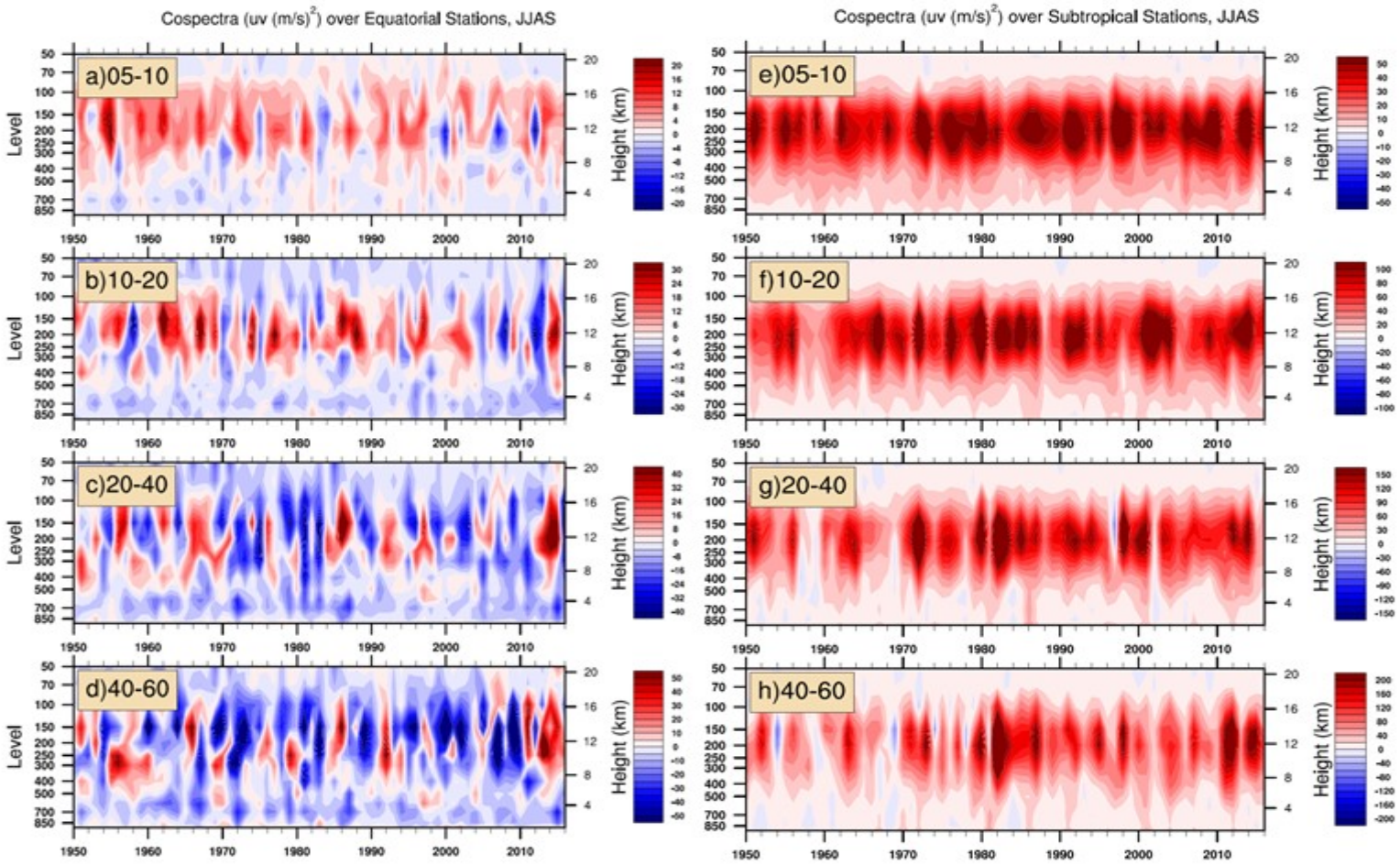

Figure 12: *Seasonal-mean (Pacific region, 1950-2016 year, JJAS months) interannual* ***uv*** *cospectra (**C_f(uv)**, shaded contour, red (positive) northward, blue (negative) equatorward), Over equatorial Pacific from (a) to (b) and over subtropical Pacific from (e) to (h) represents eddy bands of 5-10 days, 10-20 days, 20-40 days and 40-60 days respectively. (For station details Nitta, 1970).*

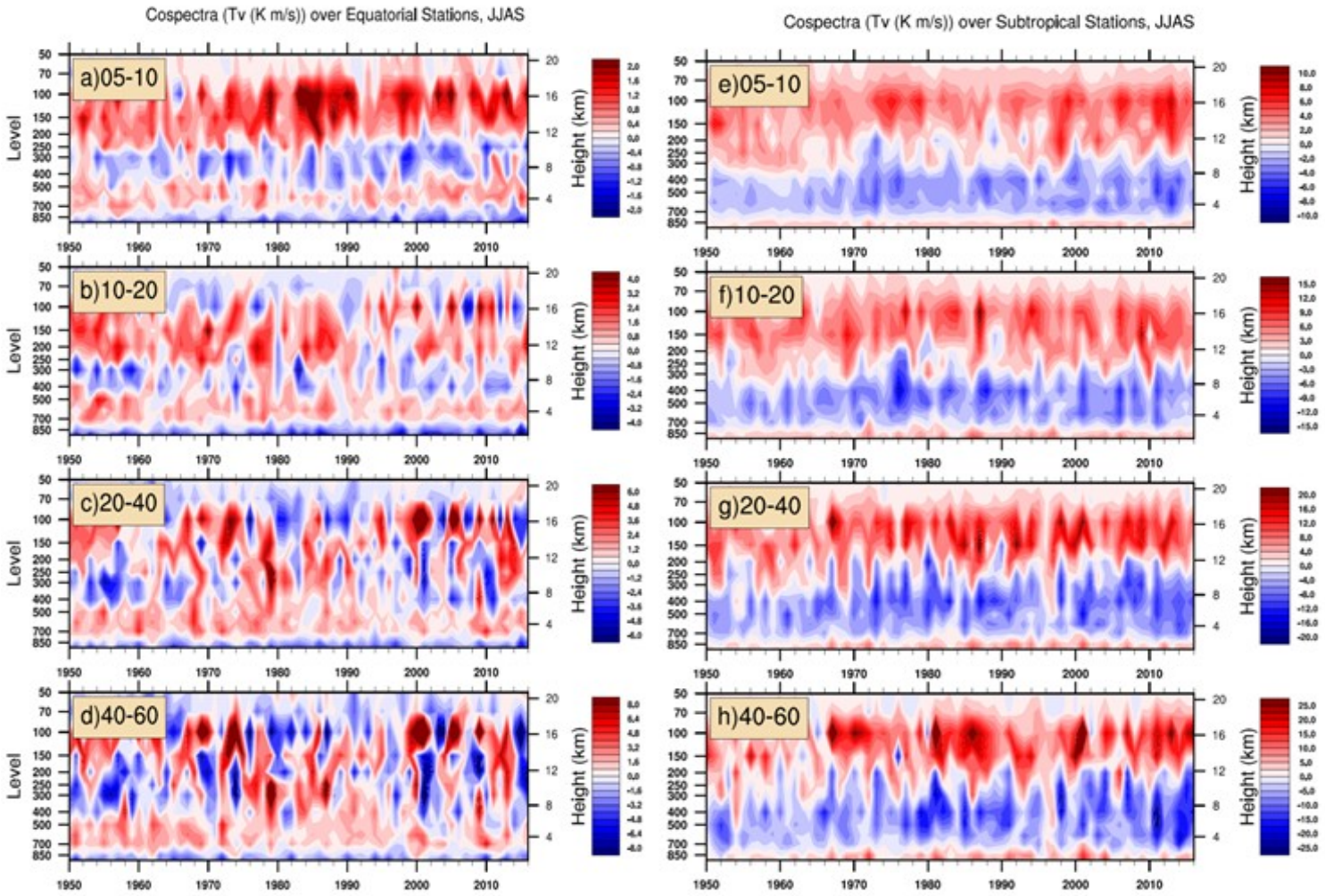

Figure 13: *Seasonal-mean (Pacific region, 1950-2016 year, JJAS months) interannual* ***Tv*** *cospectra (**C_f(Tv),** shaded contour, red(positive) northward, blue(negative) equatorward),Over equatorial Pacific from (a) to (b) and over subtropical Pacific from (e) to (h) represents eddy bands of 5-10 days, 10-20 days, 20-40 days and 40-60 days respectively. (For station details Nitta, 1970).*

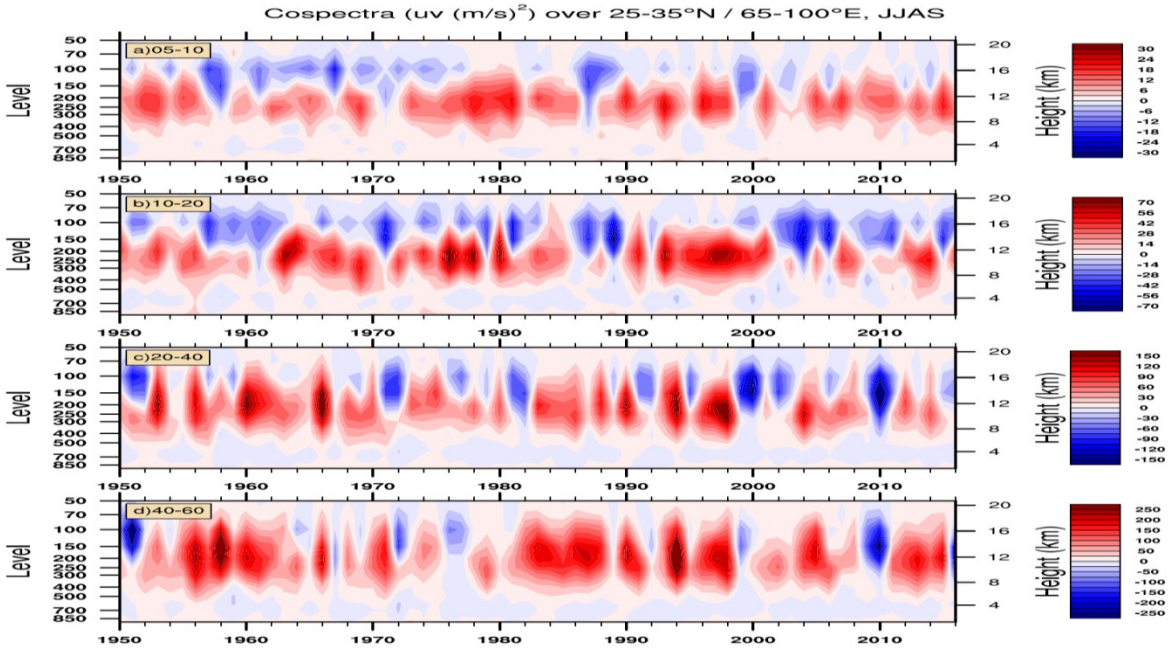

Figure 14: *Seasonal-mean (25°N-35°N, 65°E-100°E, 1950-2016 year, JJAS months) interannual* ***uv*** *cospectra (**C_f(uv)**, shaded contour, red(positive) northward, blue(negative) equatorward),eddy bands from a) 5-10 days, b) 10-20 days, c) 20-40 days and d) 40-60 days respectively.*

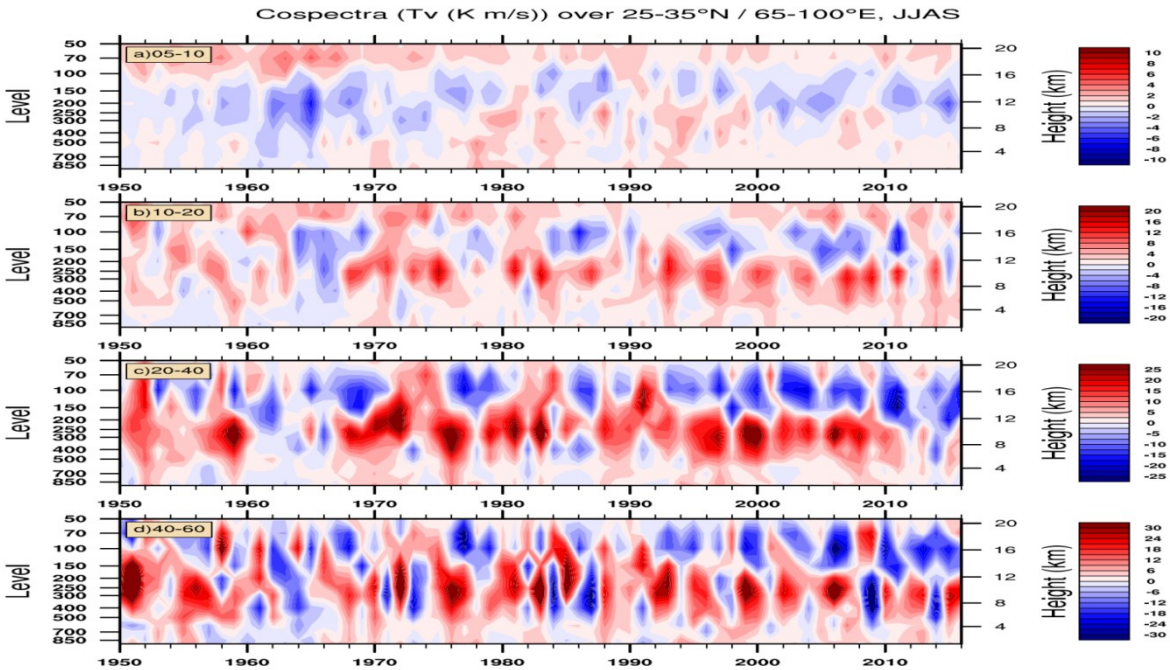

Figure 15: *Seasonal-mean (25°N-35°N, 65°E-100°E, 1950-2016 year, JJAS months) interannual* ***Tv*** *cospectra (**C_f(Tv)**, shaded contour, red(positive) northward, blue(negative) equatorward), eddy bands from a)5-10 days, b)10-20 days, c)20-40 days and d)40-60 days respectively.*

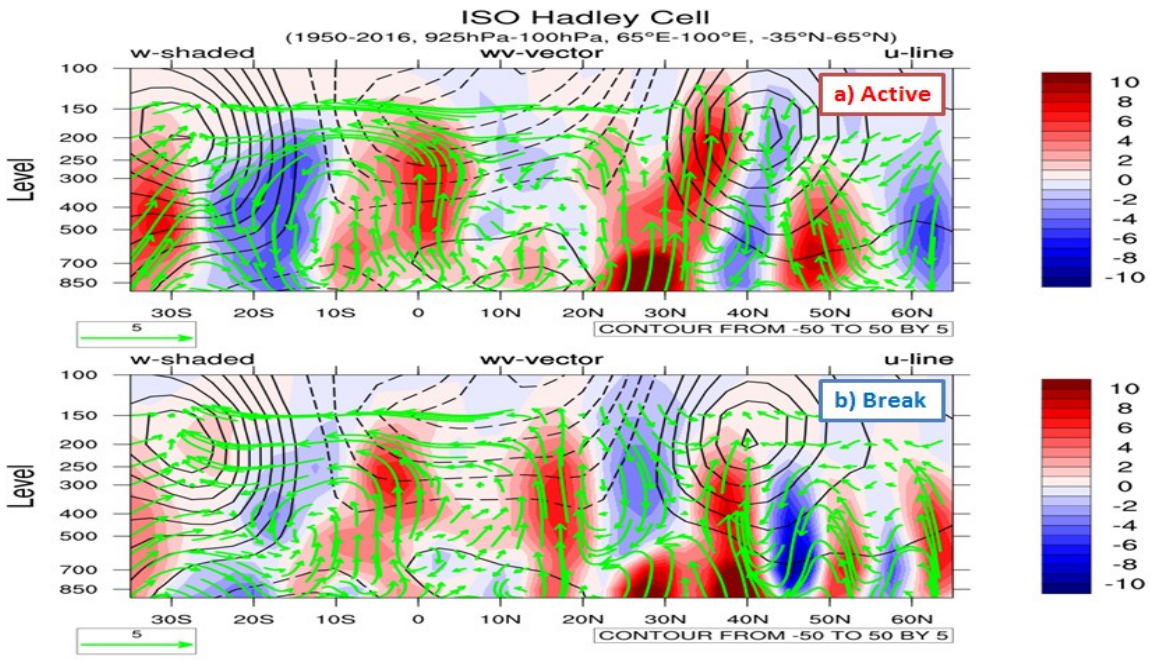

Figure 16: *Mean (65°E-100°E, 1950-2016 year, JJAS months) monsoonal Hadley cell during the dominant mode of intraseasonal oscillation (ISO), i.e., a) Active and b) Break spells, Days are classified according to Rajeevan et al., 2010. Zonal mean wind (line contour, continuous lines (westerlies), and dotted lines (easterlies)), mean meridional circulation (green arrow), and vertical mean wind component (shaded contour, red (upward), blue (downward), scaled by 100).*

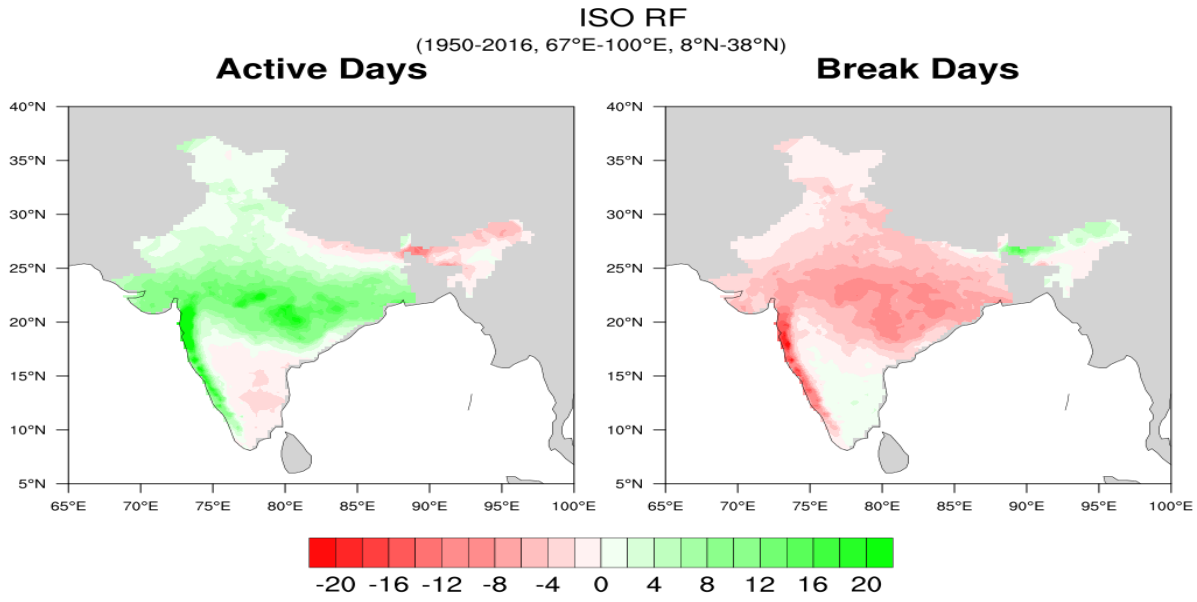

.

Figure 17: *Mean (1950-2016 year / JJAS months) spatial pattern of rainfall anomalies (mm/day) during dominant mode intraseasonal oscillation (ISO), i.e., a) Active and b) Break spells, Days are classified according to Rajeevan et al., 2010.*

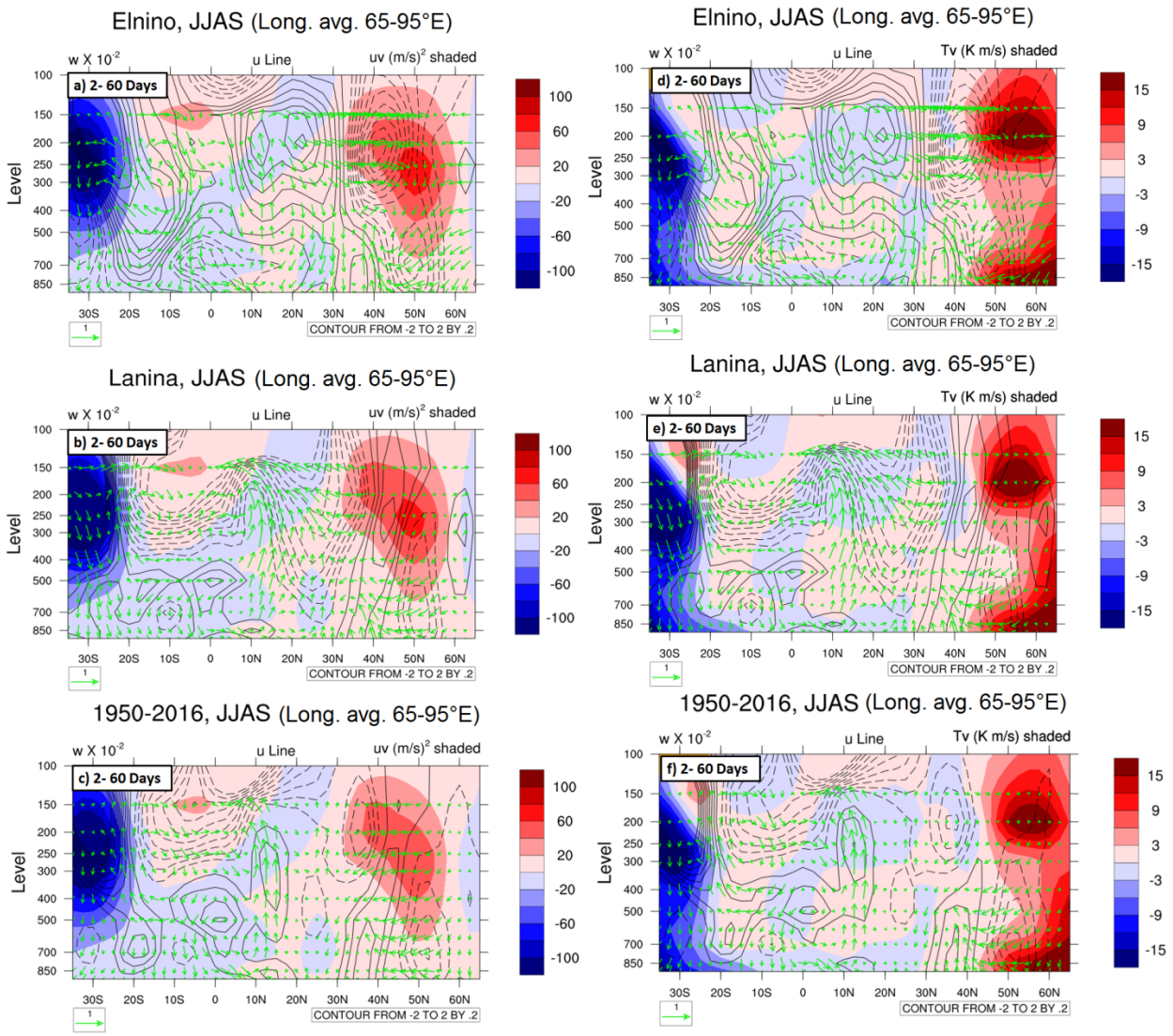

Figure 18: *Seasonal-mean(65°E-95°E, 1950-2016 year, JJAS months) meridional distribution of cospectra (shaded contour, red(positive) northward, blue(negative) equatorward) by averaged 2 to 60 days period with zonal mean wind anomalies (black line) and meridional wind vector (green arrow) for* ***C_f(uv)*** *during a) El Niño, b) La Niña and c) mean (1950 to 2016). For* ***C_f(Tv)*** *during d) El Niño, e) La Niña and f) mean (1950 to 2016) cases.*

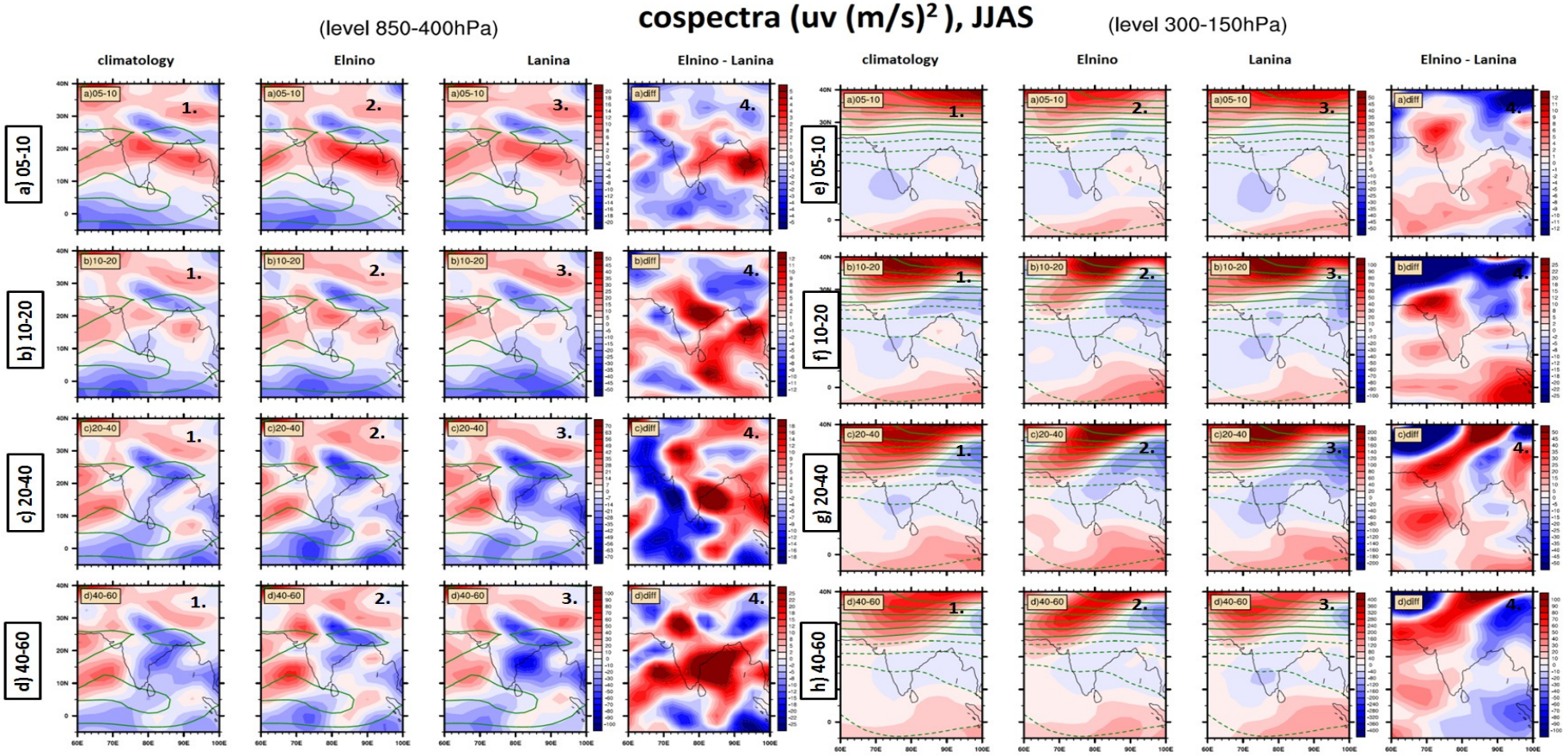

Figure 19: *Spatial distribution of* ***uv*** *cospectra (**C_f(uv)**, red(+ve) and blue(-ve) shading) with zonal wind (green line) over Indian region (5°S-40°N/60°E-100°E / JJAS) during ENSO cases. The columnar plot is 1.Climatology, 2.El Niño,3. La Niña, and 4.Difference between El Niño & La Niña. Averaged over 850hPa to 400hPa level for (a) 5-10 days, (b) 10-20 days, (c) 20-40 days and (d) 40-60 days bands. Averaged over 300hPa to 150hPa level for (e) 5-10 days, (f) 10-20 days, (g) 20-40 days and (h) 40-60 days bands. Green solid (dash) line represents positive (negative)* ***u*** *wind component (m/s, -50 to 50 by 5).*

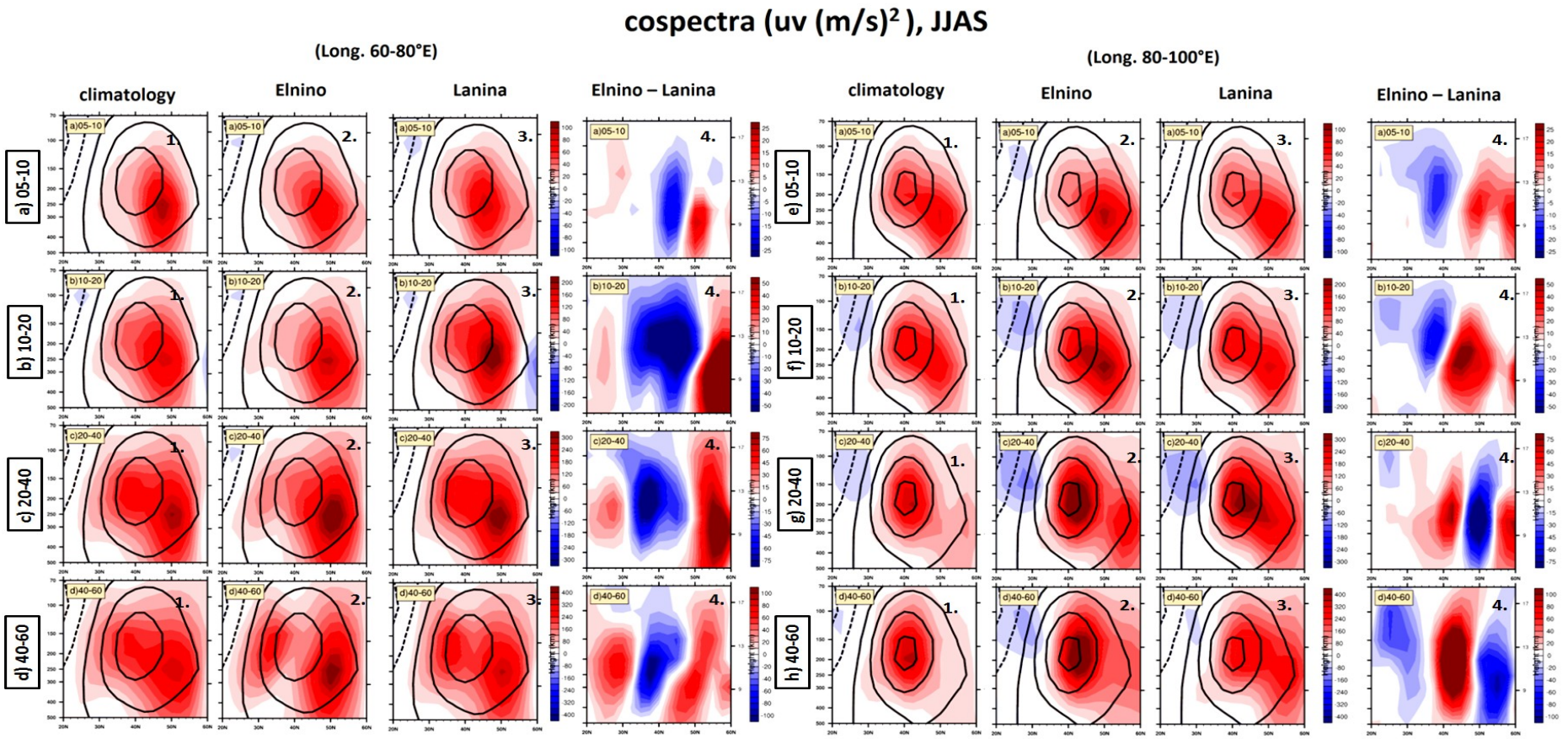

Figure 20: *Vertical distribution of* ***uv*** *cospectra (**C_f(uv)**, red(+ve) and blue(-ve) shading) with the zonal mean wind (black line) over 20°N -60°N and 500hPa-70hPa during ENSO cases. The columnar plot is 1.Climatology, 2.El Niño, 3.La Niña, and 4.Difference between El Niño & La Niña. Averaged over 60°E to 80°E longitude for (a) 5-10 days, (b) 10-20 days, (c) 20-40 days and (d) 40-60 days bands and averaged over 80°E to 100°E longitude for (e) 5-10 days, (f) 10-20 days, (g) 20-40 days and (h) 40-60 days bands. Black solid (dash) line represents positive (negative)* ***u*** *wind component (m/s, -50 to 50 by 5).*

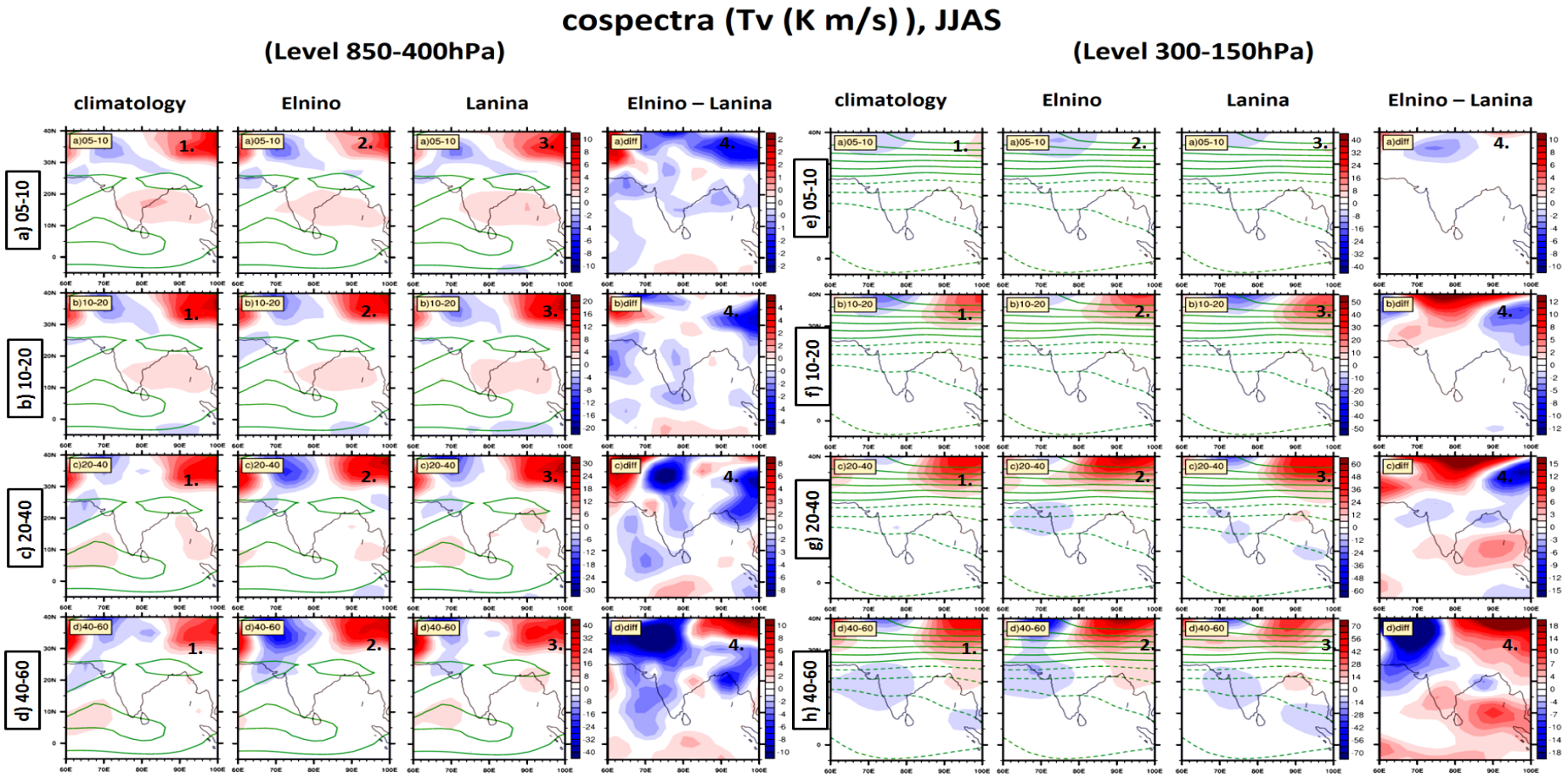

Figure 21: *Spatial distribution of* ***Tv*** *cospectra (**C_f(Tv)**, red(+ve) and blue(-ve) shading) with zonal wind (green line) over Indian region (5°S-40°N/60°E-100°E) during ENSO cases. The columnar plot is 1.Climatology, 2.El Niño, 3.La Niña, and 4.Difference between El Niño & La Niña. Averaged over 850hPa to 400hPa level for (a)5-10 days, (b)10-20 days, (c)20-40 days and (d)40-60 days bands and averaged over 300hPa to 150hPa level for(e)5-10 days, (f)10-20 days, (g)20-40 days and (h)40-60 days bands. Green solid (dash) line represents positive (negative)* ***u*** *wind component (m/s, -50 to 50 by 5).*

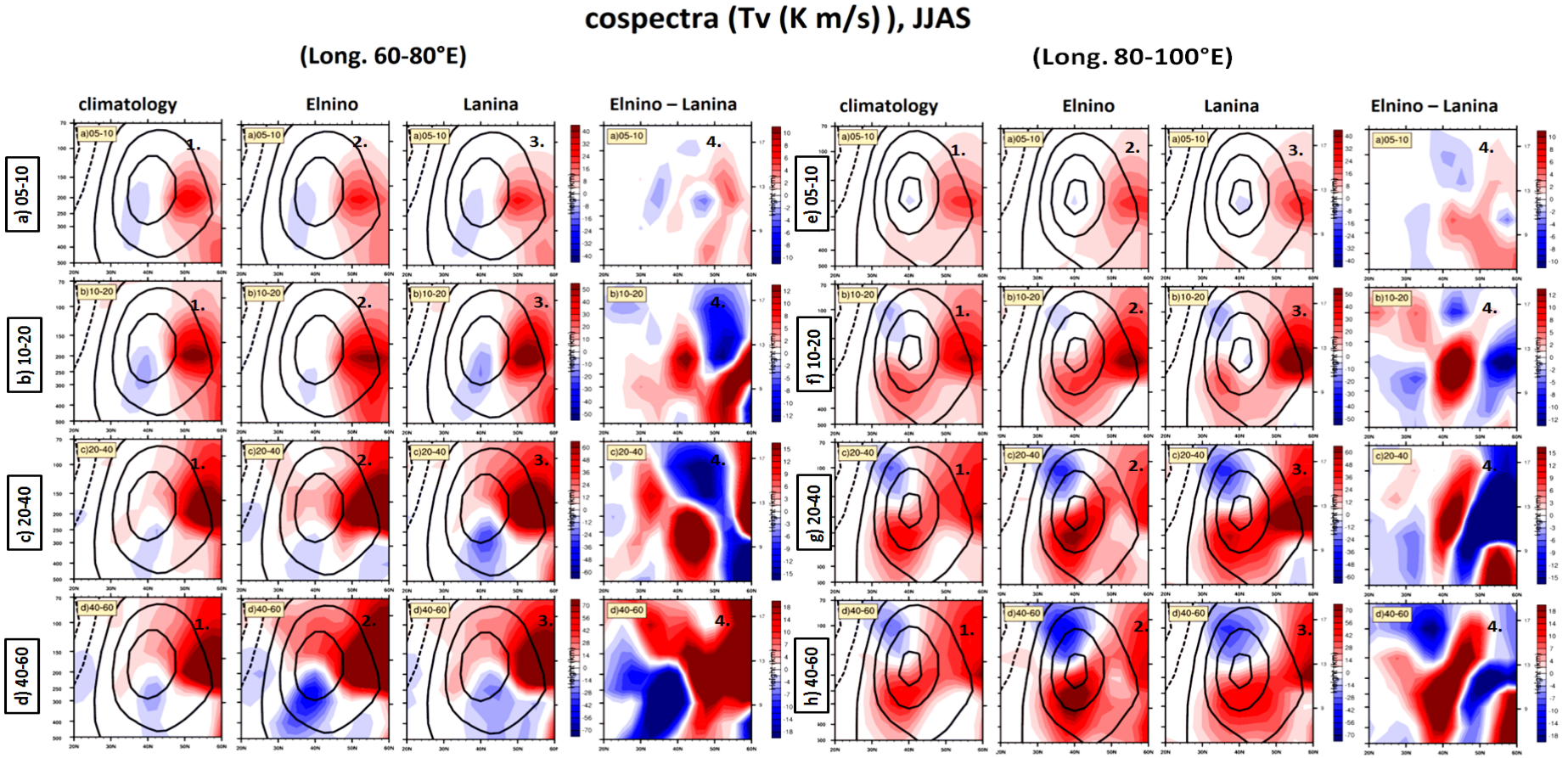

Figure 22: *Vertical distribution of* ***Tv*** *cospectra (**C_f(Tv)**, red (+ve) and blue (-ve) shading) with the zonal mean wind (black line) over 20°N -60°N and 500hPa-70hPa during ENSO cases. The columnar plot is 1.Climatology, 2.El Niño, 3.La Niña, and 4.Difference between El Niño & La Niña. Averaged over 60°E to 80°E longitude for (a) 5-10 days, (b) 10-20 days, (c) 20-40 days and (d) 40-60 days bands and averaged over 80°E to 100°E longitude for (e) 5-10 days, (f) 10-20 days, (g) 20-40 days and (h) 40-60 days bands. Black solid (dash) line represents positive (negative)* ***u*** *wind component (m/s, -50 to 50 by 5).*

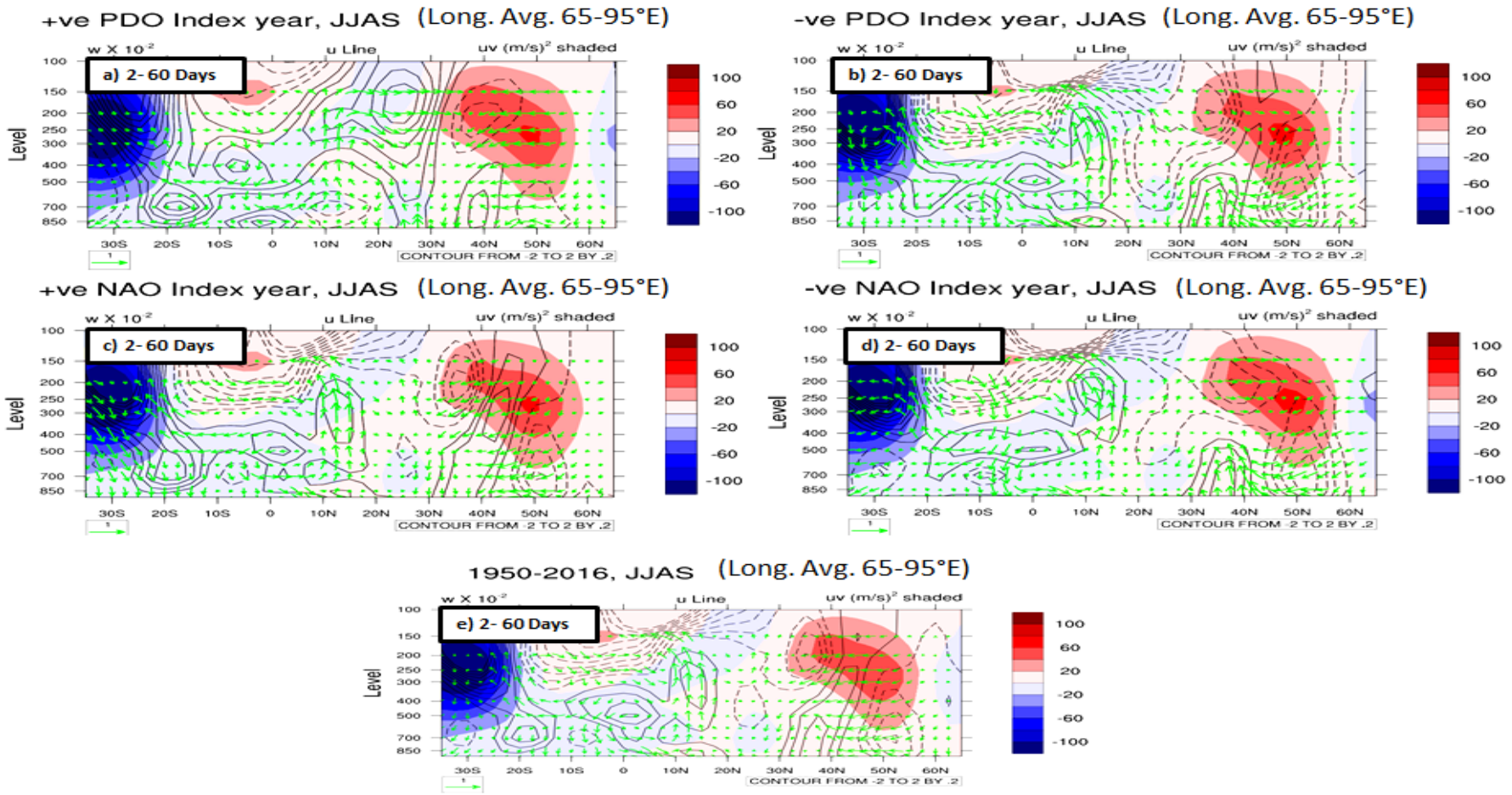

Figure 23: *Seasonal-mean (65°E-95°E / 1950-2016 year / JJAS months) meridional distribution of* ***uv*** *cospectra (**C_f(uv),** shaded contour, red(positive) northward, blue(negative) equatorward) by averaged 2 to 60 days period with zonal mean wind anomalies (black line) and meridional wind vector (green arrow) during a)+PDO, b)-PDO, c)+NAO, d)-NAO and c) mean (1950 to 2016) Cases.*

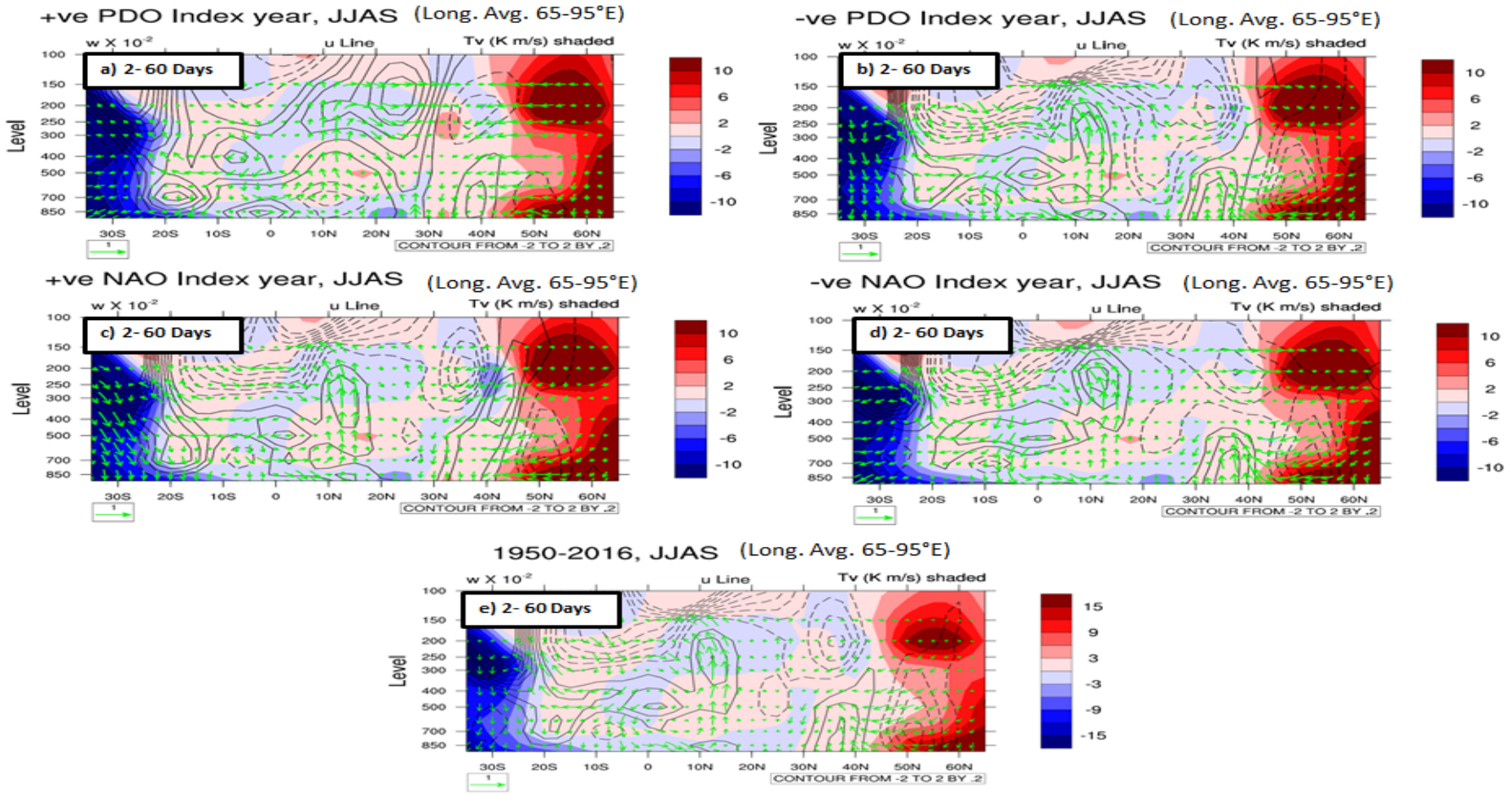

Figure 24: *Seasonal-mean (65°E-95°E / 1950-2016 year / JJAS months) meridional distribution of* ***Tv*** *cospectra (**C_f(Tv)**, shaded contour, red(positive) northward, blue(negative) equatorward) by averaged 2 to 60 days period with zonal mean wind anomalies (black line) and meridional wind vector (green arrow) during a)+PDO, b)-PDO, c)+NAO, d)-NAO and c) mean (1950 to 2016) Cases.*

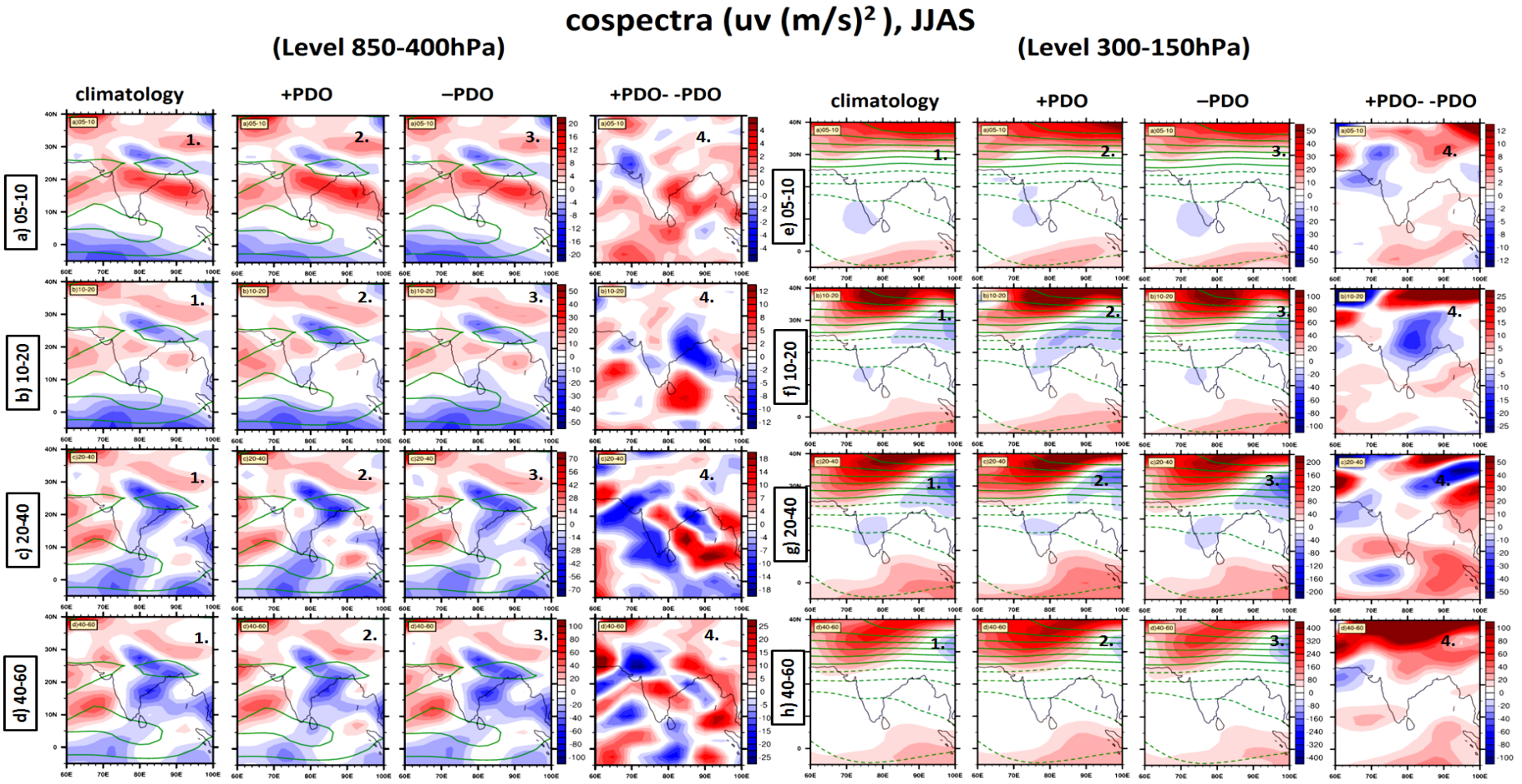

Figure 25: *Spatial distribution of* ***uv*** *cospectra (**C_f(uv)**, red(+ve) and blue(-ve) shading) with zonal wind (green line) over Indian region (5°S-40°N/60°E-100°E) during PDO cases. Columnar plot are 1.Climatology, 2. +PDO, 3.-PDO and 4.Difference between +PDO & -PDO. Averaged over 850hPa to 400hPa level by (a)5-10 days, (b)10-20 days, (c)20-40 days and (d)40-60 days bands and averaged over 300hPa to 150hPa level for (e)5-10 days, (f)10-20 days, (g)20-40 days and (h)40-60 days bands. Green solid (dash) line represents positive (negative)* ***u*** *wind component (m/s, -50 to 50 by 5).*

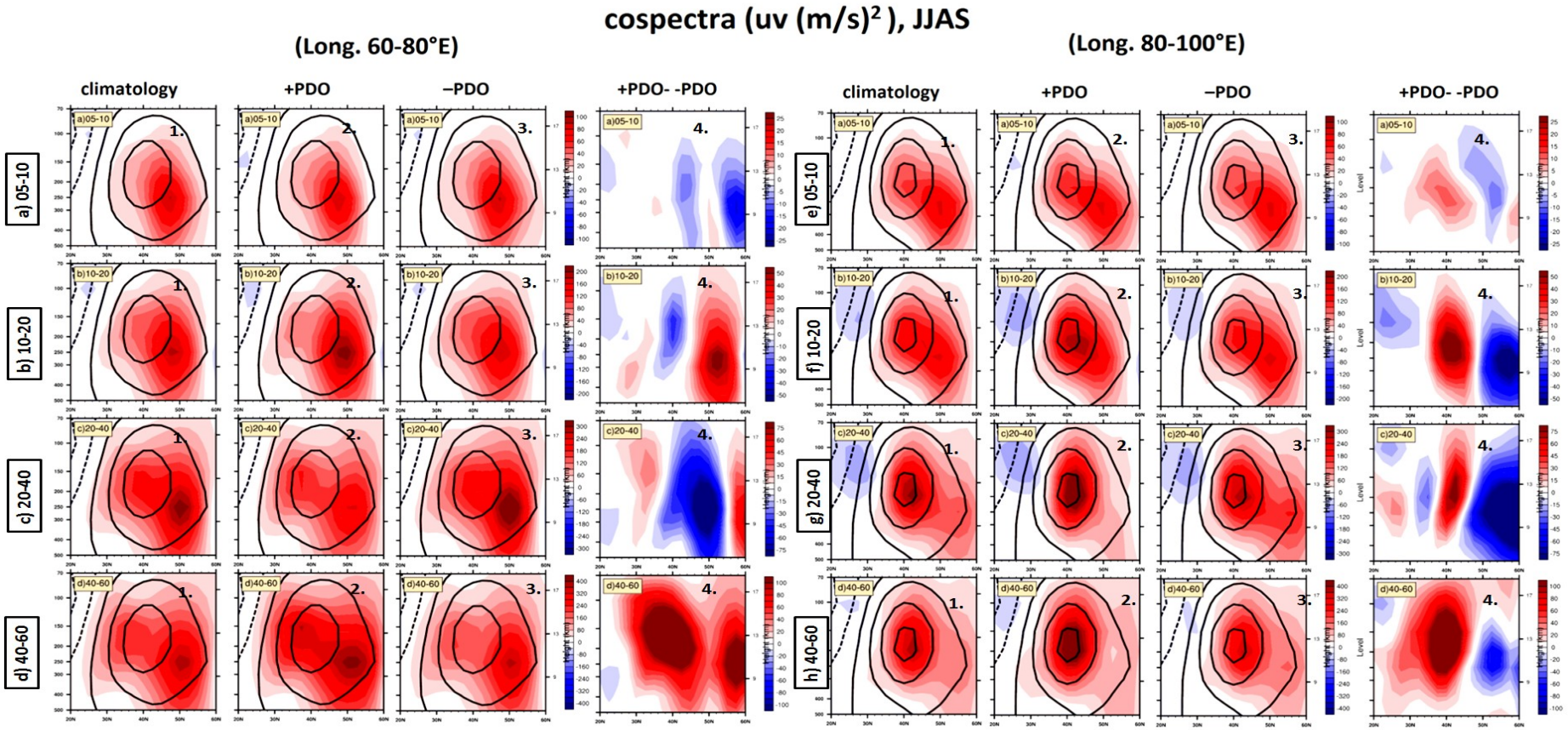

Figure 26: *Vertical distribution of* ***uv*** *cospectra (**C_f(uv)**, red (+ve) and blue (-ve) shading) with the zonal mean wind (black line) over 20°N -60°N and 500hPa-70hPa during PDO cases. Columnar plot are 1.Climatology, 2. +PDO 3.-PDO and 4.Difference between +PDO & -PDO. Averaged over 60°E to 80°E longitude for (a) 5-10 days, (b) 10-20 days, (c) 20-40 days and (d) 40-60 days bands and averaged over 80°E to 100°E longitude for (e) 5-10 days, (f) 10-20 days, (g) 20-40 days and (h) 40-60 days bands. Black solid (dash) line represents positive (negative)* ***u*** *wind component (m/s, -50 to 50 by 5).*

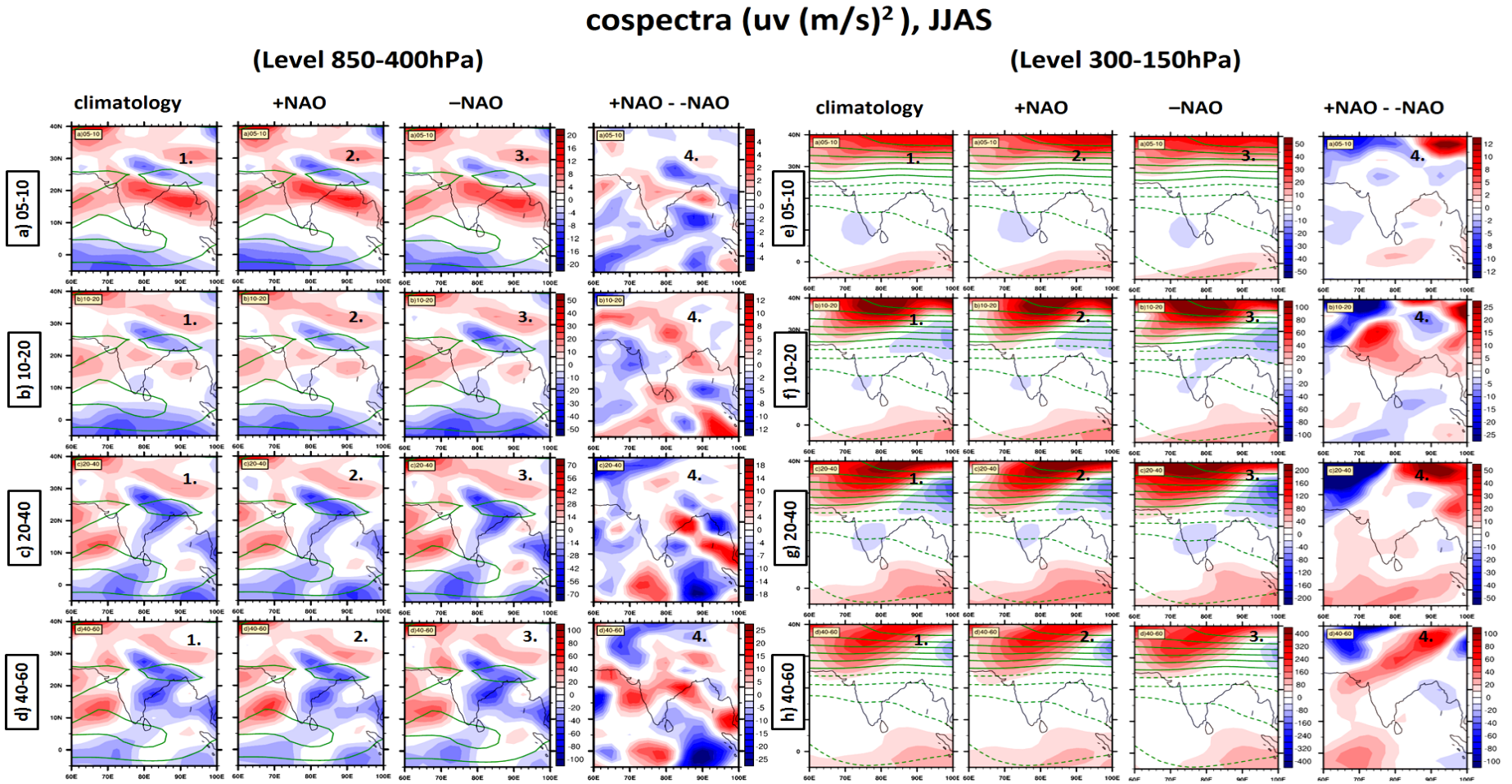

Figure 27: *Spatial distribution of* ***uv*** *cospectra (**C_f(uv)**, red(+ve) and blue(-ve) shading) with zonal wind (green line) over Indian region (5°S-40°N/60°E-100°E) during* NAO *cases. The columnar plot is 1.Climatology, 2.* +NAO*, 3.*-NAO *and 4.Difference between* +NAO*&*-NAO*. Averaged over 850hPa to 400hPa level for (a)5-10 days, (b)10-20 days, (c)20-40 days and (d)40-60 days bands and over 300hPa to 150hPa level for (e)5-10 days, (f)10-20 days, (g)20-40 days and (h)40-60 days bands. Green solid (dash) line represents positive (negative)* ***u*** *wind component (m/s, -50 to 50 by 5).*

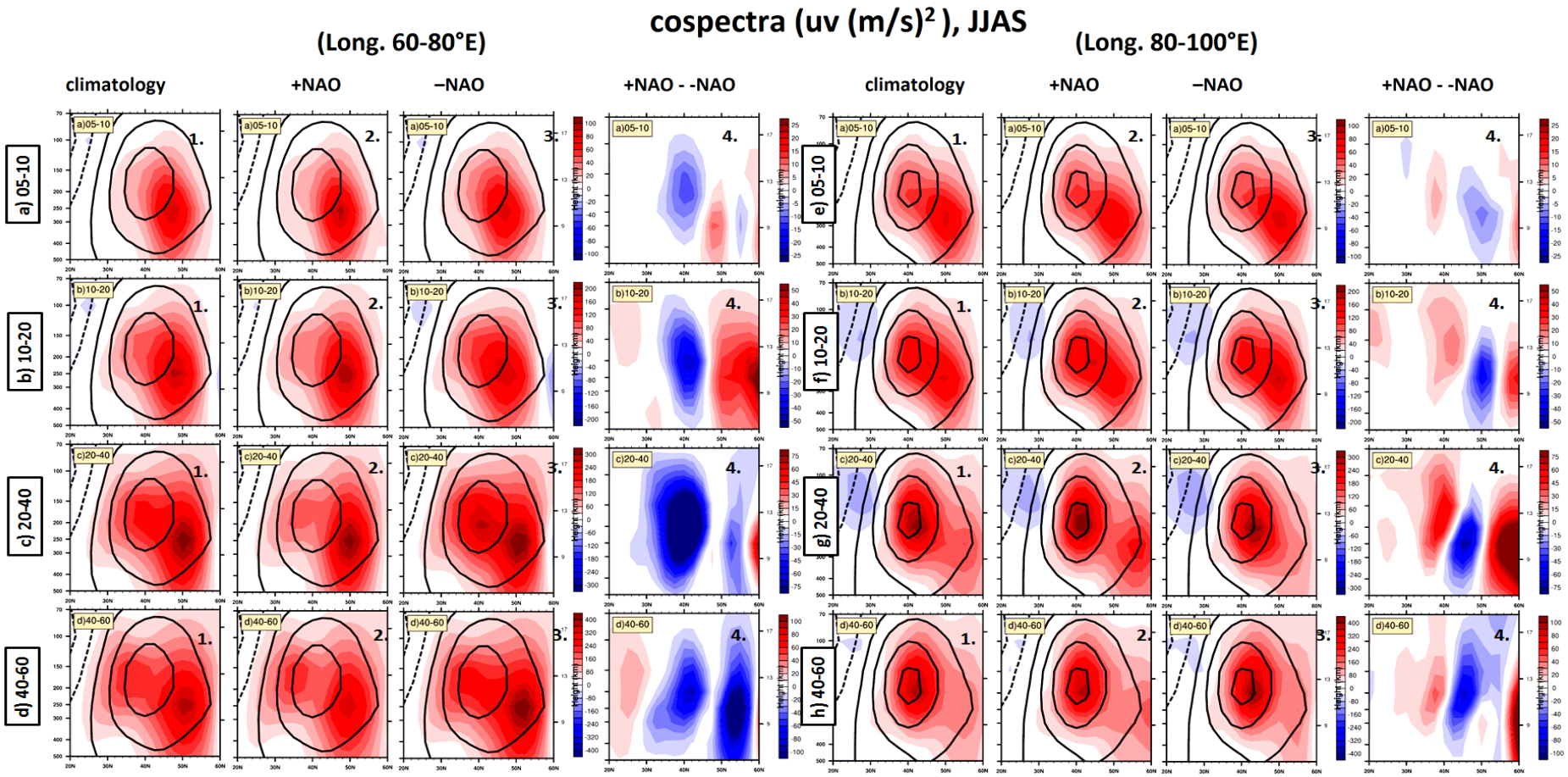

Figure 28: *Vertical distribution of* ***uv*** *cospectra (**C_f(uv)**, red (+ve) and blue (-ve) shading) with the zonal mean wind (black line) over 20°N -60°N and 500hPa-70hPa during NAO cases. The columnar plot is 1.Climatology, 2. +NAO 3.-NAO and 4.Difference between +NAO & -NAO. Averaged over 60°E to 80°E longitude for (a) 5-10 days, (b) 10-20 days, (c) 20-40 days and (d) 40-60 days bands and averaged over 80°E to 100°E longitude for (e) 5-10 days, (f) 10-20 days, (g) 20-40 days and (h) 40-60 days bands. Black solid (dash) line represents positive (negative)* ***u*** *wind component (m/s, -50 to 50 by 5).*

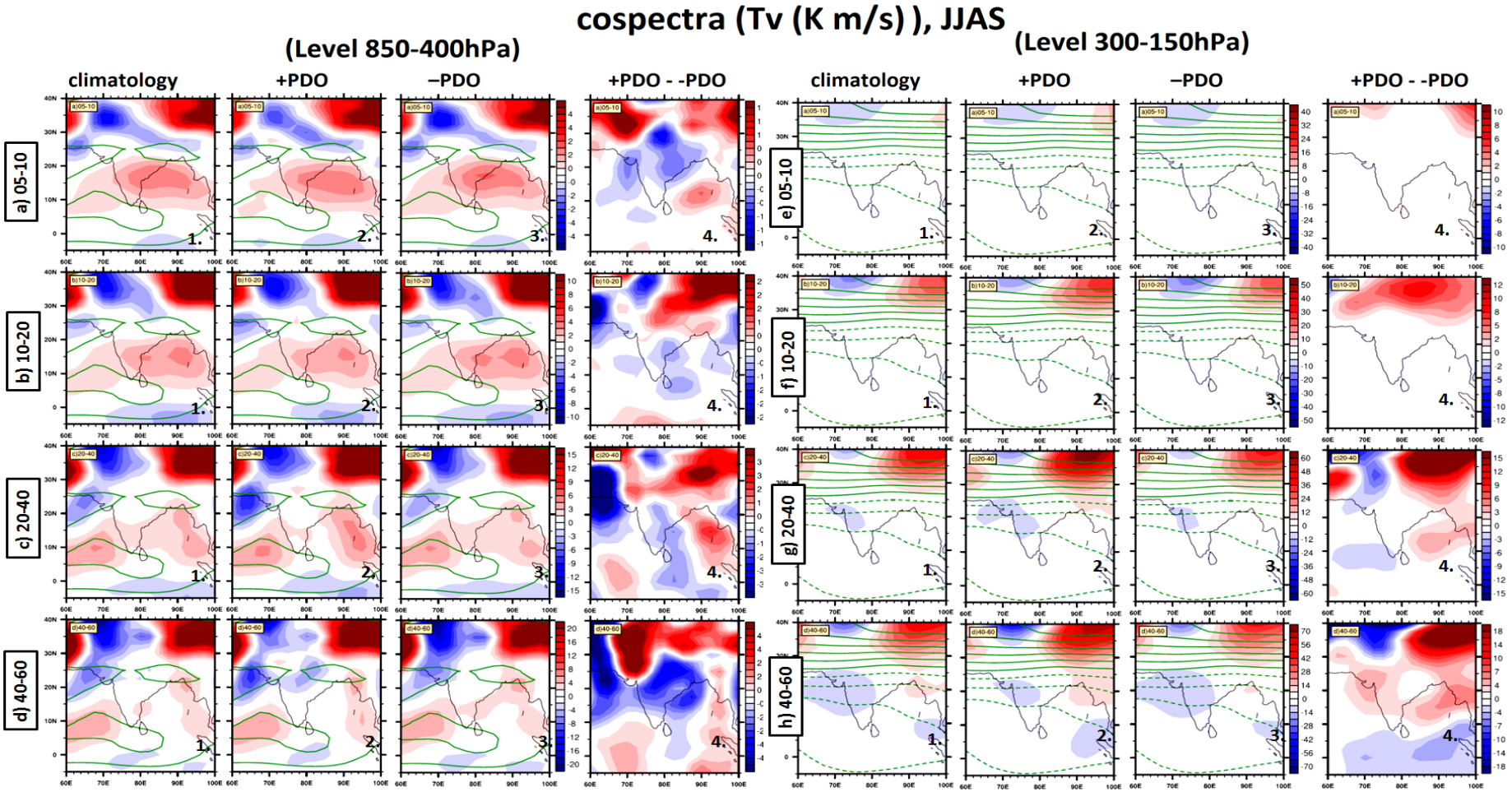

Figure 29: *Spatial distribution of* ***Tv*** *cospectra (**C_f(Tv)**, red(+ve) and blue(-ve) shading) with zonal wind (green line) over Indian region (5°S-40°N/60°E-100°E) during PDO cases. Columnar plot are 1.Climatology, 2. +PDO, 3.-PDO and 4.Difference between +PDO & -PDO. Averaged over 850hPa to 400hPa level for (a)5-10 days, (b)10-20 days, (c)20-40 days and (d)40-60 days bands and averaged over 300hPa to 150hPa level for (e)5-10 days, (f)10-20 days, (g)20-40 days and (h)40-60 days bands. Green solid (dash) line represents positive (negative)* ***u*** *wind component (m/s, -50 to 50 by 5).*

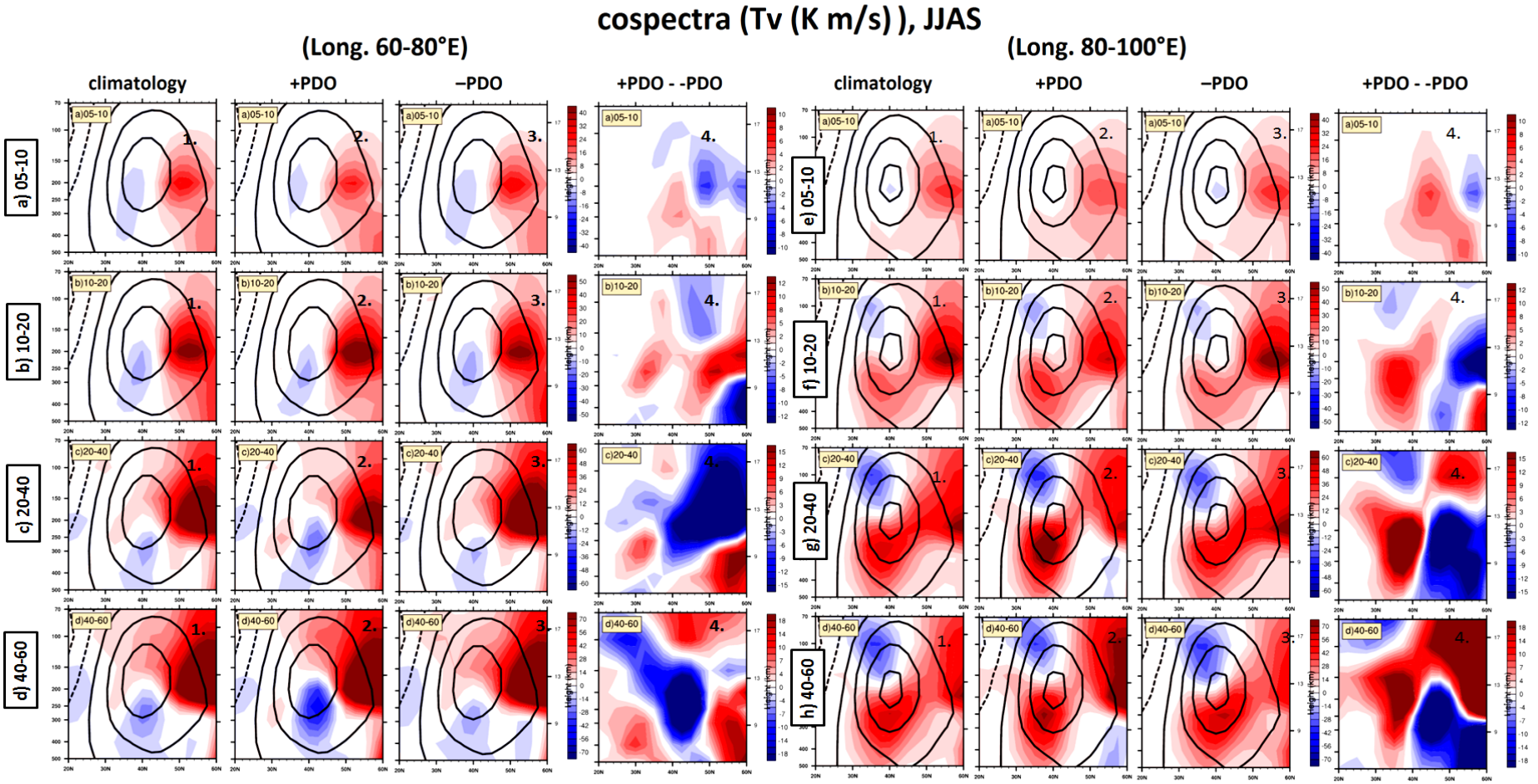

Figure 30: *Vertical distribution of* ***Tv*** *cospectra (**C_f(Tv)**, red (+ve) and blue (-ve) shading) with the zonal mean wind (black line) over 20°N -60°N and 500hPa-70hPa during PDO cases. Columnar plot are 1.Climatology, 2. +PDO 3.-PDO and 4.Difference between +PDO & -PDO. Averaged over 60°E to 80°E longitude for (a) 5-10 days, (b) 10-20 days, (c) 20-40 days and (d) 40-60 days bands and averaged over 80°E to 100°E longitude for (e) 5-10 days, (f) 10-20 days, (g) 20-40 days and (h 40-60 days bands. Black solid (dash) line represents positive (negative)* ***u*** *wind component (m/s, -50 to 50 by 5).*

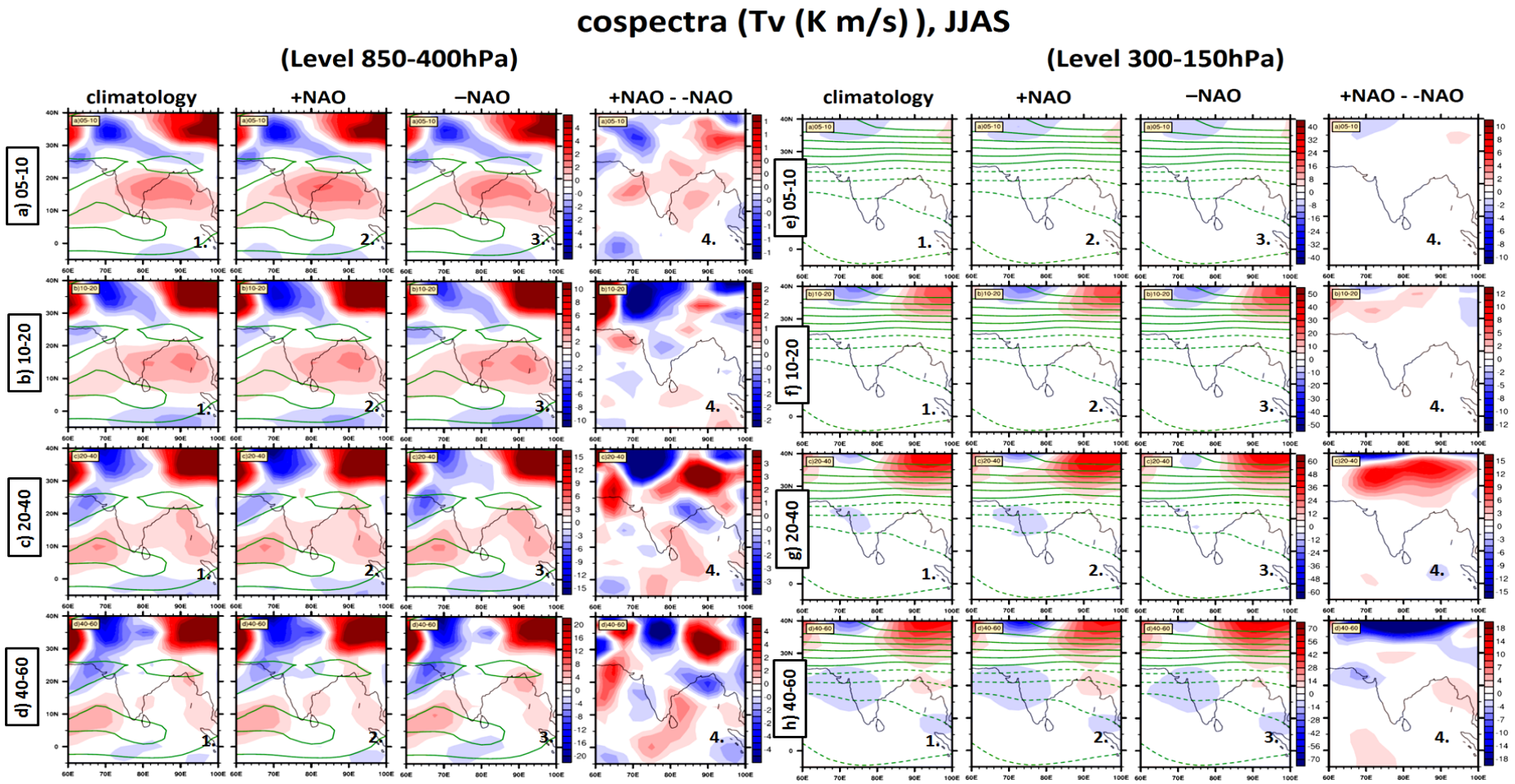

Figure 31: *Spatial distribution of* ***Tv*** *cospectra (**C_f(Tv)**, red(+ve) and blue(-ve) shading) with zonal wind (green line) over Indian region (5°S-40°N/60°E-100°E) during* NAO *cases. The columnar plot is 1.Climatology, 2.* +NAO, *3.*-NAO *and 4.Difference between* +NAO&-NAO. *Averaged over 850hPa to 400hPa level for (a)5-10 days, (b)10-20 days, (c)20-40 days and (d)40-60 days bands and averaged over 300hPa to 150hPa level for (e)5-10 days, (f)10-20 days, (g)20-40 days and (h)40-60 days bands. Green solid (dash) line represents positive (negative)* ***u*** *wind component (m/s, -50 to 50 by 5).*

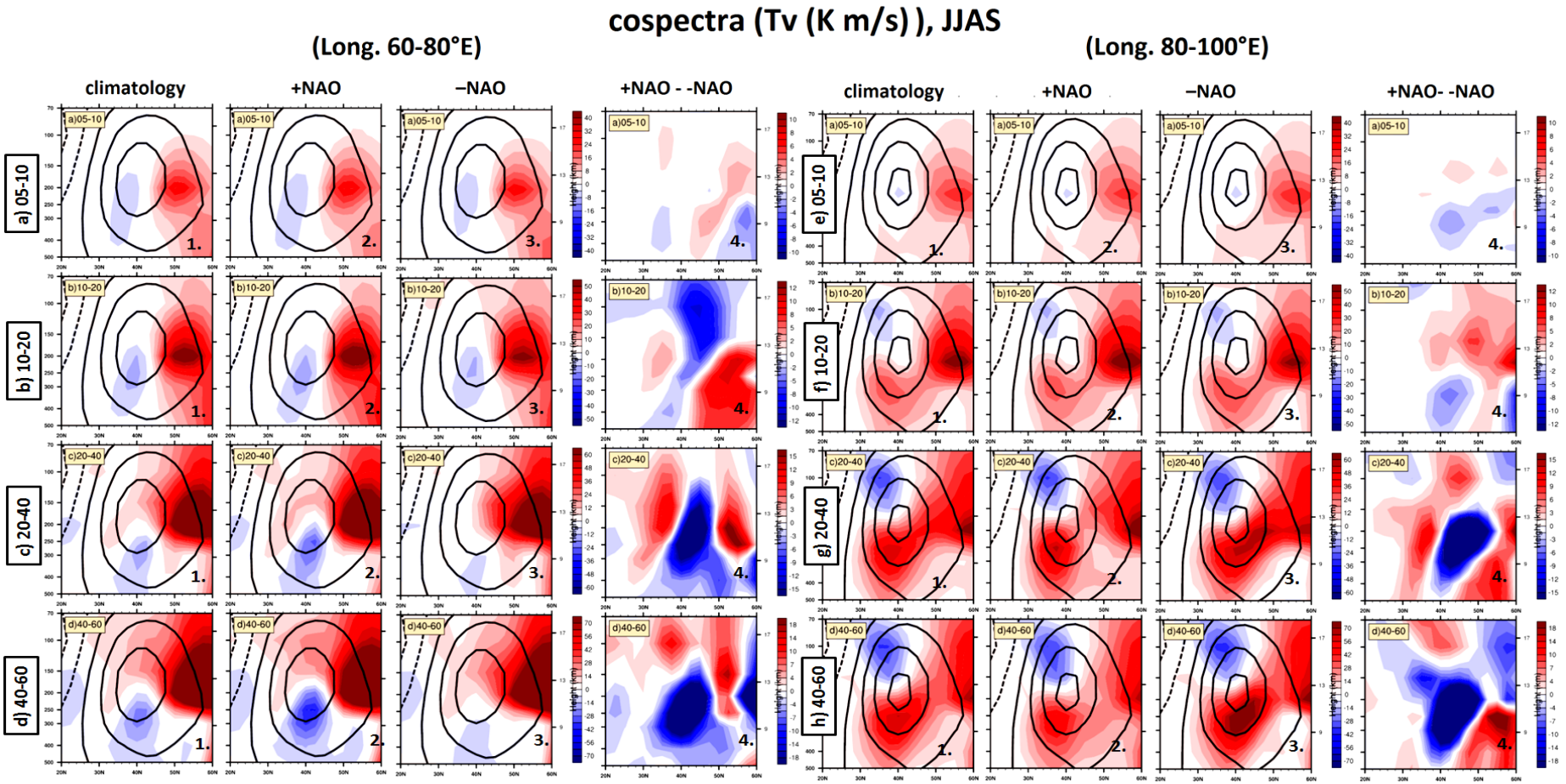

Figure 32: *Vertical distribution of* ***Tv*** *cospectra* ***(C_f(Tv)****, red (+ve) and blue (-ve) shading) with the zonal mean wind (black line) over 20°N -60°N and 500hPa-70hPa during NAO cases. The columnar plot is 1.Climatology, 2. +NAO 3. -NAO and 4.Difference between +NAO & -NAO. Averaged over 60°E to 80°E longitude for (a) 5-10 days, (b) 10-20 days, (c) 20-40 days and (d) 40-60 days bands and averaged over 80°E to 100°E longitude for (e) 5-10 days, (f) 10-20 days, (g) 20-40 days and (h) 40-60 days bands. Black solid (dash) line represents positive (negative)* ***u*** *wind component (m/s, -50 to 50 by 5).*

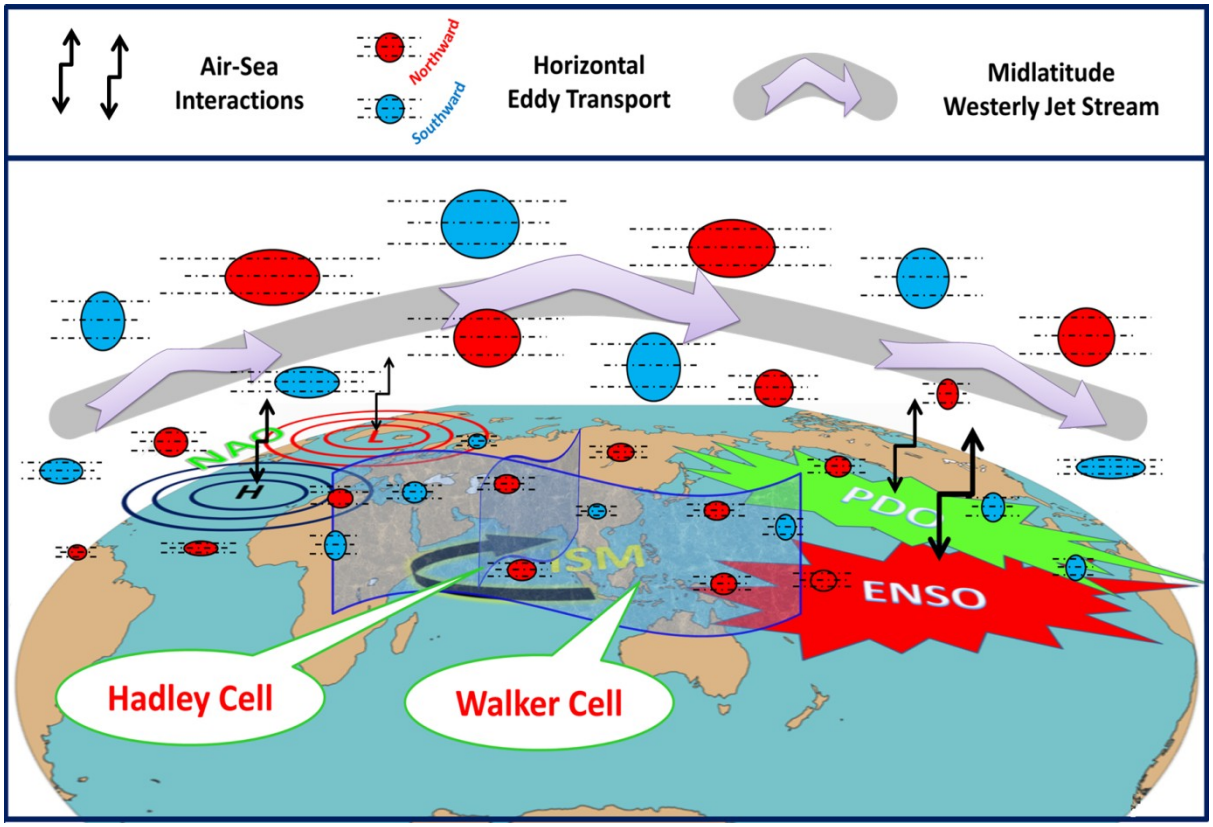

Figure 33: *Schematic representation of air-sea interaction and teleconnection which may indirectly modulate Indian summer monsoon through eddy transport. On a different scale, such eddy fluctuation may associate with known global patterns such as ENSO, PDO, and NAO.*